



**The  
University  
Of  
Sheffield.**  
Faculty of Engineering

**Feasibility Study of Plasma Treatment of Clays  
and Polymers for Nanocomposite  
Manufacture by Laser Sintering**

By:

**Alaa Madhloom Mahdi Almansoori**

A thesis submitted in partial fulfilment of the requirements for  
the degree of

**Doctor of Philosophy**

**The University of Sheffield**

**Faculty of Engineering**

**Department of Materials Science and Engineering**

**November 2018**



## **Dedication**

*This thesis and all my academic achievements are dedicated to the memories of my Father and Mother.*

## **Acknowledgements**

I would like to take this opportunity to express my sincere gratitude to my sponsor, Ministry of Higher Education and Scientific Research and its representative in London, the Cultural Attaché for their financial support. I extend special thanks to The Southern Technical University in Basra for giving me study leave to do my PhD research.

I would also like to express my sincere thanks to my supervisors, Dr Cornelia Rodenburg and Dr Candice Majewski, for giving me this opportunity to join their research group. I truly appreciate their continued assistance, encouragement, constructive discussion, and moral support they have provided.

I gratefully thank the contributions of the co-authors, Dr K. Abrams, Dr R. Masters from the research group, Dr J. Schäfer, Dr T. Gerling from Germany. Thanks to all the group member's Dr Vikas Kumar, Dr Quan Wang, Sameer Falih and Nicola Stehling for their helpful pieces of advice.

My gratitude and thanks to all the admin staff and technicians of the Department of Materials Science and Engineering, Centre for Advanced Additive Manufacturing (ADAM) and the Sorby Centre for Electron Microscopy and Microanalysis at The University of Sheffield. Special thanks to Dr Cheryl Shaw, Ben Palmer, Dean Haylock, and Wendy Birtwistle for their technical support.

I must express my gratitude and appreciation to my wife for her unfailing support and continuous encouragement throughout the four years of my PhD research.

Finally, I would say thanks to my brothers and sisters and my friends in Iraq.

## **Abstract**

Additive Manufacturing (AM) describes a powerful set of techniques which have the potential to become a reliable method for the manufacture of complex and accurate parts. Laser Sintering (LS) is one of the most promising AM techniques, capable of manufacturing 3-dimensional (3D) products from polymer powders. However, some key challenges still limit their widespread applications. The most common key challenges, specifically for the Laser Sintering AM process are limited availability of different materials, inconsistent or poor mechanical properties and surface quality, each of which is currently still restricting the functions of the end-use parts.

In some cases, nanoclay reinforcement of polymers has been shown to provide performance benefits, improving part quality, and offering new applications. However, the dispersion of those nano-sized materials still remains a critical issue for the preparation of Laser Sintering nanocomposites. A novel method of using plasma treatment to tackle these challenges was developed in this study. Plasma treatment was used to increase the surface area of nanoclay particles and with the expectation of simultaneous surface functionalisation aiming for increased homogeneity after dry mixing of polymer and nanoclay powders. SEM images of treated composite powders confirmed this expectation as the plasma treatment reduce agglomerations and improved nanoclay dispersion in the powders.

To consolidate these powders into parts a novel methodology, i.e. Downward Heat Sintering (DHS) method was initially used as a powerful replication method for the Laser Sintering technique. DHS process was employed with a hot press to process small quantities of PA12 and dry mixed composite powders into tensile test specimens after optimisation attempts based on differential scanning calorimetry (DSC) and hot-stage microscopy (HSM). SEM images of the heat sintered specimens showed clearly the plasma treatment prevented the aggregation of the nanoclay resulting in an improved elastic modulus of treated composite compared with neat PA12 and untreated composites. Moreover, the reduction in elongation at break for the treated composite was less pronounced than untreated composite.

Further work resulted in successfully LS parts with different complex and accurate shapes. No significant deterioration in LS processibility was observed and complex LS parts could be produced when including the plasma treated nanoclay. SEM images of the

cross-sections of the fabricated parts that the layer by layer structure were successfully consolidated and relatively uniform. In addition, the introduction of the plasma treated nanoclay was found to improve the elastic modulus of the LS composite parts. Most notably however, a substantially improved surface quality in part's appearance and microstructure was found as a result of incorporating plasma treated nanoclay compared to the nontreated nanoclay.

PA12 exposed to Low Pressure Air Plasma Treatment showed an increase in wettability, was relatively porous, and possessed a higher density, which resulted from surface functionalisation and materials removal during the plasma exposure. However, it showed poor melt behaviour under heating conditions typical for Laser Sintering. In contrast, brief Plasma Jet treatments demonstrated similar changes in porosity, but crucially, retained the favourable melt characteristics of PA12 powder.

To summarise, this is a unique study on the use of plasma treatment and polymer/polymer nanocomposites in LS applications, demonstrating for the first time that plasma treatment has the potential to provide crucial performance benefits for laser sintered nanocomposites.

## Table of Contents

<b>Dedication.....</b>	<b>i</b>
<b>Acknowledgements .....</b>	<b>ii</b>
<b>Abstract.....</b>	<b>iii</b>
<b>Table of Contents .....</b>	<b>v</b>
<b>Table of Figures .....</b>	<b>x</b>
<b>Table of Figures in the Appendices .....</b>	<b>xiv</b>
<b>List of Tables .....</b>	<b>xvi</b>
<b>Publications .....</b>	<b>xvii</b>
<b>Conferences and Meetings .....</b>	<b>xvii</b>
<b>Chapter 1: Introduction.....</b>	<b>1</b>
Section 1.1: Background.....	1
Section 1.2: Aims and objectives .....	3
Section 1.3: Thesis Structure.....	4
Section 1.4: References.....	6
<b>Chapter 2: Literature Review .....</b>	<b>9</b>
Section 2.1: Background .....	9
Section 2.2: Nanocomposites .....	9
<i>Section 2.2.1: Polymer nanocomposites .....</i>	<i>10</i>
<i>Section 2.2.2: Fillers.....</i>	<i>11</i>
<i>Section 2.2.3: Nanoclay/polymer nanocomposites .....</i>	<i>15</i>
Section 2.3: Manufacturing processes .....	21
<i>Section 2.3.1: Laser Sintering (LS).....</i>	<i>21</i>
<i>Section 2.3.2: Polymers nanocomposites by LS technique .....</i>	<i>22</i>
<i>Section 2.3.3: Plasma Treatments.....</i>	<i>24</i>
<i>Section 2.3.4: Plasma treatments of nanofillers .....</i>	<i>25</i>
<i>Section 2.3.5: Plasma treatments of LS polymers.....</i>	<i>26</i>

<i>Section 2.3.6: Characterisation of polymer nanocomposites</i> .....	27
<i>Section 2.3.7: Mechanical properties of LS polymer nanocomposites</i> .....	29
Section 2.4: References.....	31
<b>Chapter 3: Background and Experimental works</b> .....	<b>45</b>
Section 3.1: Background .....	45
<i>Section 3.1.1: Materials</i> .....	45
<i>Section 3.1.2: Plasma treatments</i> .....	48
Section 3.2: Materials processing .....	52
Section 3.3: Experimental procedures for materials .....	55
<i>Section 3.3.1: Morphological investigations by SEM</i> .....	55
<i>Section 3.3.2: Wettability and density measurements</i> .....	56
<i>Section 3.3.3: Fourier transform infrared spectroscopy (FTIR)</i> .....	57
<i>Section 3.3.4: X-Ray Diffraction (XRD)</i> .....	57
<i>Section 3.3.5: Thermal analysis</i> .....	57
<i>Section 3.3.6: Tensile testing</i> .....	58
Section 3.4: References.....	59
<b>Chapter 4: Nanoclay/Polymer Composite Powders for use in Laser Sintering</b>	
<b>Applications: Effects of Nanoclay Plasma Treatment</b> .....	<b>61</b>
Section 4.1: Abstract.....	61
Section 4.2: Introduction.....	61
Section 4.3: Materials, Preparation Methods, and Experimental Work .....	65
<i>Section 4.3.1: Materials and Preparation Methods</i> .....	65
<i>Section 4.3.2: Experimental work</i> .....	67
Section 4.4: Results and Discussion .....	68
<i>Section 4.4.1: Optimisation of processing conditions by HSM</i> .....	68



<i>Section 4.4.2: Effect of Plasma Treatment on the Nanoclay (Characterisation Techniques)</i> .....	71
<i>Section 4.4.3: Investigation of the properties of the etched nanoclay/polymer composites powders</i> .....	73
<i>Section 4.4.4: Testing the mechanical properties</i> .....	74
Section 4.5: Conclusion .....	78
Section 4.6: References.....	79

**Chapter 5: Novel Plasma Treatment for Preparation of Laser Sintered**

<b>Nanocomposite Parts</b> .....	<b>83</b>
Section 5.1: Abstract.....	83
Section 5.2: Introduction.....	84
Section 5.3: Materials and Materials Processing and Preparation .....	86
<i>Section 5.3.1: Nanoclays</i> .....	86
<i>Section 5.3.2: Low Pressure Air Plasma Treatment (LP-PT) technique</i> .....	87
<i>Section 5.3.3: Materials preparation for Downward Heat Sintering (DHS) and laser sintering (LS) applications</i> .....	88
Section 5.4: Materials characterisation and testing .....	89
<i>Section 5.4.1: Scanning electron microscopy (SEM) and Hot Stage Microscopy (HSM)</i> .....	90
<i>Section 5.4.2: Fourier transform infrared spectroscopy (FTIR)</i> .....	90
<i>Section 5.4.3: Thermogravimetric analysis (TGA)</i> .....	91
<i>Section 5.4.4: Tensile tests</i> .....	91
Section 5.5: Results and Discussion .....	92
<i>Section 5.5.1: Characterisation analysis and results</i> .....	92
<i>Section 5.5.2: Influence of plasma treatment on the quality of Laser sintered parts</i> .....	98

<i>Section 5.5.3: Dispersion of I.34TCN (untreated and plasma treated) in PA12</i> .....	101
<i>Section 5.5.4: Mechanical properties</i> .....	103
Section 5.6: Conclusion .....	107
Section 5.7: References .....	108
Section 5.8: Appendix (Supplementary Information).....	114
<b>Chapter 6: Surface Modification of the Laser Sintering Standard Powder</b>	
<b>Polyamide 12 by Plasma Treatments</b> .....	<b>121</b>
Section 6.1: Abstract.....	121
Section 6.2: Introduction .....	121
Section 6.3: Materials and Experimental .....	124
<i>Section 6.3.1: Materials</i> .....	124
<i>Section 6.3.2: Plasma Treatment Technologies</i> .....	125
<i>Section 6.3.3: Sample Fabrication Methods</i> .....	126
Section 6.4: Characterisation and Testing.....	126
<i>Section 6.4.1: Morphology Investigations by SEM</i> .....	126
<i>Section 6.4.2: Wettability and density measurements</i> .....	127
<i>Section 6.4.3: Fourier Transform Infrared Spectroscopy (FTIR) and Hot Stage Microscopy (HSM)</i> .....	127
Section 6.5: Results and Discussion .....	128
<i>Section 6.5.1: Visual observation and chemical reactions description</i> .....	128
<i>Section 6.5.2: Surface morphology investigations by SEM</i> .....	130
<i>Section 6.5.3: Powder wettability and density results</i> .....	131
<i>Section 6.5.4: Chemical analysis using FTIR</i> .....	133
<i>Section 6.5.5: Pores formation in powder due to LP-PT (SEM and HSM analyses)</i> ..... .....	136
Section 6.6: Parts Fabricated from Plasma Treated.....	138

Section 6.7: Conclusion .....	142
Section 6.8: References.....	143
Section 6.9: Appendix (Supplementary Information) .....	147
<b>Chapter 7: Conclusions and Future work.....</b>	<b>151</b>
Section 7.1: Conclusions.....	151
Section 7.2: Future Work.....	152

## Table of Figures

<i>Figure 2-1</i> The ideal structural diagram of a montmorillonite clay , reproduced with permission from [44]. .....	15
<i>Figure 2-2</i> possible four types of dispersion of filler: Micro-aggregated (phase separated), fully intercalated, fully exfoliated and partially intercalated-exfoliated structures. The layer thickness and distance between layers are around 1 nm. ....	17
<i>Figure 2-3</i> DSC and HSM results of PA12 heating from 50 C to 250 C at rate of 10 C/min. shows melting, crystallization and processing window temperatures. ....	23
<i>Figure 2-4</i> One of my LS building attempts showing the polymer powder was failed to produce parts due to improper choice of parameters . ....	30
<i>Figure 3-1</i> (a) The chemical reaction of amide group, and (b) PA12 repeating unit linked together by amide group.....	46
<i>Figure 3-2</i> SEM micrograph of PA12 powder (a) and (b) high magnification SEM image of single PA12 particle covered by TiO <sub>2</sub> nanoparticles. Reproduced from [4] under a CC BY 4.0 license. ....	47
<i>Figure 3-3</i> A schematic diagram shows the LP-PT procedure. Reproduced from [4] under a CC BY 4.0 license. ....	49
<i>Figure 3-4</i> (a) A photo was taken to the LP-PT vacuum chamber where the glow discharge plasma was produced. (b) A schematic shows the dissociation of oxygen molecules to re-active species, atoms, radicals, ions and electrons.....	50
<i>Figure 3-5</i> Table shows parameters of the two different APPJ pen sources used in this project. Reproduced from [4] under a CC BY 4.0 license.....	51
<i>Figure 3-6</i> Illustration of the Downward Heat Sintering (DHS) using the hot press. ....	54
<i>Figure 3-7</i> Panels (a-d) are the pictures of the LS equipment, powder container, sintered powder, and fabricated parts respectively. ....	55

**Figure 4-1:** Melting temperature for PA12 and its composites measured by DSC showing no significant changes between peaks especially if the standard deviation mentioned in the text was considered. Inset (a) is a SEM image of a cross-section of a untreated composite tensile test sample with non-melted particles; sample was made with temperature suitable for neat PA12. Inset (b) unsuccessful LS attempt for printing untreated composite at neat PA powder bed temperature. Inset (c) successful LS attempted for treated composite at DHS adjusted powder bed temperature. .... 69

**Figure 4-2:** HSM results for PA12 and its composites under different temperatures (Neat PA12 at temperatures (a) 185 °C, (b) 190 °C, and (c) 192 °C, 3% untreated C30B/PA12 at temperatures (d) 192 °C, (e) 195 °C, and (f) 200 °C, and 3% treated C30B/PA12 at temperatures (g) 190 °C, (h) 192 °C, and (i) 195 °C)..... 70

**Figure 4-3:** Influence of plasma treatment on the nanoclay using different characterization tests; (a) FTIR spectra and (b) XRD patterns, SEM images (inset i and ii) and TGA results (inset iii). .... 72

**Figure 4-4:** SEM images of 3%untreated C30B/PA12 mixed powders (a) and 3%treated/PA12 mixed powders (b)..... 74

**Figure 4-5:** Tensile test curves of PA12 and 3% C30B composites (treated and untreated). Each curve is almost the best in tensile strength..... 75

**Figure 4-6:** Tensile test curves of PA12 and 5% C30B composites (treated and untreated). Each curve is almost the best in tensile strength..... 75

**Figure 4-7:** The elongation at break values of treated and untreated composites, and the SEM image of 3%treated C30B composite showing features of ductile fracture (Inset (i)). ..... 77

**Figure 4-8** Low magnification SEM images of the fracture surface of untreated 3% C30B composite in which more brittle fracture was occurred with no clear deformation before fracture (a) and 3% treated C30B composite indicating the sample was plastically deformed before fracture (b). ..... 79

**Figure 5-1** Micrographs of the nanoclays before (as received) and after plasma treatment (a) untreated C30B which are reproduced from [30] under CC-BY-4, (b) treated C30B, (c) untreated I.34TCN, and (d) treated I.34TCN. Arrows in (c) refer to the large, round untreated particles, whereas in (d) they refer to particles were broken in to smaller particles during plasma treatment. .... 93

**Figure 5-2** FTIR spectra of untreated and plasma treated nanoclays (a) C30B, (b) I.34TCN; Pressed discs of the untreated and treated I.34TCN powders pictured in inset (i) shows a clear change in colour after air plasma. .... 94

**Figure 5-3** FTIR spectra of untreated and treated nanoclays (a-c) C30B and (d-f) I.34TCN.... 96

**Figure 5-4** TGA thermograms of untreated and plasma treated nanoclays (a) C30B, (b) I.34TCN. Inset Tables (i) and (ii) are the decomposition temperatures of untreated and plasma treated C30B and I.34TCN. .... 97

**Figure 5-5** Different shaped-LS samples (a) Neat PA12, (b) 3% untreated I.34TCN composite and (c) 3% plasma treated I.34TCN composite ..... 99

**Figure 5-6** Cross-sectional SEM images of the LS specimen (a-b) neat PA12, (c-d) untreated I.34TCN composite (e-f) treated I.34TCN composite. Images on the left display the top left region of the composites whilst the images on the right are of the middle regions. The white arrows highlight cracks and pores. PA12 fractures (a-b) are more ductile but more porous, while Figures (c-f) from the composite materials are more brittle fractures. .... 100

**Figure 5-7** High resolution low voltage SEM imaging of fractured surfaces of a) PA12, b) untreated I.34TCN composite, and c) treated I.34TCN composite on the micron scale and d) PA12, e) untreated I.34TCN composite, and f) treated I.34TCN composite on the nanoscale. 103

**Figure 5-8** Ultimate stress results obtained from PA12, untreated I.34TCN and treated I.34TCN composites at three different laser powers: 13, 17, and 21W. .... 105

**Figure 5-9** Ultimate strain results obtained from PA12, untreated I.34TCN composite and treated I.34TCN composite at three different laser powers: 13, 17, and 21W. .... 106

<b>Figure 5-10</b> Elastic modulus results obtained from PA12, untreated I.34TCN composite and treated I.34TCN composite at three different laser power: 13, 17, and 21W. ....	107
<b>Figure 6-1</b> (a) A photograph of nontreated PA12, 1 hour and 2 hour treated PA12 reveals that the PA12 colour change with the plasma treatment. (b) Cold pressed discs of nontreated and 1 hour treated PA12 show the treated pellet has a uniform coloured surface after 1 hour LP-PT exposure. (c) Schemes of the chemical reactions resulting from plasma exposure. ....	129
<b>Figure 6-2</b> SEM micrographs of the PA12 particles surfaces (a) without LP-PT plasma treatment, (b) 1hr LP-PT plasma treated PA12 (porosity examples marked with circle and arrows) .....	130
<b>Figure 6-3</b> Photographs of PA12 powders (untreated and 1 hour treated LP-PT) immersed and stirred in water (untreated is white and treated is darker): (a) before stirring, (b) 1 minute (c) 72 hours after stirring respectively. ....	132
<b>Figure 6-4</b> FTIR spectra of nontreated PA12 and 1 hr, 2hr, and 3hr LP-PT treated PA12 powder. ....	133
<b>Figure 6-5</b> High magnification SEM images of (a) PA12 without LP-PT plasma treatment (b) 1hr LP-PT treated PA12, (c) 2hr LP-PT treated PA12, and (d) 3hr LP-PT treated PA12. ....	137
<b>Figure 6-6</b> (a) HSM image of PA12 particles taken during crystallisation from melting. (b) High magnification SEM micrograph of 3hr LP-PT treated PA12 particle revealing holes on surface where the amorphous component has been removed (highlighted by the green circle ) .....	138
<b>Figure 6-7</b> (a) Top surface and cross section of the nontreated PA12 part, (b) Top surface and cross section of 1 hr treated PA12 part, (c) Cross section of the 2hr treated PA12 part and (d) Cross section of LS PA12 part sample ( green circle highlight unmelted powder). ....	140
<b>Figure 6-8</b> SEM Micrographs of PA12 subjected to K-APJ at a duration of (a-b) 1minute. And (c-d) 3 minutes.e-f) PA12 powder particles subjected to H-APJ of 6 minutes.....	141

## Table of Figures in the Appendices

<i>Figure S5-1(a) LS specimen design and build layout oriented parallel to the xy-plane, (b) Tensile test and laser extensometer setup, (c) standard dimensions (in mm) of a single tensile test specimen according to the ASTM D638-02A, and (d) A diagram represents the fracture area after tensile testing, showing the SEM scanned areas, Area 1 and Area 2 in Figure 5-6. ....</i>	<i>115</i>
<i>Figure S5-2 HSM images of (a) Untreated PA12/I.34TCN composite (b) Plasma treated PA12/I.34TCN composite. ....</i>	<i>115</i>
<i>Figure S5-3 Cross section of the LS specimens of the untreated I.34TCN composite (a) and treated I.34TCN composite (b). Examples of aggregated untreated clay particles in (a) and smaller size of treated clay particles in (b) are highlighted with green circles. Yellow and blue arrows in (a) and (b) are found to highlight rough and smooth areas respectively. ....</i>	<i>116</i>
<i>Figure S5-4 SEM micrograph of the PA12 cross section shows the presence of TiO<sub>2</sub> nanoparticles (a), 3D surface plot of the PA12 surface displays the distribution of the TiO<sub>2</sub> nanoparticles (b), TiO<sub>2</sub> particle size statistics using ImageJ shows the range of the particles size and (c). The presence of TiO<sub>2</sub> can be evidenced by the intense peaks in ImageJ 3D surface plot shown in (b). Histogram of the TiO<sub>2</sub> particles shows a range of the particle sizes (c) but about 80% of these particles has a full circularity as shown in circularity (d). More explanation about the effect of plasma on the distribution of TiO<sub>2</sub> nanoparticles on PA12 particles is found in Chapter 6.....</i>	<i>117</i>
<i>Figure S5-5 Panels a-d are the large-scale SEM images of Figure 5-7b, Figure 5-7e, Figure 5-7d and Figure 5-7f respectively in the main document. ....</i>	<i>118</i>
<i>Figure S5-6 SEM micrographs of untreated I.34TCN composite surface at different magnifications (a) low magnification image (b) high magnification image, and (i) nanoscale image shows the aggregation of untreated clay. ....</i>	<i>119</i>
<i>Figure S5-7 SEM micrographs shows a large aggregated untreated I.34TCN on PA12 surface. ....</i>	<i>119</i>



<b>Figure S6-1</b> SEM micrograph of PA12 powder (a) and (b) high magnification SEM image of single PA12 particle covered by TiO <sub>2</sub> nanoparticles. ....	147
<b>Figure S6-2</b> A schematic diagram shows the LP-PT procedure .....	148
<b>Figure S6-3</b> Table shows parameters of the two different plasma pen sources used in this work. ....	148
<b>Figure S6-4</b> A photo taken immediately after spread the untreated (white) and 1 hour treated (darker) over the top of water in petri dishes. ....	148
<b>Figure S6-5</b> Photos were taken to the nontreated and LP-PT treated PA12 powder after stirred in water (a) 1min, (b) 1hr, (c) 2hr, (d) 3hr, (e) 4hr, (f) 6hr, (g) 24hr, and (h) 72hr.....	149
<b>Figure S6-6</b> Entire FTIR spectra of untreated PA12 and 1 hr, 2hr, and 3hr LP-PT treated PA12 powder.....	149
<b>Figure S6-7</b> SEM micrograph of 2 hour LP-PT treated PA12 powder.....	149
<b>Figure S6-8</b> SEM Micrographs of PA12 powder a) Untreated b) LP-PT for 6 minutes c) H-APJ for 6 minutes.....	150

## List of Tables

<b>Table 2-1</b> Polymer Nanocomposites Applications.....	10
<b>Table 3-1</b> Surfactants information and specification (according to the suppliers' technical sheets and Ref. [6], [10]). .....	48
<b>Table 3-2</b> Laser and Heat Sintering processes parameters. ....	52
<b>Table 4-1:</b> Summary of results from previous studies on PA12 and PA12/nanoclay composites (brackets relative values with regards to neat PA12.....	64
<b>Table 4-2</b> Technical specifications of DHS.....	66
<b>Table 4-3:</b> Summary of the tensile test results of PA12 and composites (3% and 5% treated and untreated C30B). .....	76
<b>Table 5-1</b> Surfactants information and specification (according to the suppliers' technical sheets and Ref. [32], [36]). .....	87
<b>Table 5-2</b> Laser and Heat Sintering processes parameters .....	88
<b>Table 6-1</b> Change percentage of density of PA 12 powder with the time of treatment. ....	132
<b>Table 6-2</b> Major FTIR absorption bands and their assignments of PA12. ....	134
<b>Table 6-3</b> FTIR absorption bands of PA12. ....	135

## **Publications**

### **Published**

[1] Alaa Almansoori, Robert Masters, Kerry Abrams, Jan Schäfer, Torsten Gerling, Candice Majewski, Cornelia Rodenburg, *Surface modification of the laser sintering standard powder polyamide 12 by plasma treatments*, **Plasma Processes and Polymers** Volume 15, Issue 7, 1800032, (2018).

[2] Alaa Almansoori, Robert Masters, Kerry Abrams, Jan Schäfer, Torsten Gerling, Candice Majewski, Cornelia Rodenburg, *Cover Picture*, **Plasma Processes and Polymers**, Volume 15, Issue 7, 1870015, (2018).

[3] Alaa Almansoori, Candice Majewski, Cornelia Rodenburg, *Nanoclay/Polymer Composite Powders for Use in Laser Sintering Applications: Effects of Nanoclay Plasma Treatment*, **JOM** Volume 69, Issue 11, pp 2278–2285 (2017).

[4] Alaa Almansoori, Ryan Seabright, Candice Majewski, Cornelia Rodenburg, *Feasibility of Plasma Treated Clay in Clay/Polymer Nanocomposites Powders for use Laser Sintering (LS)*, **IOP Conference Series: Materials Science and Engineering**, Volume 195, conference 1, (2017).

### **Submitted**

[1] Alaa Almansoori, Kerry Abrams, Ammar Al-Rubaye, Candice Majewski, Cornelia Rodenburg, *Novel Plasma Treatment for Preparation of Laser Sintered Nanocomposite parts*, **Additive Manufacturing (Elsevier)**.

## **Conferences and Meetings**

### **Oral Presentations**

(1) NANOSTRUC 2016: The 3<sup>rd</sup> International Conference on Structural Nano Composites, 12–15 September 2016, Aberdeen, United Kingdom.

(2) ANM 2017: 9<sup>th</sup> International conference on Advanced Nanomaterials, 19-21 July 2017, Aveiro, Portugal.

(3) APM 2017: 1<sup>st</sup> International conferencme on Advanced Polymer Materials and Nanocomposites, 19-21 July 2017, Aveiro, Portugal.

(4) MAPP First International Conference, 30-31 January 2018, Sheffield, United Kingdom.

(5) CMG-RiP Meeting 2018: Clay Minerals Group Research in Progress Meeting, 27<sup>th</sup> June 2018, Sheffield, United Kingdom.

### **Poster Presentations**

(1) USES 2015: University of Sheffield Engineering Symposium (USES), 24<sup>th</sup> Jun 2015, University of Sheffield, Sheffield, United Kingdom.

(2) Electron Microscopy Characterisation of Organic-Inorganic Interfaces, 22<sup>nd</sup> Feb 2016, University of Queen Mary, London, United Kingdom.

(3) MRE 2018: Materials Research Exchange, 12-13 March 2018, London, United Kingdom.

# Chapter 1: Introduction

## Section 1.1: Background

Laser Sintering (LS) is a well-known Additive Manufacturing process, capable of producing highly complex geometries with little or no cost penalty. The demand for materials that can be used efficiently in Laser Sintering applications have raised interest in polymer-matrix nanocomposites. LS has emerged as a promising technology in a large number of applications because it has achieved the production of highest precision and accuracy on 3D complex products [1], [2]. Polymer matrices have desirable properties, in these applications, such as light weight, and low cost, [3], but their mechanical properties are limited compared to metals. Moreover, limited selection of polymers, component surface quality and performance consistency may also limit the LS applications [4]–[6]. For expanding the LS applications or to enhance the existing properties of the LS materials, researchers have focused on changing the LS parameters and investigating new materials, or a combination of these options [4], [5], [7]–[11]. Whereas surface modification based on plasma treatment has not been considered for LS applications. Plasma treatment can be used efficiently to modify either polymer matrices or filler materials for LS nanocomposites. For example, polymer surfaces can be modified to alter their surface properties for example adhesion, wettability and biocompatibility [12]–[14]. However, plasma treatment to date has been mostly used to modify solid materials and thin films, whereas powders remain much less explored. Polymer powders can be modified as well as solids and similar results to that of solids can also be obtained such as adhesion and wettability. However, polymers, particularly powders, are sensitive to rising temperature (as expected during plasma treatment) and respond quickly to the plasma action, therefore using the right plasma technique and parameters is essential to ensure the desired modification. Therefore, two plasma treatment techniques were

explored in the current study: low pressure plasma treatment and atmospheric pressure plasma jets. The most suitable plasma treatment source, parameters, conditions, process gases could vary the intended application of the LS products. For example, plasma treatment could produce materials for applications require high porosity, or wettability properties. It was suggested, as a result, the production of LS components from plasma treated powders could be the next generation of materials and applications produced by a combination of two different technologies: plasma treatment and LS.

Another unexplored application of plasma treatment is the surface modification of the nanomaterials, and more specifically nanoclays. Nanoclays are frequently used as a reinforcement, to enhance the thermo-mechanical properties of polymers [15]. However, the incompatibility between the organic polymers and mineral clays can restrict the strength of reinforcement. Hence, organic modifiers are commonly used to render nanoclay miscible with polymer [16]. To a certain extent, organo-treated nanoclays have increased the mechanical properties of polymers in the conventional manufacturing methods such as melt compounding [17]. However, when laser sintering was used, weak interaction between clays and matrices and the agglomeration of clay has reduced the strength and the elongation at break especially when mechanical mixing is employed [18]. Therefore, plasma treatment could have the potential to reduce the nanoclay agglomeration and enhance its dispersion polymer matrix. The plasma treatment of nanoclay has not been widely used [19], [20]; moreover, studies on using plasma treatment to prepare polymers nanocomposites are very rare [21], [22]. Thus, it is a crucial study to treat nanoclays using plasma treatment to increase the surface area of nanoclay particles and facilitate the dispersion of nanoclay in this LS technique.

## **Section 1.2:Aims and objectives**

The main aim of this study was to explore new areas of plasma treatment applications to enhance Laser Sintering polymer nanocomposites. This study, therefore, presents new methods to improve the dispersion of filler inside the LS polymer powder in one hand and to treat powders used for laser sintering in another hand. These aims are further explained in the next three points:

### **(I) Plasma treatment of nanoclay for replication of the LS process**

The first part of section (I) aimed to investigate the feasibility of using plasma treated nanoclay to reinforce LS polymers with an expectation of reducing nanoclay agglomerations and enhancing properties. The current approach has been started initially with Cloisite 30B nanoclay as a filler and polyamide 12 as a matrix for this part of study. In order to save time and cost through using the minimum amount of powder, a new simple casting method to mirror the idea of LS technique was suggested for initial trials. Thus, the second aim of this section was to replicate the laser sintering process; work will be presented on the development of a Downward Heat Sintering (DHS) process, carried out in a hot press, to fabricate tensile test specimens from the composite powders (plasma treated and untreated nanoclays). This section is the topic of *Chapter 4: Nanoclay/Polymer Composite Powders for use in Laser Sintering Applications: Effects of Nanoclay Plasma Treatment*

### **(II) Plasma treatment of nanoclay for LS applications**

Exploring new fields of plasma treatment in polymer nanocomposites continues in this section, but using the LS technique. This part of the thesis exploits the potential of plasma treatment to address the poor dispersion of the nanoclay into the LS polymer matrix. This novel method, therefore, aims to overcome the LS challenges: lower properties, performance consistency, and surface quality, which is caused by the limited selection of

LS materials or by the poor interaction between the nanoclay and the polymer. The composite materials of PA12 and nanoclay (Nanomer I.34TCN) were prepared for Laser Sintering method follow the heat sintering process described in previous section. This section is the topic of *Chapter 5: Novel Plasma Treatment for Preparation of Laser Sintered Nanocomposite Parts*

(III) Plasma treatment for surface modification of LS polymer powders

This chapter is part of a series of works linking plasma treatment and its advantages on laser sintering materials. However, standard LS polymer powder was modified, here, using three different plasma treatment techniques for applications which require high hydrophilicity. This is a comparable study suggested these techniques to ensure the advantages of plasma treatment are fully exploited. This part of the study also benefited from the advantages of DHS as a casting method to mirror the technology of laser sintering on smaller PA12 powder quantities. This section is the topic *Chapter 6: Surface Modification of the Laser Sintering Standard Powder Polyamide 12 by Plasma Treatments.*

### **Section 1.3:Thesis structure**

This is an alternative format thesis (approved by the supervisors and Faculty of Engineering in University of Sheffield) contains chapters (Chapter 4 and 6) were published in peer-reviewed journals or submitted (Chapter 5) as stated in thesis structure shown below:

#### ***Section 1.3.1: Thesis chapters:***

**Chapter 1: Introduction**

**Chapter 3: Literature Review**

**Chapter 2: Background and Experimental Works**

**Chapter 4: Published Paper**



## ***Nanoclay/Polymer Composite Powders for use in Laser Sintering Applications: Effects of Nanoclay Plasma Treatment***

*This chapter was published in:*

- ***JOM, Volume 69, Issue 11, pp 2278–2285, (2017);***
- ***Alaa Almansoori<sup>a, b</sup>, Candice Majewski<sup>c</sup>, and Cornelia Rodenburg<sup>a</sup>***

<sup>a</sup> *Department of Material Science and Engineering, University of Sheffield, UK*

<sup>b</sup> *Southern Technical University, Basra, Iraq*

<sup>c</sup> *Department of Mechanical Engineering, University of Sheffield, UK*

**DOI:** [doi.org/10.1007/s11837-017-2408-5](https://doi.org/10.1007/s11837-017-2408-5)

## **Chapter 5: Submitted Paper**

### ***Novel Plasma Treatment for Preparation of Laser Sintered Nanocomposite parts***

*This chapter is submitted to:*

***Additive Manufacturing Journal (Elsevier)***

***Alaa Almansoori<sup>a, b</sup>, Kerry J Abrams<sup>a</sup>, Ammar D. Ghali Al-Rubaye<sup>c, d</sup>, Candice Majewski<sup>c</sup>, and Cornelia Rodenburg<sup>a</sup>***

<sup>a</sup> *Department of Material Science and Engineering, University of Sheffield, UK*

<sup>b</sup> *Southern Technical University, Basra, Iraq*

<sup>c</sup> *Department of Mechanical Engineering, University of Sheffield, UK*

<sup>d</sup> *College of Engineering, University of Wasit, Wasit, Iraq*

## **Chapter 6: Published Paper**

### ***Surface Modification of the Laser Sintering Standard Powder Polyamide 12 by Plasma Treatments***

*This chapter was published in:*

***Plasma Processes and Polymers (PPaP), Volume 15, Issue 7, 20180032, (2018)***

***Alaa Almansoori<sup>a, b</sup>, Robert Masters<sup>a</sup>, Kerry Abrams<sup>a</sup>, Jan Schäfer<sup>c</sup>, Torsten Gerling<sup>c</sup>, Candice Majewski<sup>d</sup>, and Cornelia Rodenburg<sup>a</sup>***

<sup>a</sup> *Department of Material Science and Engineering, University of Sheffield, UK*

<sup>b</sup> *Southern Technical University, Basra, Iraq*

<sup>c</sup> *Leibniz Institute for Plasma Science and Technology, Felix-Hausdorff-Straße 2, 17489 Greifswald, Germany*

<sup>d</sup> *Department of Mechanical Engineering, University of Sheffield, UK*

**DOI:** [doi.org/10.1002/ppap.201800032](https://doi.org/10.1002/ppap.201800032)

## **Chapter 7: Conclusions and Future Work**

### ***Section 1.3.2: Published and submitted papers***

For all published chapters, the submitted manuscript text has been amended by comments and suggestions by the journal's reviewers and by comments of the examiners of the thesis. Supplementary information has been incorporated into the chapter, and figure and table listing adopted for continuity of the thesis. The text is therefore only approximately identical to the journal manuscript.

I was the lead author of these papers and I carried out the majority of the work within, including powder and bulk samples preparation, fabrication of laser sintered parts, materials characterisation (XRD, FTIR, DSC, TGA, and HSM), and imaging using Nova SEM and all tensile tests and density measurements. I performed all the analyses of the tests and experiments. I developed a method to investigate the polymer powder wettability and also developed the DHS method to replicate the LS process.

Plasma treatment used in **Chapter 4**, and **Chapter 5** is only the Low Pressure Plasma Treatment LP-PT (Plasma Cleaner Zepto from Diener Electronic). Therefore, in these chapters plasma treated and untreated were used.

In **Chapter 6**, three different plasma treatment techniques were used, therefore I used the abbreviation LP-PT to differentiate between the Low Pressure Air Plasma Treatment and the other plasma treatment techniques, i.e.: KinPen plasma jet (K-APJ) and Hairline plasma jet (H-APJ).

Articles: [doi.org/10.1007/s11837-017-2408-5](https://doi.org/10.1007/s11837-017-2408-5) and [doi.org/10.1002/ppap.201800032](https://doi.org/10.1002/ppap.201800032), in their entirety, including all figures and tables, are reproduced here under a CC-BY 4.0 license: <http://creativecommons.org/licenses/by/4.0>.

### **Section 1.4:References**

[1] G. M. Vasquez, C. E. Majewski, B. Haworth, and N. Hopkinson, "A targeted

- material selection process for polymers in laser sintering,” *Addit. Manuf.*, vol. 1, pp. 127–138, 2014.
- [2] D. L. Bourell, T. J. Watt, D. K. Leigh, and B. Fulcher, “Performance limitations in polymer laser sintering,” *Phys. Procedia*, vol. 56, no. C, pp. 147–156, 2014.
- [3] K. Müller *et al.*, “Review on the Processing and Properties of Polymer Nanocomposites and Nanocoatings and Their Applications in the Packaging, Automotive and Solar Energy Fields,” *Nanomaterials*, vol. 7, no. 4, p. 74, 2017.
- [4] S. Berretta, O. Ghita, and K. E. Evans, “Morphology of polymeric powders in Laser Sintering (LS): From Polyamide to new PEEK powders,” *Eur. Polym. J.*, vol. 59, pp. 218–229, 2014.
- [5] A. Wegner, “New polymer materials for the laser sintering process: Polypropylene and others,” *Phys. Procedia*, vol. 83, pp. 1003–1012, 2016.
- [6] H. Zarringhalam, C. Majewski, and N. Hopkinson, “Degree of particle melt in Nylon-12 selective laser-sintered parts,” *Rapid Prototyp. J.*, vol. 15, no. 2, pp. 126–132, 2009.
- [7] B. Caulfield, P. E. McHugh, and S. Lohfeld, “Dependence of mechanical properties of polyamide components on build parameters in the SLS process,” *J. Mater. Process. Technol.*, vol. 182, no. 1–3, pp. 477–488, 2007.
- [8] L. Verbelen, S. Dadbakhsh, M. Van Den Eynde, J. P. Kruth, B. Goderis, and P. Van Puyvelde, “Characterization of polyamide powders for determination of laser sintering processability,” *Eur. Polym. J.*, vol. 75, pp. 163–174, 2016.
- [9] B. Chen, S. Berretta, K. Evans, K. Smith, and O. Ghita, “A primary study into graphene/polyether ether ketone (PEEK) nanocomposite for laser sintering,” *Appl. Surf. Sci.*, vol. 428, pp. 1018–1028, 2018.
- [10] Y. Khalil, A. Kowalski, and N. Hopkinson, “Influence of laser power on tensile properties and material characteristics of laser-sintered UHMWPE,” *Manuf. Rev.*, vol. 3, p. 15, 2016.
- [11] R. D. Goodridge *et al.*, “Processing of a Polyamide-12/carbon nanofibre composite by laser sintering,” *Polym. Test.*, vol. 30, no. 1, pp. 94–100, 2011.
- [12] J. Hnilica, L. Potočňáková, M. Stupavská, and V. Kudrle, “Rapid surface treatment of polyamide 12 by microwave plasma jet,” *Appl. Surf. Sci.*, vol. 288, pp. 251–257, 2014.
- [13] J. Hanusová, D. Kováčik, M. Stupavská, M. Černák, and I. Novák, “Atmospheric pressure plasma treatment of polyamide-12 foils,” *Open Chem.*, vol. 13, no. 1, pp. 382–388, 2015.
- [14] A. Dupuis *et al.*, “Improving adhesion of powder coating on PEEK composite: Influence of atmospheric plasma parameters,” *Appl. Surf. Sci.*, vol. 357, pp. 1196–1204, 2015.
- [15] S. Pavlidou and C. D. Papaspyrides, “A review on polymer-layered silicate nanocomposites,” *Prog. Polym. Sci.*, vol. 33, no. 12, pp. 1119–1198, 2008.

- [16] S. S. Bhattacharya and A. Mandot, "Polyamide / Clay Nanocomposites Film , Synthesis and Mechanical Testing," *Int. J. Pure Appl. Sci. Technol.*, vol. 17, no. 2, pp. 36–44, 2013.
- [17] I. Y. Phang *et al.*, "Morphology, thermal and mechanical properties of nylon 12/organoclay nanocomposites prepared by melt compounding," *Polym. Int.*, vol. 54, no. 2, pp. 456–464, 2005.
- [18] P. K. Jain, P. M. Pandey, and P. V. M. Rao, "Selective laser sintering of clay-reinforced polyamide," *Polym. Compos.*, vol. 31, no. 4, pp. 732–743, 2010.
- [19] K. Fatyeyeva and F. Poncin-Epaillard, "Sulfur dioxide Plasma Treatment of the Clay (Laponite) Particles," *Plasma Chem. Plasma Process.*, vol. 31, no. 3, pp. 449–464, Jun. 2011.
- [20] A. T. Djowe, S. Laminsi, D. Njopwouo, E. Acayanka, and E. M. Gaigneaux, "Surface Modification of Smectite Clay Induced by Non-thermal Gliding Arc Plasma at Atmospheric Pressure," *Plasma Chem. Plasma Process.*, vol. 33, no. 4, pp. 707–723, Aug. 2013.
- [21] R. Scaffaro and A. Maio, "Enhancing the mechanical performance of polymer based nanocomposites by plasma-modification of nanoparticles," *Polym. Test.*, vol. 31, no. 7, pp. 889–894, 2012.
- [22] M. H. Shamsi, M. Luqman, F. Basarir, J. S. Kim, T. H. Yoon, and K. E. Geckeler, "Plasma-modified halloysite nanocomposites: Effect of plasma modification on the structure and dynamic mechanical properties of halloysite-polystyrene nanocomposites," *Polym. Int.*, vol. 59, no. 11, pp. 1492–1498, 2010.

## **Chapter 2: Literature Review**

### **Section 2.1:Background**

Three main aspects covered in this chapter are: polymer nanocomposites, laser sintering, and plasma treatments. The first section focuses mainly on nanoclay/polymer composites discussing the nanoclay dispersion benefits, challenges and its influence on polymer matrix properties. Then, laser sintering is the second main part of this chapter, and will outline the laser sintering process, materials, advantages and challenges. Previous studies, made to widen the range of materials for laser sintering, are reviewed in this section. The final part of this chapter deals with the plasma treatments of polymers and nanomaterials, particularly focusing on laser sintering materials. A summary of the previous literature is given at the end of this chapter to emphasise the importance and novelty of the current study.

### **Section 2.2:Nanocomposites**

Nanocomposites are multiphase materials fabricated from two or more materials at least one material has one or more nanoscale dimensions (less than 100 nm). They are highly heterogeneous mixture of organic and nonorganic materials; therefore, they can exhibit significantly improved properties such as mechanical, optical, thermal, barrier and flammability properties [1]–[8]. These studies are only few examples of research and review articles which are continuously published every year in the literature. Nanocomposites major materials named as matrix, reinforced with nano-sized materials at different loadings which vary from 3% or less to 30% or more. The most frequently used nanocomposite systems are: Metal Matrix Nanocomposites; Ceramic Matrix Nanocomposites and Polymer Matrix Nanocomposites [9], [10]. Even though, ceramic and metal nanocomposites have been manufactured commercially for different applications [11]–[13], polymer nanocomposites have also emerged as an essential

material and a substitute material to these expensive materials in an endless list of applications [8]. Some examples of the polymer nanocomposites are listed in **Table 2-1**. For example, using of light-weight polymer nanocomposites in automotive applications have the potential to reduce fuel consumption and emissions. Also, design of polymer composites is more flexible and ease to produce in different colours and shapes. Here, we only focus on polymer nanocomposites used for laser sintering applications.

**Table 2-1** Polymer Nanocomposites Applications

<i>Fillers</i>	<i>Properties</i>	<i>Synthesis and fabrication</i>	<i>Applications</i>	<i>References</i>
Carbon Nanotube sponges	Mechanical properties	Infiltration-Curing process	Aerospace	[1]
Carbon Nanotube	Conductivity	Spin-coating	Solar energy applications	[4]
Nanoclay	Mechanical Properties	3D Bio-printing	Biomedical	[14]
Montmorillonite	Permeability properties	in situ emulsion polymerization	Coating Applications	[15]
Nanoclay	Flame retardancy	Solution-participation	Flame retardants	[16]
TiO <sub>2</sub>	Mechanical Properties	Suspension and bulk polymerization free-radical techniques	Dental composites and bone cements	[17]
Gold nanoparticles	Electrochemical activity	Chemically synthesized gold polypyrrole.	Biosensor	[18]

### **Section 2.2.1: Polymer nanocomposites**

Polymers as matrices have preferential properties in industry such as low melting temperature, light weight, and ease of manufacturing [19], and thus, polymers, now, have an important role in a wide variety of applications in transportation, medical and communications. However, polymers alone do not satisfy all the requirements of these applications because polymer in nature has low thermal and electricity conductivity, and

low strength and thermal stability. An efficient way to improve polymer properties is by using nanofiller-reinforced polymer composites [20]. Despite the field of polymer nanocomposites progressing in the last few decades, the current preparation methods for making nanocomposites still need to be further developed to achieve enhancement in nanocomposite properties and cost saving. The major challenge to obtain the potential benefits of the polymer reinforcement is the dispersion of the fillers (e.g. carbon nanotube or clay) in a polymer matrix [5], [21], [22].

### ***Section 2.2.2: Fillers***

#### *Section 2.2.2.1: Introduction to nanofillers*

Nanofillers are a relatively new class of materials in which at least one nano-sized dimension which could bring significant physical and chemical changes for polymeric materials. Nanofillers of various materials are categorised based on their functions, chemical nature, shape, orientation and so on. On the basis of their functionalities, nanofiller groups can be divided into, for example, conductive and nonconductive nanomaterials. In terms of their chemical nature, Nanofillers can also be classified into, organic and inorganic or natural and synthetic. These general classifications, in some cases, may not be very helpful because several classes of materials may fall into more than one of these classifications for example, nanocarbon tubes are organic and conductive. For most purposes, scientific name (e.g. multi-walled carbon nanotubes) or commercial name (e.g. Cloisite<sup>®</sup> 30B) of nanofillers are more acceptable. A wide range of nanofillers are used to reinforce polymers for different applications, but so far, a limited selection of reinforcing materials is only explored for LS applications. For these purposes, few types of inorganic layered silicates (nanoclays) [23]–[25], organic nanofillers- carbon containing materials (carbon nanofiber-CNF, carbon nanotube-CNT and carbon black-CB) [26], and metal oxides (nano- $\text{Al}_2\text{O}_3$  [27] or nano-silica [28]) have attracted much

interest than other nanofillers. Compared to the layered silicates, other reinforcements require additional preparation processes, for example, Melt mixing followed by grinding in a cryogenic milling process were used to prepare CNF composite [29]. Such these processes cause irregular powder morphology which is un-preferred for LS applications [30], [31]. Other studies have shown that CNT and CB composites, Salmoria et al [32] and Athreya et al [33] respectively, can be prepared via mechanical mixing process, but fails to avoid nanofiller aggregation. A study by Zhang et al [27] has shown that a polystyrene (PS) coating of Nano- $\text{Al}_2\text{O}_3$  by emulsion polymerisation for PS composites improved the nanofiller homogeneity, but it sacrificed the polymer binder. Similarly, nanosilica was coated with PA12 to reinforce PA12 using dissolution- precipitation process [28].

In summary, additional processes and extra materials are required to maintain the LS-favourable near-spherical powder morphology and achieve homogeneous nanofiller dispersion [34]. However, a patented method was developed by Jiaming Bai et al [34], [35] has shown that CNT/PA12 nanocomposites can be produced with enhanced mechanical properties and without any change in PA12 powder morphology. High cost of CNT and its negative impact on health and environment could be a disincentive for some of their potential uses [29], [36], [37]. Compared to CNT, Nanoclays including montmorillonite, halloysite, kaolin, and bentonite are safe and exhibited no toxicity [38], whilst organomodified nanoclays have higher degree of toxicity as performed by Alixandra Wagner [39]. However, a full examination of these materials at all stages of their life (manufacturing and end of their life stages) has not completed yet which is required to maintain their favourable properties for biomedical applications [39]. Notable results showed that the nanoclay byproducts have exhibited a loss in toxicity as a results of the degradation of the nanoclay organic modifier [39]. Therefore, any process like



plasma treatment could be useful for the bio-manufacturing if it causes a reduction in the organo-modifier of the nanoclays while maintaining favourable properties of nanoclay reinforcement properties. The preferential production of nanoclay composites is via mechanical mixing to maintain near-spherical powder morphology but the nanoclay particles aggregation is expected to occur which could weaken the mechanical properties of the LS parts [23]. Such as this process, however, is more favourable than any other process which could change the powder morphology such as the grinding of composite pellets causing irregular powder morphology. Generally, Nanoclays are available, much cheaper and environmentally friendly materials [40]–[42]. Uncertain toxic organic modifiers need further works to understand the physical and chemical properties which could affect the potential toxicity [39]. Hence, we have exclusively focused on the layered silicates nanoclays which will be explained and discussed in detail in the next section. Another health and safety issues with the combination of nanomaterials (e.g. nanoclays) with the LS powder contained in the LS building chamber

The large quantities of polymer nanocomposite powders contained in the LS building chamber during the LS process may raise the health and safety issues. However, up-to-date, there is no previous study in this field has considered these issues.

#### *Section 2.2.2.2: Layered silicate clay*

Layered silicates are named for regular stacks of aluminosilicates layers constructed in two different arrangements: Kaolinites and phyllosilicates. Kaolin clays (also called China clay) have layered structure as one tetrahedral layer linked to one Octahedral layer [1(T):1(O)] with a chemical formula of  $(Al_2Si_2O_5(OH)_5)$ . The Kaolinite's layers are tightly held together by hydrogen bonds, not expandable, and thus polymers are not able to intercalate between these minerals sheets. Therefore, these filling materials are used in materials, for which no intercalation is required but the appearance of the product is more

important such as ceramics, rubber, paints, and paper [43]. Whilst, phyllosilicates such as smectite and mica are built from 2:1 Tetrahedral-Octahedral structure. Micaceous, similar to Kaolinite, are not expandable but their interlayer bonding is relatively strong. In contrast, Smectite is the most appropriate group for intercalation process of polymers resulting from the interlayer weak van der Waals bonding and exchangeable ions [3]. Smectite mineral clays are either naturally occurring such as sodium montmorillonite ( $\text{Na}^+$  MMT), hectorite and saponite, or could be synthesised like laponite.  $\text{Na}^+$  MMT is still the most popular among the others due to its high surface area, high aspect ratio and availability. *Figure 2-1* illustrates structural diagram for ideal layered silicate Montmorillonite clay [44]. Furthermore, it is possible to hydrate interlayer cations in aqueous solution leading to an increasing in the gallery and facilitate the intercalation process [19]. MMT's particles with a platy structure are stuck together to form irregular macro to micron size powder agglomerations.

A challenge with using  $\text{Na}^+$  MMT as filler is the weak dispersion of the hydrophilic  $\text{Na}^+$  MMT in a hydrophobic polymer. To make better intercalation between these materials, the nano  $\text{Na}^+$  MMT has been modified organically in order to convert it from hydrophilic clay to organophilic clay by adding surfactants. Surfactants with Quaternary Ammonium Salts reduce the surface energy of the clay and increase the interlayer space making it generally compatible with hydrophobic polymers [5]. Clays after modification are called as organomodified (nano) clays or organoclays, but commercially they are produced under manufacturer's brands based on the chemical structure of the organic surfactant. For example, Southern Clay Products had produced several organo-nanoclays under the trade name Cloisite™ trade name (C), such as C15A, C20A and C30B. Nanocor® (wholly owned subsidiary of Minerals Technologies Inc.) has also produced nanoclays under Nanomer® trade name for instance, I.34TCN, I.24TL and I.30T. Studies have shown that

the organomodified nanoclays (e.g. Cloisites) have enhanced barrier [6], electrical [45], thermal [45] and mechanical [46] properties higher than the polymer matrices and nonmodified MMT/polymer composites. Nanoclays (organic-modified) C30B and I.34TCN are the project filling materials. I have begun to use C30B to create nanocomposite for LS applications but, afterward, the supplier of this nanoclay does not exist anymore and C30B is no longer available. Therefore, C30B was used for the DHS method, while the I.34TCN for the LS only as will be discussed in *Chapter Five*.

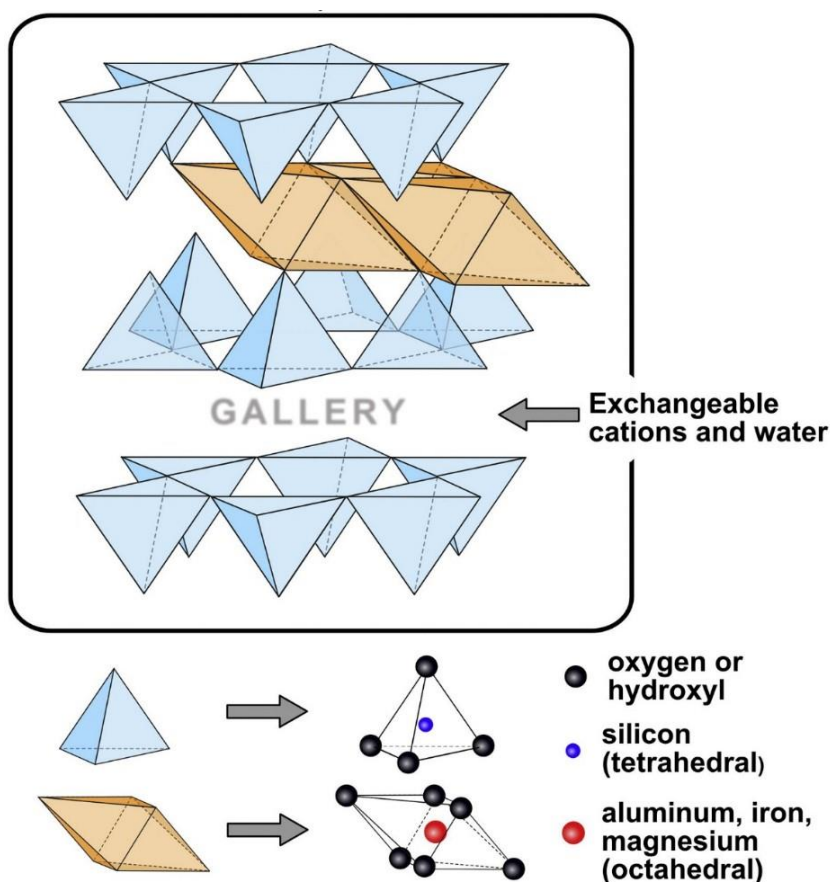


**Figure 2-1** The ideal structural diagram of a montmorillonite clay, reproduced with permission from [44].

### **Section 2.2.3: Nanoclay/polymer nanocomposites**

Nanoclays as filling materials have been proved remarkable reinforcement to polymers [6] which have been widely used commercially in different applications such as in automobile, air plane, and space parts because of the unique properties of the produced

parts compared to conventional macro and micro composites. Within the last decade many studies have been conducted in the nanocomposite field, but the first known work was presented by Toyota Research Centre in Japan in the early 1990s [47].

After that, Emmanuel P. Giannelis worked with his group in this area. Giannelis [48] reviewed and summarised their previous works on polymer layered silicates composites. They showed that polymer chains intercalate into the interlayer spaces (galleries) which resulted in an improved mechanical and thermal properties of polymer nanocomposites. They also found that, the quantity of the layered silicates fillers is far less compared to other fillers like mineral and glass-based fillers that is reduced the product overall weight. Finally, they reported commercial applications have already benefited from the light weight, enhanced properties, and low cost of using layered silicates nanocomposites, and more are still under development.

Since that then, many researchers have widely studied the field of polymer nanocomposite worldwide. The new manufacturing processes, computerised techniques, practical characterisation laboratories have greatly helped researchers and developers to work in agile and supportive environment. Over the past two decades, the dispersion of the nanoclay in polymers has attracted intense interest from these researchers and it plays an important role in the development of the polymer nanocomposites.

#### *Section 2.2.3.1: Dispersion of nanoclays*

There are two possible structures for nanoclay dispersion into polymers matrices: Immiscible and miscible structures. When the morphology of nanocomposites is immiscible, the nanoclay layers are stacked together with very bad adhesion between nanoclay and polymers leading to a phase-separated structure. The miscible formation of nanocomposites has three possible structures: fully intercalated, fully exfoliated and partially intercalated partially exfoliated. Intercalated nanoclay has a constant interlayer

space and the polymer molecules are inserted into the interlayer space, while in exfoliated from the nanoclay does not have a constant gallery instead the nanoclay layers are well dispersed into polymer matrix. Also, partial exfoliation and partial intercalation can occur. The four types of dispersion methods are shown in **Figure 2-2**. Using clay monolayers of nm-scale dimension as idealisation. Real clay layers, even for nanoparticles, will have multilayer thickness of 10s or 100s of nm.

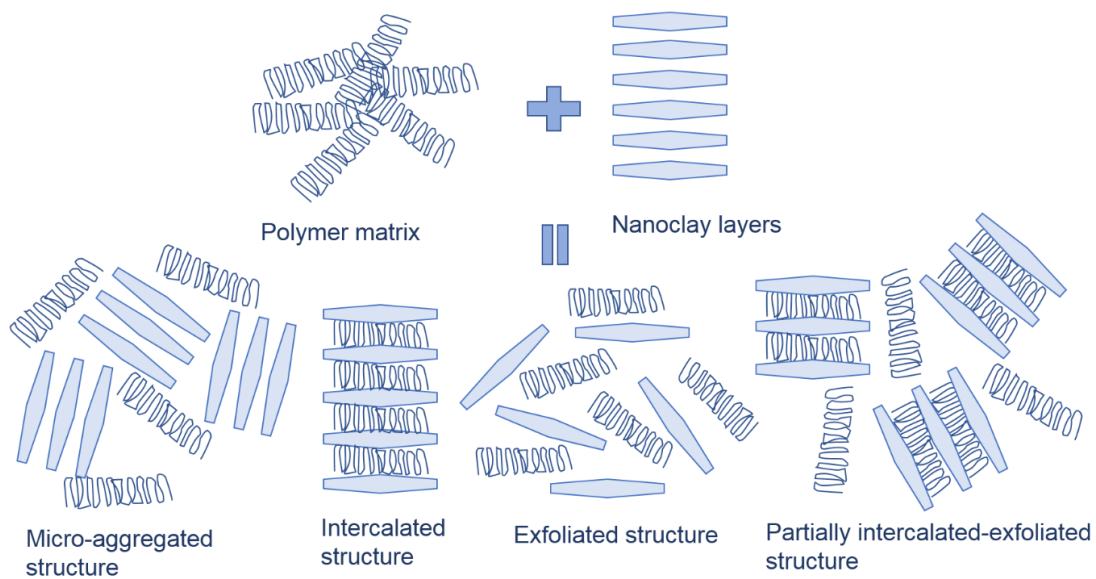


**Figure 2-2** possible four types of dispersion of filler: *Micro-aggregated (phase separated), fully intercalated, fully exfoliated and partially intercalated-exfoliated structures. The ideal layer thickness and distance between layers are 1-2 nm.*

#### Section 2.2.3.2: Preparation methods

Polymer nanocomposites are governed partially by the preparation processes; therefore, any development attempts start from the method of materials mixing.

Mainly, four preparation methods were and are still used intensively to prepare polymer nanocomposites including: mixing in solvent, mixing in polymerization, mixing in melting, and mixing by mechanical means.

**Mixing in solvent;** in this process, the polymer is dissolved in a solvent and the layered silicate clay is dispersed and exfoliated in the resultant solution. The polymer is

intercalated between layered silicates or the nanoclay layers were completely separated when the solvent is evaporated or precipitated. The compatibility between polymer and clay will control the resultant nanocomposite: intercalated or exfoliated [19]. Water as solvent can be used with water soluble polymers [19]. However, potential toxicity of solvents is an important issue especially if organic solvent is used [49].

**Mixing in polymerisation;** this method, so called “In situ polymerization”, was used to prepare polymer nanocomposites by Toyota Research group. This process, afterwards, is frequently used but with limitations such as the cost of environmental hazardous organic solvents. In situ polymerization, the layered silicates clay (modified or unmodified) is swollen in monomer solution and polymer intercalated into layer galleries. This process has been used to prepare either thermoset polymers for example Epoxy or thermoplastics like polyamide with modified or unmodified clay [19].

**Mixing in melting;** the layered silicate clay and polymer are mixed together through a molten state without any solvent. Thermoplastic polymer is preferred to be used in this method to produce intercalated or exfoliated nanocomposites through injection moulding [50] or extruders [51]. To produce a well-dispersed exfoliated nanocomposite, adding a compatibilizer is required [50], [51].

**Liquid mixing by mechanical means;** in this process the polymer and filler are mixing in liquid state. High speed magnetic stir bars are used to create the vortex effect and leading to well-dispersed composites as demonstrated by S. Zainuddin and coworkers [52]. However, in this process air bubbles may be created and leadsto increase the microvoids inside the resultant composite which should be avoided in LS applications.

**Dry mixing by mechanical means,** high speed dry mixer or stirrer followed by sonication is used to prepare LS nanocomposite materials. After the mechanical mixing,

powder morphology is not changed which raise the benefits of this process, the homogeneity of the nanoclay in polymer matrix using injection moulding [53] or LS [23] processes is a key issue.

Although, there is not perfect method to prepare nanocomposite, the last method, dry mixing, is much easier and not needing solvents or additives and no extra lengthy processes. In addition, some solvents are not eco-friendly such as diethyl ether and petroleum ether [54]; therefore environmental issues should be considered for those solvents. Furthermore, the mechanical properties of the LS polymer composites prepared by solution method was lower than the unfilled polymer [55].

#### *Section 2.2.3.3: Mechanical properties*

Enhancing the Mechanical properties of polymers is still a major challenge, although considerable research is being carried out every year since the first study was conducted by Toyota group in the early 1990s. Tensile test, flexural test, and hardness test have been used successfully to evaluate the improvement in mechanical properties, the tensile test is the most popular technique which has been used to evaluate the strength and stiffness of polymers nanocomposites. Polymer stiffness and strength are relatively low; therefore, adding nanofillers, most important nanoclays is a common option to improve these properties. However, the incorporation of nanoclays into polymers does not always increase the properties of the polymer matrix. The difference in polarity between polymers and nanoclays, preparation methods and nanoclay loading play an important role in improving the tensile test properties. For example, Byung-Wang Ju et al [46] proved that the mechanical and thermal properties of nanocomposites would be improved if the nanoclay was well dispersed into polymer matrix. They found that the use of organomodified Cloisite 30B and 25A in polymer nanocomposites exhibited better exfoliation than Na<sup>+</sup> MMT. The results showed Young Modulus of Na<sup>+</sup> MMT

nanocomposites was not increased compared to the pure polymer due to the poor dispersion of nanoclay in polymer matrix. Also, using more than 5% Cloisite 30B or 25A nanoclay led to the decrease the performance of nanocomposites because a lower degree of exfoliated clay was presented. Similar studies in literature have showed the reinforcement is discontinuous with higher loading percentage of fillers for instance nanoclay/epoxy nanocomposite [52] and carbon nanotube/epoxy nanocomposites [56].

#### *Section 2.2.3.4: Theoretical modelling*

Theoretical studies using analytical models coupled with experimental methods could make a qualitative description to predict the overall stiffness of the polymer nanocomposites. Analytical models: Mori-Tanaka and Halpin-Tsai are the most widely used micromechanical methods. The difference between those models is geometrical and physical [57]. The physical difference between those models is: Mori-Tanaka is independent of the Poisson's ratio and in Halpin-Tsai is independent of aspect ratio [57]. Based on geometry, Mori-Tanaka assumed the fiber and disc particles as ellipsoidal shape, while Halpin-Tsai assumed the disc as a rectangular and the fiber as a fiber [57]. Also, in literature, the disc could be assumed as a circular shape [58]. Thus, geometric and dispersion of filler are essential in these models. Due to the complexity of geometric, some assumptions are made in such studies. Some of these studies are assumed the distribution of fillers is well-exfoliation [57] or partially exfoliated and intercalation [3]. The orientation of particles is also important for Mori-Tanaka model; therefore, this model is divided into three approaches depending on the orientation of particles, i.e. oriented particles, 2D and 3D randomly distributed particles [59]. Parameters such as particle volume ratio, aspect ratio, and particle/polymer elastic modules are also recorded as important parameters for those approaches.



The use of Finite Element Methods with these models is limited especially for high aspect ratio plate-like particles [59]. Another limitation of using these models is the accuracy of elastic modulus (E) is necessary and this is difficult to achieve it [59].

### **Section 2.3: Manufacturing processes**

Polymer and polymer nanocomposites could be produced either by conventional or non-conventional fabrication techniques. Conventional manufacturing technology includes extrusion and injection moulding are widely used in plastic industries to manufacture high volume products by injection into a mould or by extrusion pressure. Although these traditional processes are frequently used and gained industrial acceptance, dimensional accuracy of products does not meet all the manufacturing needs for high precision products [60]. Parts made from thermoplastic polymers such as nylon, polypropylene and polystyrene are the most commonly produced using this technology. Temperature and pressure are required in the fabrication process; therefore a thermal degradation is expected in produced materials. On the other hand, additive manufacturing processes have attracted increasing attention due to their promising potential for the direct part production of final 3D high-accuracy products using mould-less and pressure-less manufacturing process. Different types of additive manufacturing are currently available in the manufacturing market, but here we only focus on laser-based additive manufacturing techniques. This manufacturing technique uses high power laser to sinter polymeric powder in Laser Sintering (LS) machine or fuse (melt) metallic powder in a different machine named as Laser Melting (LM) [61]. Thus, the main focus of this thesis is Laser Sintering and its applications in polymers and polymer nanocomposites.

#### ***Section 2.3.1: Laser Sintering (LS)***

Laser Sintering (LS), also known as a rapid prototyping, is a layer-by-layer manufacturing technique designed to produce high precise and more complex 3 dimensional (3D)

products. A computer aided design (CAD) model in a computer connected to the LS machine is used to simulate three dimensional shapes and then fabricate the designed objects from powdered materials using laser power. The possibility to produce parts in a high geometric complexity is the main advantage of using LS technique [62]. LS produces final or near-final objects without the need for post machining could reduce processing time and cost. However, a limited selection of materials and inconsistent mechanical properties are still challenges restricting the overall potential of LS [62]–[65]. Porosity and surface quality could also affect the functions of the end-use parts [66], [67]. Pore formation is highly affected by the melt flow and thermal stability and is also influenced by the powder particle shape, distribution and processing parameters (laser power and scan speed) [64], [68], [69].

### ***Section 2.3.2: Polymers nanocomposites by LS technique***

**Matrix polymers;** Polyamides especially polyamide 12 (PA12) is the most frequently used polymer in LS. Benefits offer by PA12 are processability (easy to sinter), availability (relatively inexpensive) and successfully produced (large sintering window) [31]. It is important to include an example of my DSC-HSM results (**Figure 2-3**) here in this section to give general idea about the thermal properties of PA12 and further discussion are found in Chapter4-6. DSC results coupled with hot stage microscopy images in **Figure 2-3**, shows the melting, crystallization temperature and processing window of PA12: 185.5 °C, 145.7 °C and 39.8 °C respectively. Thus, PA12 in LS has been insightful research rather than other materials.

Attempts to use other polymers in LS are reported for example: polyethylene (PE) [70], poly (Ether-Ether-Keton) (PEEK) [63] and poly (Ether-Keton) (PEK) [71]. Despite this potential, the produced parts still do not meet the requirements in many applications.

Challenges such as porosity, surface quality, inconsistent mechanical properties and part shrinkage are still restricting the overall potential of LS [66], [67], [70], [71].

However, polymeric materials are capable to be reinforced by adding reinforcement materials such as nanoclay to improve their materials properties.

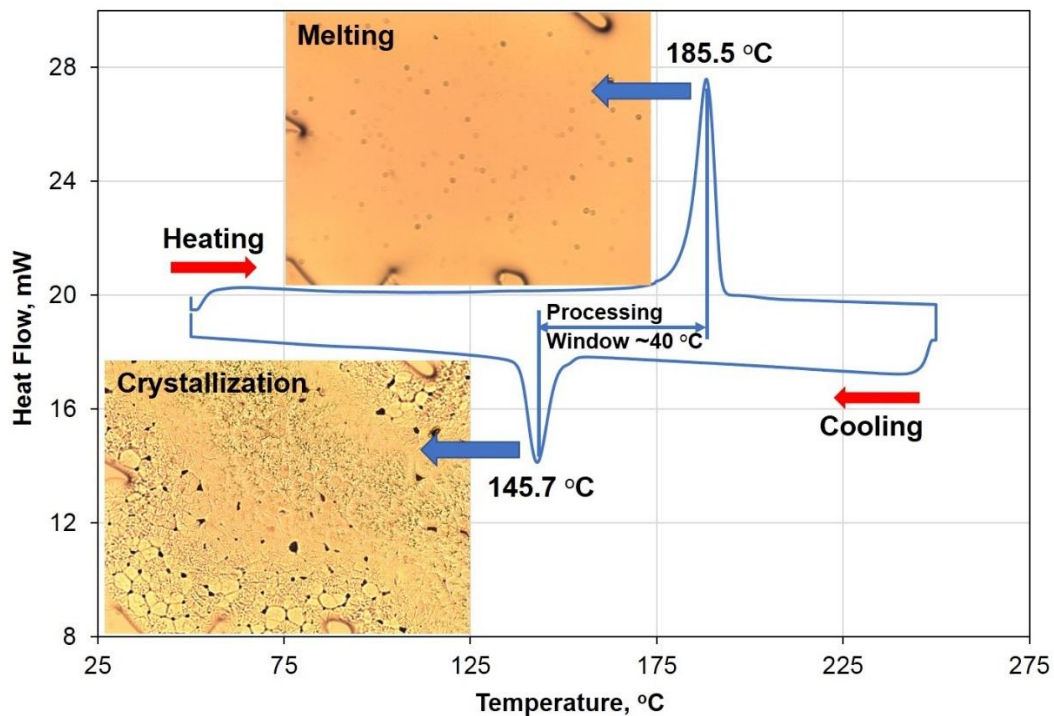


**Figure 2-3** DSC and HSM results of PA12 heating from 50 C to 250 C at rate of 10 C/min. shows melting, crystallization and processing window temperatures.

### Nanofillers

Nanoclays, are frequently used nanofillers in polymer nanocomposite applications, nanomaterials, offer significantly improved matrix polymer properties, such as strength, thermal and electrical conductivity. However, the dispersion of nanoclay still remains a challenge for the overall performance of laser sintering nanocomposites. Poor interaction between organic polymer matrices and inorganic nanoclays leads to a micro-aggregation phenomenon and is a problem for the mechanical properties [5].

Jain and coresearchers [23] have conducted an experimental study to investigate the effect of organomodified MMT on the mechanical properties of Polyamide PA2200 and sintering parameters as well. They used a high speed mechanical mixer to prepare the nanocomposites. Morphological observations revealed inhomogeneous distribution of nanofiller in polymer matrix. The dispersion of filler was poor and the filler was clearly agglomerated. As a result, the mechanical properties were not improved. This is an example of how the sintered nanocomposite did fail to improve the properties of nanocomposites compared to the neat polymer. Another example of the effect of nanoclay on the properties of sintering polyamides was carried out by Yan [72]. They used a dissolution-precipitation method to prepare OMMT/nylon12 nanocomposite before laser sintering. Morphological, the results showed well dispersed filler. The tensile test properties were relatively improved except the 17.5% decrease in elongation at break that was reported after adding the clay. Tensile test fracture morphology, solid samples porosity and nano-dispersion of the nanoclay were not discussed in this study. Alternatively, the authors have shown that the micro-dispersion of nanoclay was observed by the low magnification SEM image of the impact test fracture surface.

In summary, LS materials are capable to be reinforced by fillers, but the reinforcement is not fully satisfied, therefore, we exploit the potential of plasma treatment to address the poor dispersion of the nanoclay into the polymer matrix.

### ***Section 2.3.3: Plasma Treatments***

Besides the mechanical properties of LS materials, these materials have also restricted applications where adhesion, bonding, wettability or printability is required, due to their hydrophobization. Although several studies were made on the plasma treatments of LS materials (e.g. PA12) to alter surface properties such as hydrophilicity and wettability [73]–[76], these were more concentrated on bulk materials and thin films.

On the other hand, polymers nanocomposites still do not meet the needs for LS applications in many areas due to inhomogeneous distribution of nanofillers and poor adhesion between nanocomposite materials. During the past decade, for these purposes, plasma treatments were not a research priority. Studies were more concentrated on chemical modification of clay for example; inorganic acids [77], [78], or organic grafting [79], [80].

Plasma treatment as a physical surface modification technique have the potential to modify polymeric (matrices) and non-polymeric materials (fillers) in a chemical-free, low-cost and environmental friendly process. Studies on plasma treatments were mainly concentrated on bulk materials and thin films. Here we established a novel method for using plasma treatments in LS applications as: a nanoclay dispersion enhancer for LS polymer nanocomposite powder and a surface modifier for LS polymer powder.

#### ***Section 2.3.4: Plasma treatments of nanofillers***

Several attempts were made to modify nanofillers for different purposes for example carbon nanotubes, natural fibers and nanoclays. Carbon nanotubes were plasma treated to improve nanotube dispersion into the epoxy matrix [81], or for dispersion improvement in water [82], or for better electrical properties [83]. Natural fibres were also subjected to plasma treatment to enhance the mechanical properties of fibres [84]. The surface modification of the clay/nanoclay for the reinforcement of polymers is rarely covered and only a few studies were carried out on this topic [85], [86]. In addition, no previous studies have been done to explore the Plasma Treatment effect for fillers for laser sintering applications. Nanoclay has stacks of platelets which can aggregated to form microscale tactoids with negative effects on LS processing. Breaking up such aggregates to small sizes tactoids or individual platelets, if possible, requires further modifications or very elaborate techniques for example using organic solvents or melt mixing, therefore, we

suggested using a cheap, dry method that does not require any chemicals: i.e. Plasma Treatment. Plasma treatment of nanoclays is described in chapters four and five.

### ***Section 2.3.5: Plasma treatments of LS polymers***

A plasma discharge may cause a production of chemical functionalities of the exposed polymer depending on the process gas and plasma conditions, and even the chemical composition of the polymeric surfaces. Plasma treatments use routinely inert gas plasma (Argon), Fluorine based plasmas such as CF<sub>4</sub> and oxygen gas for the surface modification of polymers [73], [87]–[92].

Several attempts have been carried out to modify a wide range of polymers using plasmas for different purposes [73], [87]–[92]. Some of these attempts were made on the plasma treatment of PA12 (bulk or thin films) to alter surface properties such as hydrophilicity and wettability [75], [93]–[95]. Hnilica et al [75] used microwave plasma jet using argon gas at atmospheric pressure and they found that the PA12 surface wettability was significantly increased. They concluded, based on the AFM, ATR-FTIR, and XPS results, the wettability was increased due to both chemical and morphological changes. Surface Barrier Discharge Plasma at atmospheric pressure in Oxygen and Nitrogen (O<sub>2</sub> and N<sub>2</sub>) and Radio-Frequency Discharge Plasma in Air were used to modify the surface and adhesion properties of PA12 foils as described by Novak [95]. ATR-FTIR and XPS have detected changes in the chemical structure of the plasma modified PA12 foils, for example an increase of the oxygen containing groups and more hydrophilic functional groups were obtained.

The topmost surface layer of the solid materials is the most influenced by the plasma action [96]. Within this surface layer, the chemical structure and properties (e. g. mechanical properties) differ significantly from those of pristine materials or the bulk [75], [91], [95], therefore, a phase separation in the region between the surface and bulk

materials can occur [97]. Aging and degradation of the plasma-assisted active sites after exposure to the ambient environment is another common issue which is caused by the interaction between the surfaces free radicals and environmental oxygen [91], [98]. Laser Sintering of plasma treated powder is in its infancy, although a recent work used a plasma jet in ambient atmosphere for 120 seconds on powder before sintering to increase surface tension [99]. The authors aimed to present a correlation between the measured and estimated surface tension of the powder and melt for understanding the LS processes and additional qualifying new materials. However, the wettability and surface morphology were not described in this study.

We believed that, the surface morphology is an important role in studying the plasma treated powder. Plasma treatment could make a significant change to the powder morphology as well as powder chemistry. Plasma treatment of polymer powder will be discussed in chapter 6.

### ***Section 2.3.6: Characterisation of polymer nanocomposites***

Structural characterisation and microstructure analysis of polymer nanocomposites is required to investigate the effect of nanofiller on the polymer matrix. The description of the exfoliation/intercalation and dispersion of filler in polymers using X-ray diffraction and Scanning Electron Analysis is required to identify the structural changes in the nanoscale. Scanning electron microscope (SEM) is widely used technique in micro/nano-structure observation of polymer composites. Insight into the morphology of the nanocomposites has resulted in a deeper understanding of the reasons for changes in properties. For instance, if the filler was well dispersed, nanocomposites properties such as mechanical and thermal properties would be significantly enhanced [48]. In contrast, the aggregation of filler always led to undesirable properties [100]. Flammability of PLS is also affected by intercalated/delaminated structure [101]. As a result, SEM has

approved to be a powerful tool in nanocomposites researches. Field-Emission Gun (FEG) SEM such as NovaSEM can make nanocomposites research easier by providing images with high resolution and high magnification up to few nanometres. Based on the above reasons, SEM has been widely used as an efficient technique [7], [21], [23], [102]. In addition, SEM has been used as a powerful tool in the observation of the LS surface and cross-section morphologies [31][63], [103]. Despite the fact that SEM is widely used to predict the morphology of composites, to our knowledge nobody has predicted the mechanical properties of a composite depending on the dispersion of filler which was made by the effect of plasma treatment. Thus, the current study is motivated by the need to find a new methodology in making composite as will discuss in chapters 4-6. Furthermore, in this study, SEM micrographs were obtained without the need of coating, which can obscure the presence of nano-fillers.

Dynamic scanning calorimetry (DSC), Hot Stage Microscopy (HSM), Thermo-Graphical Analysis (TGA) and Fourier-transform infrared spectroscopy (FTIR) are powerful techniques used frequently to characterize LS polymer nanocomposites. DSC is a thermo-analytical technique used to measure melting and re-crystallization behaviours of materials usually solids or powders [103]–[105]. In DSC experiments, LS materials are heated from low temperature (usually room temperature or above) to a temperature above the melting temperature (e.g. PA12, its melting point around 185 °C, heated to 250 °C) before cooling down to the initial point. The main temperatures and heat flow are measured automatically using the machine software. The appropriate selection of LS bed temperature is quite sensitive because it may leads to two undesirable phenomenon in sintered parts; curling (very low temperature) and caking (very high temperature). These can be avoided by measuring the melting and crystallization temperatures and calculating the processing window using the DSC. However, HSM can also be an efficient way to



determine visually the onset points, melting and crystallization temperatures. Moreover, the progress of coalescence for polymer/composite powder and the mechanism of neck formation can also be imaged using its optical microscope [103], [104], [106], [107]. For the amorphous structure polymers, there is no specified melting temperature, only a glass transition temperature, therefore in sintering the polymer powder should be heated above the glass temperature [31].

TGA is most widely used, especially to determine the weight loss under temperature and the heat degradation of polymers and nanoclays and their composites [108]–[110] [111]. Polymeric materials and their composites are heated from ambient temperature to around 650 °C to determine the decomposition steps, temperatures and residual. These values are highly affected by the polymer's molecular structure, the surfactant's chemical structure and the dispersion of the nanoclay in the polymer matrix. TGA analyses, therefore, should be coupled with the chemical analysis of the nanocomposite materials using the most efficiently technique: FTIR [112].

### ***Section 2.3.7: Mechanical properties of LS polymer nanocomposites***

Improving the mechanical properties of LS produced parts is of increasing interest to fulfil industrial requirements. In LS applications, similar to the conventional methods, stiffness, toughness and ductility are the most important mechanical properties which measured directly from the tensile test. However, the mechanical properties of LS parts, depend on many LS processing parameters (laser power, scan speed, layer thickness, part orientation), as well as the nanoclay loadings. These parameters could significantly change mechanical properties of the laser sintering parts, even when the same materials are processed. For example, B. Caulfield (2007) [113] found that the mechanical properties of LS samples were strongly affected by laser energy and part orientation (zero and 90°). Andreas Wegner and Gerd Witt (2012) [114] established a correlation between

the LS parameters and the mechanical properties. They demonstrated that in most cases there was a nonlinear and complex correlation between mechanical properties and LS parameters. Similar studies were carried out by Soeren Griessbach et al (2010) [115], Uzoma Ajoku (2006) [116]. And Eva C. Hofland et al (2017) [117].

Optimising the LS parameters of the polymer nanocomposites is governed by the three influencing components: polymer matrix, nanofillers and matrix-nanofiller interface. Failed samples or poor mechanical properties are expected if the LS parameters are not properly selected (see **Figure 2-4**). Additionally, the dispersion of nanoclay is still a critical role in the LS performance. For example, a study carried out by Jain and coresearchers, revealed no increase in mechanical properties after adding nanoclay [23]. They explained that was due to the presence of some un-melted PA2200 particles and the aggregation of clay within polyamide [23].



**Figure 2-4** *One of my LS building attempts showing the polymer powder was failed to produce parts due to improper choice of parameters .*

As a summary to the up-to-date literature, a correlation between these parameters (LS parameters and dispersion of nanoclay) and plasma treatment is not studied yet. LS parameters are only considered if new nanofillers [32], [34], [118] or polymer matrices

[70], [119] or new LS compounding materials [67], [69] were investigated but plasma treatment technologies were not considered in these and other studies. Thus, this is the first time to explore a relationship between the laser power and plasma treatment and dispersion of nanoclay. Such this correlation could open the door for new generation of material applications which could reduce the common LS challenges which are frequently reported in literature for examples references [62]–[65].

Similarly, plasma treatment of polymer powder was hardly considered in the enormous number of published studies on LS applications. Furthermore, the wettability and meltability of polymer powders (treated and nontreated) have not been studied so far. Studies are only concentrated on bulk and thin films [75], [76], [93]–[95]. Also, using of different plasma treatment technologies (low pressure plasma and plasma jet) for the same material could investigate the powder properties at different conditions for example the powder meltability. Here, therefore, we presented new methods, have not been used before, for measuring the meltability and wettability of plasma treated LS polymer powder.

## **Section 2.4:References**

- [1] W. Zhao *et al.*, “Mechanical properties of nanocomposites reinforced by carbon nanotube sponges,” *J. Mater.*, vol. 4, pp. 0–7, 2018.
- [2] J. Liu *et al.*, “Graphene-Alumina Nanocomposites with Improved Mechanical Properties for Biomedical Applications,” *ACS Appl. Mater. Interfaces*, vol. 8, no. 4, pp. 2607–2616, 2016.
- [3] J. J. Luo and I. M. Daniel, “Characterization and modeling of mechanical behavior of polymer/clay nanocomposites,” *Compos. Sci. Technol.*, vol. 63, no. 11, pp. 1607–1616, 2003.
- [4] G. T. Mola *et al.*, “Nano Composite for Solar Energy Application,” vol. 20, no. April, pp. 90–107, 2018.

- [5] S. Pavlidou and C. D. Papaspyrides, "A review on polymer-layered silicate nanocomposites," *Prog. Polym. Sci.*, vol. 33, no. 12, pp. 1119–1198, 2008.
- [6] D. Kint, G. Seeley, M. Gio-Batta, and A. Burgess, "Structure and Properties of Epoxy-Based Layered Silicate Nanocomposites," *J. Macromol. Sci. Part B Phys.*, vol. 44, no. 6, pp. 1021–1040, 2005.
- [7] D. Pedrazzoli, A. Pegoretti, and K. Kalaitzidou, "Synergistic effect of graphite nanoplatelets and glass fibers in polypropylene composites," *J. Appl. Polym. Sci.*, vol. 132, no. 12, pp. 1–8, 2015.
- [8] K. Müller *et al.*, "Review on the Processing and Properties of Polymer Nanocomposites and Nanocoatings and Their Applications in the Packaging, Automotive and Solar Energy Fields," *Nanomaterials*, vol. 7, no. 4, p. 74, 2017.
- [9] N. Raman, S. Sudharsan, and K. Pothiraj, "Synthesis and structural reactivity of inorganic-organic hybrid nanocomposites - A review," *J. Saudi Chem. Soc.*, vol. 16, no. 4, pp. 339–352, 2012.
- [10] S. Kumar, M. Nehra, N. Dilbaghi, K. Tankeshwar, and K. Kim, "Progress in Polymer Science Recent advances and remaining challenges for polymeric nanocomposites in healthcare applications," *Prog. Polym. Sci.*, vol. 80, pp. 1–38, 2018.
- [11] V. T. Rathod, J. S. Kumar, and A. Jain, "Polymer and ceramic nanocomposites for aerospace applications," *Appl. Nanosci.*, vol. 7, no. 8, pp. 519–548, 2017.
- [12] S. C. Tjong, "Novel nanoparticle-reinforced metal matrix composites with enhanced mechanical properties," *Adv. Eng. Mater.*, vol. 9, no. 8, pp. 639–652, 2007.
- [13] A. Lateef and R. Nazir, "Metal Nanocomposites : Synthesis , Characterization and their Applications," in *Science and applications of Tailored Nanostructures*, P. Di Sia, Ed. One central press, 2017, pp. 239–256.
- [14] X. Zhai *et al.*, "3D-Printed High Strength Bioactive Supramolecular Polymer/Clay Nanocomposite Hydrogel Scaffold for Bone Regeneration," *ACS Biomater. Sci. Eng.*, vol. 3, no. 6, pp. 1109–1118, 2017.
- [15] G. Diaconu, M. Paulis, and J. R. Leiza, "Towards the synthesis of high solids

- content waterborne poly(methyl methacrylate-co-butyl acrylate)/montmorillonite nanocomposites,” *Polymer (Guildf)*., vol. 49, no. 10, pp. 2444–2454, 2008.
- [16] G. Huang, J. Yang, X. Wang, and J. Gao, “Nanoclay, intumescent flame retardants, and their combination with chemical modification for the improvement of the flame retardant properties of polymer nanocomposites,” *Macromol. Res.*, vol. 21, no. 1, pp. 27–34, 2013.
- [17] S. M. Khaled, R. Sui, P. A. Charpentier, and A. S. Rizkalla, “Synthesis of TiO<sub>2</sub>–PMMA Nanocomposites: Using Methacrylic Acid as a Coupling Agent,” *Langmuir*, vol. 23, no. 7, pp. 3988–3995, 2007.
- [18] J. Njagi and S. Andreescu, “Stable enzyme biosensors based on chemically synthesized Au-polypyrrole nanocomposites,” *Biosens. Bioelectron.*, vol. 23, no. 2, pp. 168–175, 2007.
- [19] A. Olad, “Polymer / clay nanocomposites,” in *Advanced in Diverse Industrial Applications of Nanocomposites*, B. Reddy, Ed. Intech, 2011, pp. 113–139.
- [20] J. Njuguna, K. Pielichowski, and S. Desai, “Nanofiller Fibre-Reinforced Polymer Nanocomposites,” *Polym. Adv. Technol.*, vol. 19, no. 8, pp. 947–959, 2008.
- [21] S. S. Bhattacharya and A. Mandot, “Polyamide / Clay Nanocomposites Film , Synthesis and Mechanical Testing,” *Int. J. Pure Appl. Sci. Technol.*, vol. 17, no. 2, pp. 36–44, 2013.
- [22] S. Ghoshal, “Polymer/Carbon Nanotubes (CNT) Nanocomposites Processing Using Additive Manufacturing (Three-Dimensional Printing) Technique: An Overview,” *Fibers*, vol. 5, no. 4, p. 40, 2017.
- [23] P. K. Jain, P. M. Pandey, and P. V. M. Rao, “Selective laser sintering of clay-reinforced polyamide,” *Polym. Compos.*, vol. 31, no. 4, pp. 732–743, 2010.
- [24] J. Kim and T. S. Creasy, “Selective laser sintering characteristics of nylon 6/clay-reinforced nanocomposite,” *Polym. Test.*, vol. 23, no. 6, pp. 629–636, 2004.
- [25] Y. Wang, Y. Shi, and S. Huang, “Selective laser sintering of polyamide-rectorite composite,” *Proc. Inst. Mech. Eng. Part L J. Mater. Des. Appl.*, vol. 219, no. 1, pp. 11–16, 2005.
- [26] A. Warnakula and S. Singamneni, “Selective Laser Sintering of Nano Al<sub>2</sub>O<sub>3</sub>

- Infused Polyamide,” *Materials (Basel)*., vol. 10, no. 8, p. 864, 2017.
- [27] H. Zheng, J. Zhang, S. Lu, G. Wang, and Z. Xu, “Effect of core-shell composite particles on the sintering behavior and properties of nano-Al<sub>2</sub>O<sub>3</sub>/polystyrene composite prepared by SLS,” *Mater. Lett.*, vol. 60, no. 9–10, pp. 1219–1223, 2006.
- [28] Y. Chunze, S. Yusheng, Y. Jinsong, and L. Jinhui, “A nanosilica/nylon-12 composite powder for selective laser sintering,” *J. Reinf. Plast. Compos.*, vol. 28, no. 23, pp. 2889–2902, 2009.
- [29] R. D. Goodridge *et al.*, “Processing of a Polyamide-12/carbon nanofibre composite by laser sintering,” *Polym. Test.*, vol. 30, no. 1, pp. 94–100, 2011.
- [30] R. D. Goodridge, K. W. Dalgarno, and D. J. Wood, “Indirect selective laser sintering of an apatite-mullite glass-ceramic for potential use in bone replacement applications,” *Proc. Inst. Mech. Eng. Part H J. Eng. Med.*, vol. 220, no. 1, pp. 57–68, 2005.
- [31] R. D. Goodridge, C. J. Tuck, and R. J. M. Hague, “Laser sintering of polyamides and other polymers,” *Prog. Mater. Sci.*, vol. 57, no. 2, pp. 229–267, 2012.
- [32] G. V. Salmoria, R. A. Paggi, A. Lago, and V. E. Beal, “Microstructural and mechanical characterization of PA12/MWCNTs nanocomposite manufactured by selective laser sintering,” *Polym. Test.*, vol. 30, no. 6, pp. 611–615, 2011.
- [33] S. R. Athreya, K. Kalaitzidou, and S. Das, “Processing and characterization of a carbon black-filled electrically conductive Nylon-12 nanocomposite produced by selective laser sintering,” *Mater. Sci. Eng. A*, vol. 527, no. 10–11, pp. 2637–2642, 2010.
- [34] J. Bai, R. D. Goodridge, R. J. M. Hague, and M. Song, “Improving the mechanical properties of laser-sintered polyamide 12 through incorporation of carbon nanotubes,” *Polym. Eng. Sci.*, vol. 53, no. 9, pp. 1937–1946, Sep. 2013.
- [35] J. Bai, R. D. Goodridge, R. J. M. Hague, M. Song, and M. Okamoto, “Influence of carbon nanotubes on the rheology and dynamic mechanical properties of polyamide-12 for laser sintering,” *Polym. Test.*, vol. 36, pp. 95–100, 2014.
- [36] A. Dhawan and V. Sharma, “Toxicity assessment of nanomaterials: Methods and challenges,” *Anal. Bioanal. Chem.*, vol. 398, no. 2, pp. 589–605, 2010.

- [37] S. Y. Y. Madani, A. Mandel, and A. M. M. Seifalian, "A concise review of carbon nanotube's toxicology," *Nano Rev.*, vol. 4, no. 1, p. 21521, 2013.
- [38] M. Kryuchkova, A. Danilushkina, Y. Lvov, and R. Fakhrullin, "Evaluation of toxicity of nanoclays and graphene oxide: in vivo A *Paramecium caudatum* study," *Environ. Sci. Nano*, vol. 3, no. 2, pp. 442–452, 2016.
- [39] A. Wagner *et al.*, "Early Assessment and Correlations of Nanoclay's Toxicity to Their Physical and Chemical Properties," *ACS Appl. Mater. Interfaces*, vol. 9, no. 37, pp. 32323–32335, 2017.
- [40] V. K. K. Thakur and M. K. K. Thakur, *Eco-friendly Polymer Nanocomposites : Chemistry and Applications*, vol. 74. 2015.
- [41] M. Ghorbanpour, K. Manika, and A. Varma, *Nanoscience and plant-soil systems*, 1st ed. Springer International Publishing, 2017.
- [42] L. A. A. Utracki, M. Sepehr, and E. Boccaleri, "Synthetic, layered nanoparticles for polymeric nanocomposites (PNCs)," *Polymers for Advanced Technologies*, vol. 18, no. 1. Wiley-Blackwell, pp. 1–37, Jan-2007.
- [43] D. A. C. Manning, "Industrial clays: kaolin (china clay), ball clay and bentonite," in *Introduction to Industrial Minerals*, Dordrecht: Springer Netherlands, 2012, pp. 35–71.
- [44] T. V. V. Duncan, "Applications of nanotechnology in food packaging and food safety: Barrier materials, antimicrobials and sensors," *J. Colloid Interface Sci.*, vol. 363, no. 1, pp. 1–24, 2011.
- [45] L. Unnikrishnan, S. Mohanty, S. K. Nayak, and N. Singh, "Synthesis and characterization of polysulfone/clay nanocomposite membranes for fuel cell application," *J. Appl. Polym. Sci.*, vol. 124, no. SUPPL. 1, pp. E309–E318, Jun. 2012.
- [46] B. W. Jo, S. K. Park, and D. K. Kim, "Mechanical properties of nano-MMT reinforced polymer composite and polymer concrete," *Constr. Build. Mater.*, vol. 22, no. 1, pp. 14–20, 2008.
- [47] Kojima Yoshitsugu *et al.*, "Mechanical properties of nylon 6-clay hybrid," *J. Mater. Res.*, vol. 8, no. 5, pp. 1185–1189, May 1993.

- [48] E. P. Giannelis, "Polymer layered silicate nanocomposites," *Adv. Mater.*, vol. 8, no. 1, pp. 29–35, Jan. 1996.
- [49] S.-H. Cha, J. Bae, and K. J. J. Lee, "Enhancement of adhesion between inorganic nanoparticles and polymeric matrix in nanocomposite by introducing polymeric thin film onto nanoparticles," *Polym. Eng. Sci.*, vol. 55, no. 8, pp. 1906–1911, Aug. 2015.
- [50] A. Costantino, V. Pettarin, J. Viana, A. Pontes, A. Pouzada, and P. Frontini, "Microstructure of PP/clay nanocomposites produced by shear induced injection moulding," *Procedia Mater. Sci.*, vol. 1, no. 1, pp. 34–43, 2012.
- [51] R. R. Hegde, G. S. Bhat, and B. Deshpande, "Morphology and properties of nylon 6 blown films reinforced with different weight percentage of nanoclay additives," *Int. J. Polym. Sci.*, vol. 2012, pp. 1–14, Jun. 2012.
- [52] S. Zainuddin, M. V. Hosur, Y. Zhou, A. T. Narteh, A. Kumar, and S. Jeelani, "Experimental and numerical investigations on flexural and thermal properties of nanoclay-epoxy nanocomposites," *Mater. Sci. Eng. A*, vol. 527, no. 29–30, pp. 7920–7926, 2010.
- [53] M. L. Chan, K. T. Lau, T. T. Wong, M. P. Ho, and D. Hui, "Mechanism of reinforcement in a nanoclay/polymer composite," *Compos. Part B Eng.*, vol. 42, no. 6, pp. 1708–1712, 2011.
- [54] P. Singla, R. Mehta, and S. N. Upadhyay, "Clay Modification by the Use of Organic Cations," *Green Sustain. Chem.*, vol. 02, no. 01, pp. 21–25, 2012.
- [55] M. S. Wahab, H. W. Dalgarno, R. F. Cochrane, and S. Hassan, "Development of Polymer Nanocomposites for Rapid Prototyping Process," *Proc. World Congr. Eng.*, vol. II, pp. 1–6, 2009.
- [56] L. S. Schadler, S. C. Giannaris, and P. M. Ajayan, "Load transfer in carbon nanotube epoxy composites," *Appl. Phys. Lett.*, vol. 73, no. 26, pp. 3842–3844, 1998.
- [57] T. D. Fornes and D. R. Paul, "Modeling properties of nylon 6/clay nanocomposites using composite theories," *Polymer (Guildf)*, vol. 44, no. 17, pp. 4993–5013, 2003.



- [58] N. Sheng, M. C. Boyce, D. M. Parks, G. C. Rutledge, J. I. Abes, and R. E. Cohen, "Multiscale micromechanical modeling of polymer/clay nanocomposites and the effective clay particle," *Polymer (Guildf)*, vol. 45, no. 2, pp. 487–506, 2004.
- [59] S. Aldajah, Y. Haik, K. Moustafa, and A. Alomar, "FEM Modeling of Nanocomposites Low Speed Impact Behavior," *Int. J. Eng. Technol.*, vol. 6, no. 4, pp. 258–261, 2014.
- [60] N. R. Council, *Polymer Science and Engineering*. Washington, D.C.: National Academies Press, 1994.
- [61] H. Lee, C. H. J. Lim, M. J. Low, N. Tham, V. M. Murukeshan, and Y. J. Kim, "Lasers in additive manufacturing: A review," *Int. J. Precis. Eng. Manuf. - Green Technol.*, vol. 4, no. 3, pp. 307–322, 2017.
- [62] C. E. Majewski, H. Zarringhalam, D. Toon, U. Ajoku, N. Hopkinson, and M. P. Caine, "The use of off-line part production to predict the tensile properties of parts produced by Selective Laser Sintering," *J. Mater. Process. Technol.*, vol. 209, no. 6, pp. 2855–2863, Mar. 2009.
- [63] S. Berretta, O. Ghita, and K. E. Evans, "Morphology of polymeric powders in Laser Sintering (LS): From Polyamide to new PEEK powders," *Eur. Polym. J.*, vol. 59, pp. 218–229, 2014.
- [64] D. L. Bourell, T. J. Watt, D. K. Leigh, and B. Fulcher, "Performance limitations in polymer laser sintering," *Phys. Procedia*, vol. 56, no. C, pp. 147–156, 2014.
- [65] A. Wegner, "New polymer materials for the laser sintering process: Polypropylene and others," *Phys. Procedia*, vol. 83, pp. 1003–1012, 2016.
- [66] S. A. M. Tofail, E. P. Koumoulos, A. Bandyopadhyay, S. Bose, L. O'Donoghue, and C. Charitidis, "Additive manufacturing: scientific and technological challenges, market uptake and opportunities," *Mater. Today*, vol. 21, no. 1, pp. 22–37, 2018.
- [67] S. C. Ligon, R. Liska, J. Stampfl, M. Gurr, and R. Mülhaupt, "Polymers for 3D Printing and Customized Additive Manufacturing," *Chem. Rev.*, vol. 117, no. 15, pp. 10212–10290, 2017.
- [68] L. Hao, M. M. Savalani, Y. Zhang, K. E. Tanner, and R. A. Harris, "Effects of

- material morphology and processing conditions on the characteristics of hydroxyapatite and high-density polyethylene biocomposites by selective laser sintering,” *Proc. Inst. Mech. Eng. Part L J. Mater. Des. Appl.*, vol. 220, no. 3, pp. 125–137, 2006.
- [69] G. V. Salmoria, J. L. Leite, and R. A. Paggi, “The microstructural characterization of PA6/PA12 blend specimens fabricated by selective laser sintering,” *Polym. Test.*, vol. 28, no. 7, pp. 746–751, 2009.
- [70] Y. Khalil, A. Kowalski, and N. Hopkinson, “Influence of laser power on tensile properties and material characteristics of laser-sintered UHMWPE,” *Manuf. Rev.*, vol. 3, p. 15, 2016.
- [71] O. Ghita *et al.*, “High Temperature Laser Sintering (HT-LS): An investigation into mechanical properties and shrinkage characteristics of Poly (Ether Ketone) (PEK) structures,” *Mater. Des.*, vol. 61, pp. 124–132, 2014.
- [72] C. Z. Yan, Y. S. Shi, J. S. Yang, and J. H. Liu, “An organically modified montmorillonite/nylon-12 composite powder for selective laser sintering,” *Rapid Prototyp. J.*, vol. 17, no. 1, pp. 28–36, 2011.
- [73] P. Slepíčka, N. S. Kasálková, E. Stránská, L. Bačáková, and V. Švorčík, “Surface characterization of plasma treated polymers for applications as biocompatible carriers,” *Express Polym. Lett.*, vol. 7, no. 6, pp. 535–545, 2013.
- [74] U. Lommatzsch, D. Pasedag, A. Baalman, G. Ellinghorst, and H. E. Wagner, “Atmospheric pressure plasma jet treatment of polyethylene surfaces for adhesion improvement,” *Plasma Process. Polym.*, vol. 4, no. SUPPL.1, pp. 1041–1045, 2007.
- [75] J. Hnilica, L. Potočnáková, M. Stupavská, and V. Kudrle, “Rapid surface treatment of polyamide 12 by microwave plasma jet,” *Appl. Surf. Sci.*, vol. 288, pp. 251–257, 2014.
- [76] J. Hanusová, D. Kováčik, M. Stupavská, M. Černák, and I. Novák, “Atmospheric pressure plasma treatment of polyamide-12 foils,” *Open Chem.*, vol. 13, no. 1, pp. 382–388, 2015.
- [77] B. Tyagi, C. D. Chudasama, and R. V. Jasra, “Determination of structural

- modification in acid activated montmorillonite clay by FT-IR spectroscopy,” *Spectrochim. Acta - Part A Mol. Biomol. Spectrosc.*, vol. 64, no. 2, pp. 273–278, May 2006.
- [78] V. Krupskaya *et al.*, “Experimental Study of Montmorillonite Structure and Transformation of Its Properties under Treatment with Inorganic Acid Solutions,” *Minerals*, vol. 7, no. 4, p. 49, 2017.
- [79] S. Matsumura *et al.*, “Ionomers for proton exchange membrane fuel cells with sulfonic acid groups on the end-groups: Novel branched poly(ether-ketone)s,” *Am. Chem. Soc. Polym. Prepr. Div. Polym. Chem.*, vol. 49, no. 1, pp. 511–512, 2008.
- [80] M. Atai *et al.*, “PMMA-grafted nanoclay as novel filler for dental adhesives,” *Dent. Mater.*, vol. 25, no. 3, pp. 339–347, 2009.
- [81] C.-H. Tseng, C.-C. Wang, and C.-Y. Chen, “Functionalizing Carbon Nanotubes by Plasma Modification for the Preparation of Covalent-Integrated Epoxy Composites,” 2007.
- [82] C. Chen, A. Ogino, X. Wang, and M. Nagatsu, “Plasma treatment of multiwall carbon nanotubes for dispersion improvement in water,” *Appl. Phys. Lett.*, vol. 96, no. 13, p. 131504, Mar. 2010.
- [83] W. M. Chang, C. C. Wang, and C. Y. Chen, “Plasma Treatment of Carbon Nanotubes Applied to Improve the High Performance of Carbon Nanofiber Supercapacitors,” *Electrochim. Acta*, vol. 186, pp. 530–541, Dec. 2015.
- [84] J. Cruz and R. Figueiro, “Surface Modification of Natural Fibers: A Review,” *Procedia Eng.*, vol. 155, pp. 285–288, Jan. 2016.
- [85] A. T. Djowe, S. Laminsi, D. Njopwouo, E. Acayanka, and E. M. Gaigneaux, “Surface Modification of Smectite Clay Induced by Non-thermal Gliding Arc Plasma at Atmospheric Pressure,” *Plasma Chem. Plasma Process.*, vol. 33, no. 4, pp. 707–723, Aug. 2013.
- [86] K. Fatyeyeva and F. Poncin-Epaillard, “Sulfur dioxide Plasma Treatment of the Clay (Laponite) Particles,” *Plasma Chem. Plasma Process.*, vol. 31, no. 3, pp. 449–464, Jun. 2011.
- [87] C. K. Akkan *et al.*, “Surface topography and wetting modifications of PEEK for

- implant applications,” *Lasers Med. Sci.*, vol. 29, no. 5, pp. 1633–1639, 2014.
- [88] A. Dupuis *et al.*, “Improving adhesion of powder coating on PEEK composite: Influence of atmospheric plasma parameters,” *Appl. Surf. Sci.*, vol. 357, pp. 1196–1204, 2015.
- [89] Y. Kim, Y. Lee, S. Han, and K. J. Kim, “Improvement of hydrophobic properties of polymer surfaces by plasma source ion implantation,” *Surf. Coatings Technol.*, vol. 200, no. 16–17, pp. 4763–4769, 2006.
- [90] K. Matsubara, M. Danno, M. Inoue, H. Nishizawa, Y. Honda, and T. Abe, “Hydrophobization of polymer particles by tetrafluoromethane (CF<sub>4</sub>) plasma irradiation using a barrel-plasma-treatment system,” *Appl. Surf. Sci.*, vol. 284, pp. 340–347, 2013.
- [91] L. Zhou, Y. Qian, Y. Zhu, H. Liu, K. Gan, and J. Guo, “The effect of different surface treatments on the bond strength of PEEK composite materials (DEMA-D-13-00481),” *Dent. Mater.*, vol. 30, no. 8, pp. e209–e215, 2014.
- [92] S. W. Ha, R. Hauert, K. H. Ernst, and E. Wintermantel, “Surface analysis of chemically-etched and plasma-treated polyetheretherketone (PEEK) for biomedical applications,” *Surf. Coatings Technol.*, vol. 96, no. 2–3, pp. 293–299, 1997.
- [93] F. Dreux, S. Marais, F. Poncin-Epaillard, M. Metayer, M. Labbe, and J. M. Saiter, “Water and toluene barrier properties of a polyamide 12 modified by a surface treatment using cold plasma,” *Mater. Res. Innov.*, vol. 7, no. 3, pp. 183–190, 2003.
- [94] P. Lennon, E. Espuche, H. Sautereau, and D. Sage, “Influence of microwave plasma treatment on the wettability and the adhesive properties of polyamides films with an epoxy resin,” vol. 19, pp. 273–279, 1999.
- [95] I. Novák, M. Števiar, and I. Chodák, “Surface energy and adhesive properties of polyamide 12 modified by barrier and radio-frequency discharge plasma,” *Monatshefte für Chemie*, vol. 137, no. 7, pp. 943–952, 2006.
- [96] D. Cheneler and J. Bowen, “Degradation of polymer films,” *Soft Matter*, vol. 9, no. 2, pp. 344–358, 2013.
- [97] P. Gröning, M. Collaud Coen, and L. Schlapbach, “Polymers and cold plasmas,”

*Chimia (Aarau)*, vol. 55, no. 3, pp. 171–177, 2001.

- [98] C. Canal, R. Molina, E. Bertran, and P. Erra, “Wettability, ageing and recovery process of plasma-treated polyamide 6,” *J. Adhes. Sci. Technol.*, vol. 18, no. 9, pp. 1077–1089, 2004.
- [99] K. Wudy, D. Drummer, and M. Drexler, “Characterization of polymer materials and powders for selective laser melting,” *AIP Conf. Proc.*, vol. 1593, no. May, pp. 702–707, 2014.
- [100] M. Šupová, G. S. Martynková, and K. Barabaszová, “Effect of Nanofillers Dispersion in Polymer Matrices: A Review,” *Sci. Adv. Mater.*, vol. 3, no. 1, pp. 1–25, 2011.
- [101] J. Gilman, “Flammability and thermal stability studies of polymer layered-silicate (clay) nanocomposites,” *Appl. Clay Sci.*, vol. 15, pp. 31–49, 1999.
- [102] T. McNally, W. R. Murphy, C. Y. Lew, R. J. Turner, and G. P. Brennan, “Polyamide-12 layered silicate nanocomposites by melt blending,” *Polymer (Guildf)*, vol. 44, no. 9, pp. 2761–2772, 2003.
- [103] S. Berretta, Y. Wang, R. Davies, and O. R. Ghita, “Polymer viscosity, particle coalescence and mechanical performance in high-temperature laser sintering,” *J. Mater. Sci.*, vol. 51, no. 10, pp. 4778–4794, 2016.
- [104] L. Verbelen, S. Dadbakhsh, M. Van Den Eynde, J. P. Kruth, B. Goderis, and P. Van Puyvelde, “Characterization of polyamide powders for determination of laser sintering processability,” *Eur. Polym. J.*, vol. 75, pp. 163–174, 2016.
- [105] H. Zarringhalam, C. Majewski, and N. Hopkinson, “Degree of particle melt in Nylon-12 selective laser-sintered parts,” *Rapid Prototyp. J.*, vol. 15, no. 2, pp. 126–132, 2009.
- [106] G. M. Vasquez, C. E. Majewski, B. Haworth, and N. Hopkinson, “A targeted material selection process for polymers in laser sintering,” *Addit. Manuf.*, vol. 1, pp. 127–138, 2014.
- [107] B. Chen, S. Berretta, K. Evans, K. Smith, and O. Ghita, “A primary study into graphene/polyether ether ketone (PEEK) nanocomposite for laser sintering,” *Appl. Surf. Sci.*, vol. 428, pp. 1018–1028, 2018.

- [108] A. S. Hadj-Hamou, S. Matassi, H. Abderrahmane, and F. Yahiaoui, "Effect of cloisite 30B on the thermal and tensile behavior of poly(butylene adipate-co-terephthalate)/poly(vinyl chloride) nanoblends," *Polym. Bull.*, vol. 71, no. 6, pp. 1483–1503, 2014.
- [109] C. Zhao, H. Qin, F. Gong, M. Feng, S. Zhang, and M. Yang, "Mechanical, thermal and flammability properties of polyethylene/clay nanocomposites," *Polym. Degrad. Stab.*, vol. 87, no. 1, pp. 183–189, 2005.
- [110] C. E. Corcione and M. Frigione, "Characterization of nanocomposites by thermal analysis," *Materials (Basel)*, vol. 5, no. 12, pp. 2960–2980, 2012.
- [111] W. Xie, Z. Gao, K. Liu, W. Pan, and R. Vaia, "Thermal characterization of organically modified montmorillonite," vol. 368, pp. 0–11, 2001.
- [112] J. M. Cervantes-Uc, J. V. Cauich-Rodríguez, H. Vázquez-Torres, L. F. Garfias-Mesías, and D. R. Paul, "Thermal degradation of commercially available organoclays studied by TGA-FTIR," *Thermochim. Acta*, vol. 457, no. 1–2, pp. 92–102, 2007.
- [113] B. Caulfield, P. E. McHugh, and S. Lohfeld, "Dependence of mechanical properties of polyamide components on build parameters in the SLS process," *J. Mater. Process. Technol.*, vol. 182, no. 1–3, pp. 477–488, 2007.
- [114] A. Wegner and G. Witt, "Correlation of Process Parameters and Part Properties in Laser Sintering using Response Surface Modeling," in *Physics Procedia*, 2012, vol. 39, pp. 480–490.
- [115] S. Griessbach, R. Lach, and W. Grellmann, "Structure-property correlations of laser sintered nylon 12 for dynamic dye testing of plastic parts," *Polym. Test.*, vol. 29, no. 8, pp. 1026–1030, 2010.
- [116] U. Ajoku, N. Hopkinson, and M. Caine, "Experimental measurement and finite element modelling of the compressive properties of laser sintered Nylon-12," 2006.
- [117] E. C. Hofland, I. Baran, and D. A. Wismeijer, "Correlation of Process Parameters with Mechanical Properties of Laser Sintered PA12 Parts," vol. 2017, 2017.
- [118] A. A. Mousa, "The Effects of Content and Surface Modification of Filler on the

Mechanical Properties of Selective Laser Sintered Polyamide12 Composites,” vol. 8, no. 5, pp. 265–274, 2014.

- [119] A. Franco and L. Romoli, “Characterization of laser energy consumption in sintering of polymer based powders,” *J. Mater. Process. Technol.*, vol. 212, no. 4, pp. 917–926, 2012.





## Chapter 3: Background and Experimental works

This chapter, in *Section 3.1:Background* provides a background information to the processes materials, plasma treatments, composite preparations, and manufacturing techniques. *Section 3.3:Experimental procedures for materials* illustrates briefly all the experiments, characterisation and testing techniques were performed to optimise the processes parameters and materials conditions and loadings. Experimental and preparation methods, and background information including Figures (*Figure 3-2*, *Figure 3-3* and *Figure 3-5*) and Tables (*Table 3-1* and *Table 3-2*) mentioned here in this chapter are adapted from my published and submitted articles listed in *Chapter One* under CC-BY-4.0.

### Section 3.1:Background

#### *Section 3.1.1: Materials*

This study focuses on polymer matrix and polymer reinforced by mineral nanoclays materials. Polyamide 12 (PA12) was the polymer matrix while Cloisite 30B (C30B) and Nanomer I.34TCN (I.34TCN) were used as reinforcement materials.

PA12 (often named as Nylon12) supplied by e-Manufacturing Solution (EOS) is a white, odourless, thermoplastic and semicrystalline polymer. PA12 was selected for this study as, by far, it is the most established and commonly used laser sintering powder. PA12 is a linear synthesised polymer composed of long repeatable units of a single molecule (monomer) linked together by amide functional groups (CO-NH) which is produced by the interaction between carboxyl group (C(=O)OH) and amine group (NH<sub>2</sub>) as shown in *Figure 3-1*. Therefore, PA12 has two bonds: hydrogen bonds in the amide linkage and van der Waals bonding between the methylene chains. The presence of these polar group in PA12 causes lower degree of swelling in polar solvents, such as water and alcohol but it swells more than other polyamides in nonpolar aromatic hydrocarbon like benzene [1].

**(a) Amide group chemical reaction**



**(b) PA12 repeating unit linked by amide group**

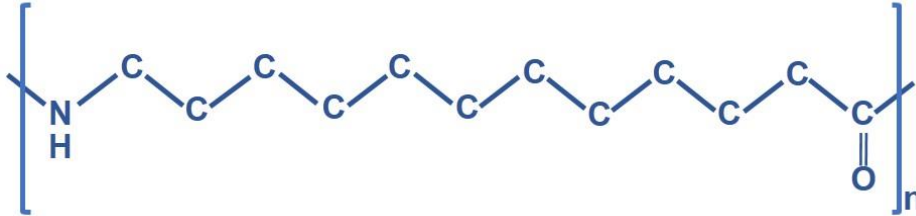


**Figure 3-1** (a) The chemical reaction of amide group, and (b) PA12 repeating unit linked together by amide group.

The powder batch used in this paper comprised 50% recovered powder from previous Laser Sintering (LS) builds, blended with 50% virgin powder. PA12 particles, as shown in **Figure 3-2a**, often have rounded or potato shape with an average size of 60-80  $\mu\text{m}$  particles. Virgin PA12 powder is made by a solution-participation process in ethanol and  $\text{TiO}_2$ , is added to the PA12 powder supplied by EOS to improve the powder whiteness and flowability [2]. In **Figure 3-2b**, is a higher magnification SEM image of a single PA12 particle, shows a non-porous solid surface covered by white nanosized particles which are assumed to be  $\text{TiO}_2$ . These nanoparticles look whiter due to their higher refractive index, which means the  $\text{TiO}_2$  has a higher scattering light affinity than the PA12 particles [3].

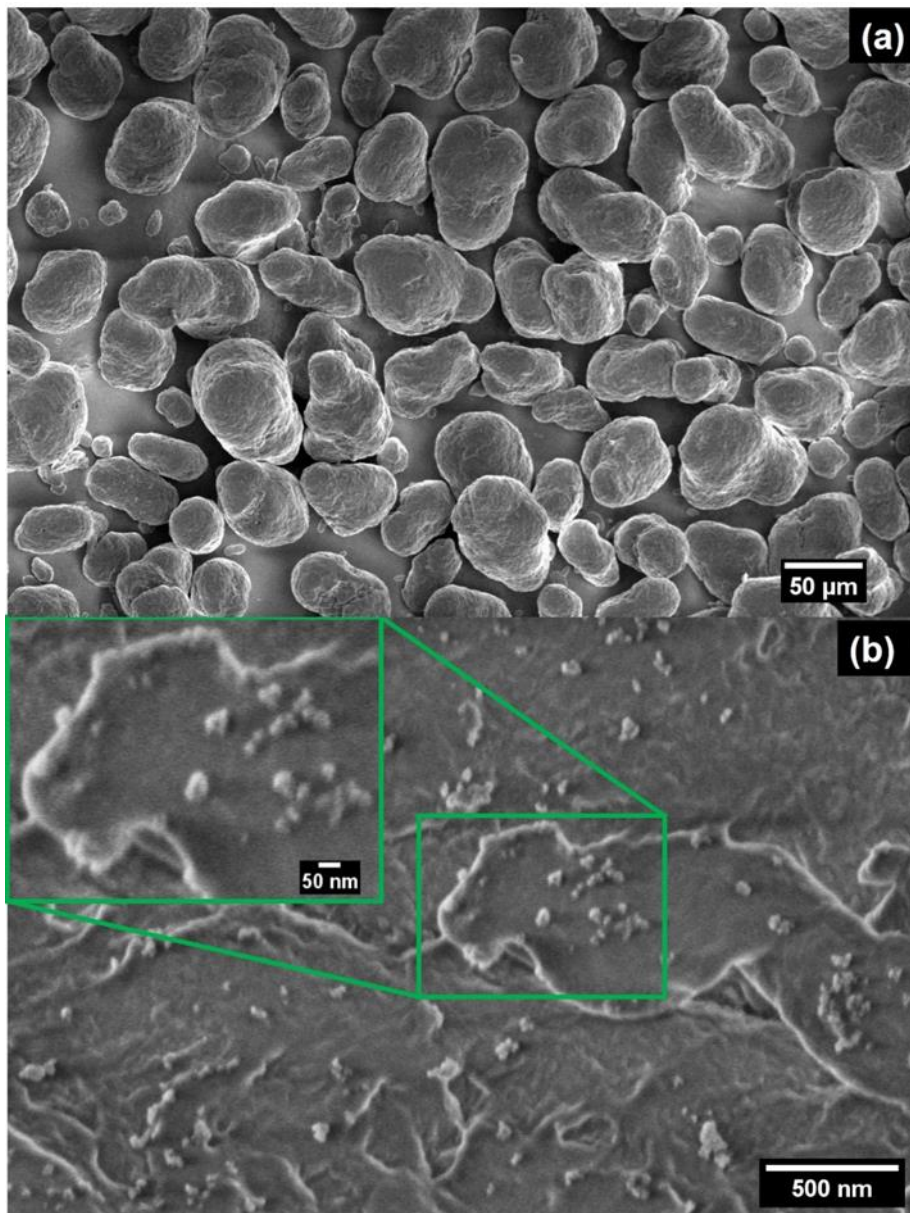


**Figure 3-2** SEM micrograph of PA12 powder (a) and (b) high magnification SEM image of single PA12 particle covered by TiO<sub>2</sub> nanoparticles. Reproduced from [4] under a CC BY 4.0 license.

Two different layered silicates clays were used: Cloisite 30B (C30B) (purchased from the clays former supplier: Southern Clay products, USA) and Nanomer (I.34TCN) (provided by Sigma Aldrich chemicals, UK). C30B and I.34TCN are montmorillonite-based nanoclays, organomodified with surfactants. The chemical structure and technical information of the surfactants are given in **Table 3-1**. C30B and I.34TCN were selected because they only differ in the structure of the surfactant. The alkyl ammonium salt of the C30B surfactant has a single alkyl tallow whereas two alkyl tallows are used to treat the

I.34TCN [5]. However, both surfactants possess a hydroxyl group which may lead to the formation of a hydrogen bond between the hydroxyl group in the surfactant and the polyamide (possessing a polar nature) resulting in a strong interaction between the organic polyamide and organomodified clays [6]. However, C30B and I.34TCN with the dihydroxyl-surfactant are more likely to suffer decomposing via Hofmann elimination reaction [7], catalyzing the degradation of polymer matrix [8],[9].

**Table 3-1** *Surfactants information and specification (according to the suppliers' technical sheets and Ref. [6], [10]).*

Clay	Surfactant	Chemical Structure	Content
C30B	Methyl bis-2 hydroxyethyl tallow alkyl quaternary ammonium chloride: [(HE) <sub>2</sub> M <sub>1</sub> T <sub>1</sub> ]  HE: Hydroxyethyl  M: Methyl  (T) Tallow: CH <sub>2</sub> (CH <sub>2</sub> ) <sub>11-15</sub> (CH=CH) <sub>0.5</sub> CH <sub>3</sub>	$  \begin{array}{c}  \text{CH}_2\text{CH}_2\text{OH} \\    \\  \text{CH}_3 - \text{N}^+ - \text{T} \\    \\  \text{CH}_2\text{CH}_2\text{OH}  \end{array}  $	25-30 %
I.34TCN	Methyl dihydroxyethyl hydrogenated tallow ammonium chloride: [(HE) <sub>2</sub> M <sub>1</sub> HT <sub>1</sub> ]  HE: Hydroxyethyl  M: Methyl  (HT) Hydrogenated Tallow:  CH <sub>2</sub> (CH <sub>2</sub> ) <sub>12-16</sub> CH <sub>3</sub>	$  \begin{array}{c}  \text{CH}_2\text{CH}_2\text{OH} \\    \\  \text{CH}_3 - \text{N}^+ - \text{HT} \\    \\  \text{CH}_2\text{CH}_2\text{OH}  \end{array}  $	25-30 %

The chemical composition of the Tallow (T) is: of 65% C18, 30% C16, and 5% C14.

N<sup>+</sup>: Quaternary ammonium salt

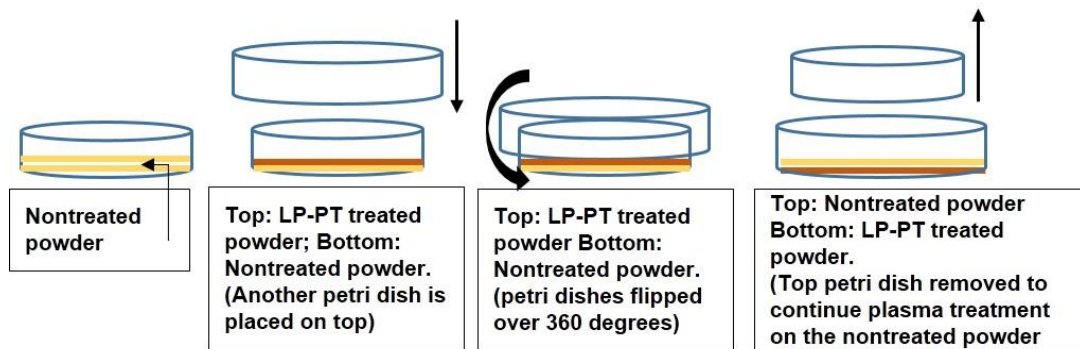
### **Section 3.1.2: Plasma treatments**

Plasmas, generated when gases (most commonly Air, O<sub>2</sub>, N<sub>2</sub>, Argon, and CF<sub>4</sub> gases) are ionized in energetic medium by an external excitation (e.g. microwave excitation sources). Plasmas composed of excited ions, atoms, radicals and molecules.

(a) Low pressure air plasma treatment (LP-PT)

Polymer (PA12) and nanoclays (C30 and I.34TCN) were subjected to LP-PT using Zepto plasma cleaner from Diener Electronics for two different purposes: LP-PT treated PA12 as an alternative LS powder or LP-PT treated nanoclays to reinforce the LS standard powder PA12.

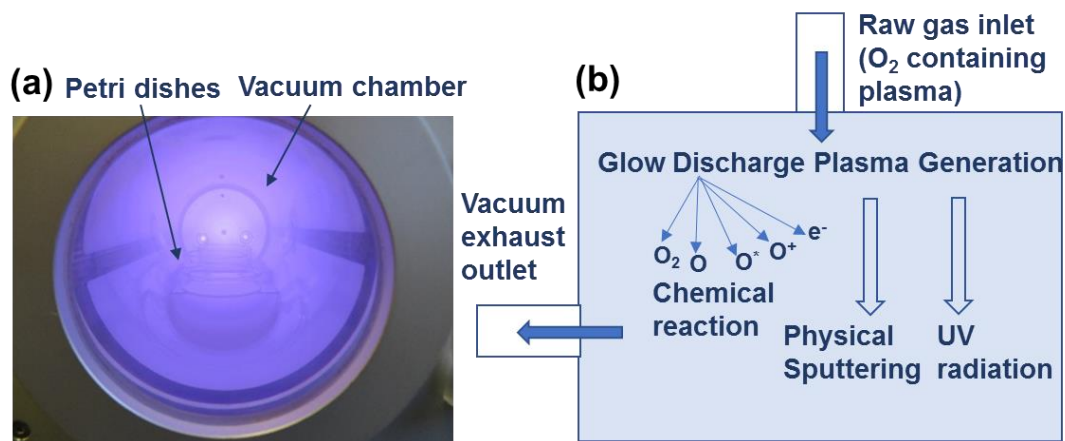
PA12 powder or the nanoclay (~3g) was placed in thin layers in a glass petri dishes in the plasma cleaner chamber (glass cylindrical chamber), exposing only the surface of the powder layer to the plasma. Thus, the powder was turned half way through the stated treatment time as shown in **Figure 3-3** to increase the homogeneity of the treatment.



**Figure 3-3** A schematic diagram shows the LP-PT procedure. Reproduced from [4] under a CC BY 4.0 license.

The main components of the plasma system are: - a vacuum pump, a vacuum chamber, and a high frequency plasma generator. As shown in **Figure 3-4a**, powder was placed into the plasma chamber, then the vacuum pump was switched on to evacuate the plasma chamber to a working pressure of <3 mbar before the process gas was fed into the chamber. Inside the glass vacuum chamber, a strong electric field created between two electrodes was applied on air to produce plasma at a full generating power of 100 W. Afterwards, a glow discharge occurred, and air was ionized producing atoms, ions, molecules, and free radicals, then the powder inside the chamber was exposed to these reactant species. The plasma system received continuously fresh gas while the contaminated gas was evacuated. As can be seen in **Figure 3-4b**, oxygen molecules are

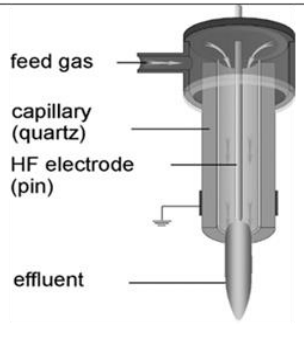
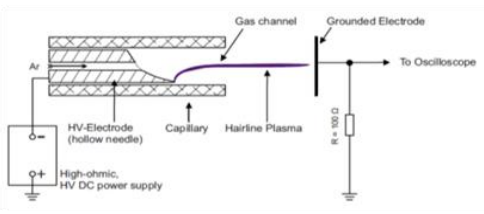
activated and dissociated into reactive species, atoms, radicals, ions, and electrons. PA12 powders were treated at for 1, 2, and 3 hours respectively, while the nanoclays (C30B and I.34TCN) were treated for 30 minutes. The treated powders PA12 or the nanoclays were then removed and stored in sealed glass jars.



**Figure 3-4** (a) A photo was taken to the LP-PT vacuum chamber where the glow discharge plasma was produced. (b) A schematic shows the dissociation of oxygen molecules to re-active species, atoms, radicals, ions and electrons.

(b) Atmospheric pressure plasma jet (APPJ)

Further treatment of PA12 powder were also conducted using two different cold atmospheric pressure plasma jets i.e. kINPen (K-APPJ) was provided by neoplas GmbH and Hairline (H-APPJ) was provided by the Institute for Plasma Science & Technology (INP) Greifswald. The differences between the two APPJ pen sources are shown in table in **Figure 3-5**- essentially the K-APPJ has a higher power than H-APPJ. The operating gas mixture for both APPJ pens is Argon operated in ambient air. PA12 powder was treated at atmospheric pressure for 1, 3 and 6 minutes. A thin layer of PA12 powder was placed on a small metal stub with a distance ~1 cm between the plasma pen and the powder.

Source	K-APPJ (Atmospheric Plasma KinPen)	H-APPJ (Atmospheric Plasma Hairline Pen)
Geometry		
Characteristic diameter	1.6 mm (capillary) 1.6 mm (effluent)	1 mm (capillary) 0.1 mm (filamentary discharge)
Reactive gas	Argon	Argon
Flow rate	4.7 slm	0.5 slm
Excitation frequency	1.1 MHz	1-3 kHz self pulsed (FWHM 10 ns)
Power	1-5 W	0.1 – 0.5 W

*Figure 3-5 Table shows parameters of the two different APPJ pen sources used in this project. Reproduced from [4] under a CC BY 4.0 license.*

In summary, three different plasma treatment approaches on three different materials are adopted as will be seen in the next three experimental chapters PA12, C30B/PA12 composite and I.34TCN composite:

(a) Polyamide 12 (PA12) powder was exposed for up to 3 hours to LP-PT and several minutes by two different atmospheric pressure plasma jets (PJ) i.e. K-APPJ and H-APPJ, (Chapter Three). The nontreated and LP-PT PA12 were fabricated using our new method, Downward Heat Sintering (DHS) (**Chapter 4**) to investigate the PA12 powder meltability.

(b) Composite materials: nontreated and LP-PT treated C30B/PA12 (NT-C30B/PA12 and PT-C30B/PA12) and nontreated and LP-PT treated I.34TCN/PA12 (NT-I.34TCN/PA12

and PT-I.34TCN/PA12) were processed together to make nanocomposite via a dry mixing process. However, the C30B based composites were fabricated using DHS (Chapter Four), while the I.34TCN composite parts were made using the laser sintering (LS) (Chapter Five). In the next paragraphs, the material processing including: dry mixing, DHS, and LS are explained:

### Section 3.2: Materials processing

(a) Composite powder preparation: Dry mixing to obtain composite powder

The nontreated and LP-PT C30B nanoclay, respectively were added to the PA12 in a small glass jars in the concentrations shown in *Table 3-2*.

*Table 3-2 Laser and Heat Sintering processes parameters.*

Clay	Materials weight*	Process	Parameters
C30B	50-100g of PA12 3% and 5% plasma treated C30B and untreated C30B	Downward Heat Sintering (DHS) (30min. mixing and 30min. sonicating before sintering)	DHS carried out in a hot press under the following parameters**: PreT 185 °C for all DHS samples (15 min.) PA12: AppT 190 °C (15 min.) Plasma treated C30B/PA12 composite: AppT 192°C (15min.) Untreated C30B/PA12 composite: AppT 195°C (15min.)
I.34TCN	3kg of PA12 3% plasma treated I.34TCN and untreated I.34TCN	Laser Sintering (LS) (1hr. mixing and 30min. sonicating before sintering)	LS parameters are the same for all samples as follows: CO <sub>2</sub> laser with a wavelength of 10.6 μm; Bed temperature 172°C; laser power (energy density***) 13W (0.208 J/mm <sup>3</sup> ), 17W (0.272 J/mm <sup>3</sup> ) and 21W (0.336 J/mm <sup>3</sup> ); laser speed scan 2500mm/sec; layer thickness 0.1mm and scan spacing 0.25mm. Under Nitrogen environment.

\* Materials weight is a minimum one set of samples.

\*\* PreT-Preheating temperature (The hot press lower part temperature); and AppT-Applied temperature (The hot press upper Part Temperature).

\*\*\* The energy densities were determined according to equation developed by Kruth et al [11].



The composite powders contained in the glass jars were mixed together using magnetic stirring bars for 30 min at a speed of 800 rpm. The glass jars, afterwards, were placed in an ultrasonic bath for sonication, to improve mixing quality, for another 30 min. The resulting powders were left, then, in its glass jar (sealed) for less than one month.

(b) Part fabrication method: Downward Heat Sintering (DHS)

The composite powders (NT-C30B/PA12 and PT-C30B/PA12) and the neat PA12 powder were formed into tensile test specimens in a hot press. Powders were placed in a hollow mould (made from stainless) in between the upper and lower parts of the hot press for thirty minutes in two stages to make tensile test samples according the British Standard (BS ISO 527). First, the powder was preheated in contact with the lower part at a temperature 185 °C for 15 minutes before the upper part at a temperature 190-195 °C (depends on the processed materials) was brought down for another 15 minutes. The temperatures of the upper and lower parts were adjusted by two electronic thermometers were attached on the hot press. Thus, parts were produced without applied external pressure with a downward supplied heat energy, therefore the DHS was considered as a good indicator for the laser sintering. A schematic diagram of the Downward Heat Sintering process is shown in *Figure 3-6*.

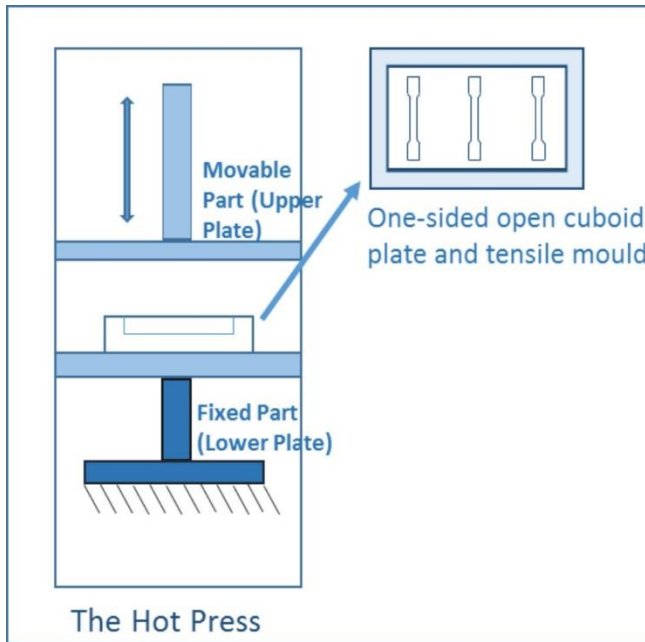


**Figure 3-6** Illustration of the Downward Heat Sintering (DHS) using the hot press.

(c) Part fabrication method: Laser Sintering (LS)

Formiga P100 LS from EOS was used to produce parts and tensile test samples from PA12, NT-I.34TCN and PT-I.34TCN composites following the DHS processes. In the laser sintering process, parts are produced by the CO<sub>2</sub>-laser energy supplied layer-by-layer to a preheated powder bed. The CO<sub>2</sub>-laser light selectively fuses the preheated powder to create 3D geometries in a mouldless process. **Table 3-2** shows briefly the DHS and LS processes parameters. The multi-picture **Figure 3-7** shows, LS machine, powder container, sintered powder and fabricated parts.

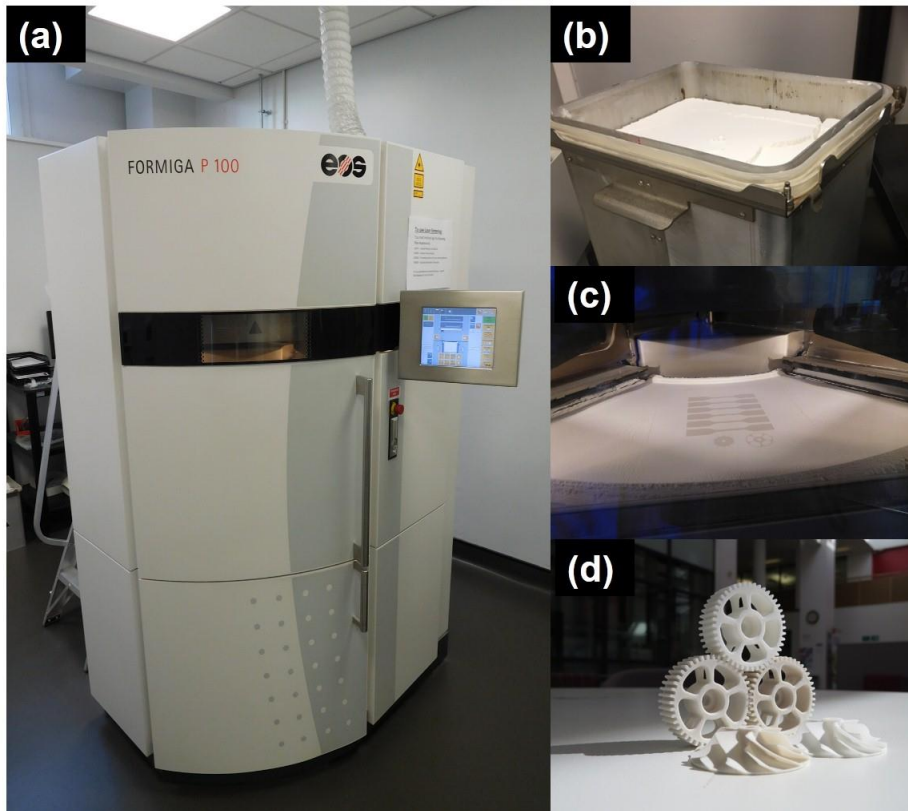


*Figure 3-7 Panels (a-d) are the pictures of the LS equipment, powder container, sintered powder, and fabricated parts respectively.*

### **Section 3.3: Experimental procedures for materials**

This section introduces the experiments, test equipment and instrumentation used for the characterisation of the materials and investigation of their properties. All the experimental tests and investigations were carried out in the laboratories of the department of Materials Science and Engineering at the University of Sheffield.

#### ***Section 3.3.1: Morphological investigations by SEM***

Low Voltage Scanning Electron Microscopy (NovaSEM) was used to analyse the morphology of the materials in Chapter 4, Chapter 5 and Chapter 6. An electron beam with a low beam energy (2.2 KeV) was used to reduce the specimen surface charging and damage. Note no metal coating was applied to the polymer surface. In addition, two different detectors were used to image the powder and bulk samples; a Through-lens-detector (TLD) for secondary electron (SE) imaging at low magnification and concentric

back scatter detector (CBS) using back-scattered electrons (BSE) to obtain high magnification images. A Low Voltage FEI Sirion (FEGSEM) was used for imaging the 1 and 3 minute K-APPJ treated PA12 (in *Chapter 6*) at low voltage up to 1kV primary beam and 4.8-4.9 mm working distance, with SE collected using the immersion-lens TLD. A Low Voltage FEI Helios SEM specifically designed for high resolution imaging at low voltages <1kV and working distance of 4 mm was used to probe the nontreated and H-APPJ treated PA12 powders in *Chapter 6*. All micrographs were processed using ImageJ [reference], to ensure the full range of grey levels is displayed. The ImageJ “Analyse Particles” function was used to find the sizes of holes and particles. ‘Enhanced Contrast’ using ImageJ was required for some of the low resolution SEM images.

### ***Section 3.3.2: Wettability, density measurements and powder distribution***

As a solid and flat surface is commonly required in the contact angle measurements, a simple alternative experiment was developed in this study to investigate the plasma effect of the wettability of polymer powders. Nontreated and 1hour LP-PT treated PA12 powders, respectively were mixed with tap water and stirred gently using a magnetic stirrer for 15 minutes in a glass jars. Then the glass jars were left at ambient temperature and images recorded before stirring, and after, every hour for up to 72 hours.

The densities of PA12 (nontreated, one hour and two hours treated) were measured using Accupyc II 1340 gas Pycnometer from micromeritics. Pycnometer used gas displacement method using Helium as a process gas to measure true volume of a known mass of powder (0.3 gram) by filling pores as small as one angstrom in diameter. PA12 powders (untreated and plasma treated) at ambient conditions and results are displayed in *Chapter 6*.

The powder distribution of PA12 and its composites (untreated I.34TCN and plasma treated I.34TCN composites) were studied using Mastersizer 2000 Particle Size Analyser

from Malvern Instruments. Each sample was tested ten times and data were analysed using software Mastersizer v3.4.

### ***Section 3.3.3: Fourier transform infrared spectroscopy (FTIR)***

FTIR analysis was performed using a PerkinElmer Frontier spectrophotometer equipped by Golden Gate™-single reflection Diamond ATR accessory in the department of materials science and engineering at the University of Sheffield. FTIR measurements were carried on powders (without KBr dilution) by recording 10 scans of the wavenumber range from 500 to 4000  $\text{cm}^{-1}$  with a spectral resolution of 4  $\text{cm}^{-1}$ . Before obtaining spectra from the samples, a background spectrum with no sample was taken as a control. FTIR measurements were performed on PA12 and its composites in Chapters 4, 5 and 6.

### ***Section 3.3.4: X-Ray Diffraction (XRD)***

XRD of powder and solid samples was carried out on Siemens D5000 (Cu, GAXRD) in the department of materials science and engineering at the University of Sheffield. X-ray scans were obtained at room temperature from  $2\theta = 2^\circ$  to  $27^\circ$  in a step of  $0.02^\circ$  and time of 1 sec per step, and the machine was operated at 40 KV and 40 mA. The obtained data was analysed using DIFFRAC.EVA application from Bruker. The XRD were carried out on C30B powder which was placed in the standard sample holder and results are displayed in Chapter 4.

FTIR and XRD are an efficient tools used to detect any changes in the chemical structure of materials (powders or bulk materials).

### ***Section 3.3.5: Thermal analysis***

#### **(a) Thermogravimetric Analysis (TGA)**

The thermal stability and decomposition of the nanoclays (both LP-PT and nontreated) and were performed on Thermogravimetric Analyser (Pyris 1 TGA from PerkinElmer) in

the department of materials science and engineering at the University of Sheffield. A known weight of powder (~5mg) placed in an aluminium pan was heated, in Nitrogen atmosphere, from 30 °C to 630 °C with a heating rate of 10 °C/min. The results of the TGA testing are shown in *Chapter 4* and *Chapter 5*.

(b) Differential Scanning Calorimetry (DSC) and Hot Stage Microscope (HSM)

Two mainly techniques, Differential Scanning Calorimetry (DSC 8500 from Perkin Elmer) and Hot Stage Microscope (HSM) in the department of mechanical engineering at the University of Sheffield, were used to optimize the melting temperature of PA12 and its nanocomposites. In DSC, powdered material weighted ~5mg was enclosed in a DSC-standard aluminium pan, then the pan was punched before placed in the DSC furnace. DSC Melting and cooling curves were collected using associated software (Pyris™). HSM was performed on BX50 light microscope from Olympus attached to a temperature-controlled microscope stage from Linkam. Samples for both DSC and HSM were melted from ambient to 250 °C in a rate of 10 °C. The DSC combined with HSM results were illustrated in *Chapter 4* and HSM imaging in *Chapter 6*.

DSC and HSM are commonly used to investigate the thermal properties of materials which are required to adjust the processing parameters of the manufacturing techniques.

***Section 3.3.6: Tensile testing***

The tensile tests were carried out to evaluate the mechanical properties of DHS and LS samples. The DHS samples were tested using Hounsfield Tensometer according to British Standard ISO 527 in the department of materials science and engineering at the University of Sheffield described in *Chapter 4*.

While tensile tests carried out on LS samples, were performed according the ASTM D638-02a, using a Tinius Olsen H5KS tensile testing machine fitted with a laser

extensometer in the department of mechanical engineering at the University of Sheffield. Ultimate stress and strain, and elastic modulus were measured using the Horizon Software. The tensile tests were carried out, *Chapter 5*, under the conditions: speed 5mm/min, preload 5N, maximum load cell 5kN and number of samples are 6.

### Section 3.4:References

- [1] V. R. Sastri, "Other Polymers," in *Plastics in Medical Devices*, Elsevier Science, 2010, pp. 217–262.
- [2] L. Verbelen, S. Dadbakhsh, M. Van Den Eynde, J. P. Kruth, B. Goderis, and P. Van Puyvelde, "Characterization of polyamide powders for determination of laser sintering processability," *Eur. Polym. J.*, vol. 75, pp. 163–174, 2016.
- [3] P. Tao *et al.*, "TiO<sub>2</sub> nanocomposites with high refractive index and transparency," *J. Mater. Chem.*, vol. 21, no. 46, p. 18623, 2011.
- [4] A. Almansoori *et al.*, "Surface modification of the laser sintering standard powder polyamide 12 by plasma treatments," *Plasma Process. Polym.*, vol. 15, no. 7, p. 1800032, Jul. 2018.
- [5] I. K. Yang and P. H. Tsai, "Preparation and characterization of polyether-block-amide copolymer/clay nanocomposites," *Polym. Eng. Sci.*, vol. 47, no. 3, pp. 235–243, Mar. 2007.
- [6] Z. Zhang, J. H. Lee, S. H. Lee, S. B. Heo, and C. U. Pittman, "Morphology, thermal stability and rheology of poly(propylene carbonate)/organoclay nanocomposites with different pillaring agents," *Polymer (Guildf)*, vol. 49, no. 12, pp. 2947–2956, 2008.
- [7] J. M. Cervantes-Uc, J. V. Cauich-Rodríguez, H. Vázquez-Torres, L. F. Garfias-Mesías, and D. R. Paul, "Thermal degradation of commercially available organoclays studied by TGA-FTIR," *Thermochim. Acta*, vol. 457, no. 1–2, pp. 92–102, 2007.
- [8] A. S. Hadj-Hamou, S. Matassi, H. Abderrahmane, and F. Yahiaoui, "Effect of cloisite 30B on the thermal and tensile behavior of poly(butylene adipate-co-terephthalate)/poly(vinyl chloride) nanoblends," *Polym. Bull.*, vol. 71, no. 6, pp.

1483–1503, 2014.

- [9] S. Pavlidou and C. D. Papaspyrides, “A review on polymer-layered silicate nanocomposites,” *Prog. Polym. Sci.*, vol. 33, no. 12, pp. 1119–1198, 2008.
- [10] E. Pérez, C. J. Pérez, V. A. Alvarez, and C. Bernal, “Fracture behavior of a commercial starch/polycaprolactone blend reinforced with different layered silicates,” *Carbohydr. Polym.*, vol. 97, no. 2, pp. 269–276, 2013.
- [11] J. P. Kruth, B. Vadenbroucke, J. V. Vaerenbergh, Naert I; “Digital manufacturing of biocompatible metal frameworks for complex dental prostheses by means of SLS/SLM”, In: Proceedings of the 2nd International Conference on Advanced Research and Rapid Prototyping, Leiria, Portugal, pp. 139-45, (2005).



## **Chapter 4: Nanoclay/Polymer Composite Powders for use in Laser Sintering Applications: Effects of Nanoclay Plasma Treatment**

### **Section 4.1: Abstract**

*Plasma treated nanoclay reinforced Polyamide 12 (PA12) powder was prepared with its intended use in laser sintering (LS) applications. To replicate the laser sintering process we presented a Downward Heat Sintering (DHS) process, carried out in a hot press, to fabricate tensile test specimens from the composite powders. The DHS parameters were optimized through Hot Stage Microscopy (HSM), which revealed that the treated nanoclay Cloisite 30B (treated C30B)-based PA12 (treated nanocomposite) powder melts at a temperature 2°C higher than that of neat PA12, and 1-3°C lower than that of the untreated clay-based nanocomposite (untreated nanocomposite). We showed that these temperature differences were critical to successful LS. The distribution of treated and untreated clay C30B onto PA12 was investigated by scanning electron microscopy (SEM). SEM images showed clearly that the plasma treatment prevents the micron scale aggregation of the nanoclay, resulting in an improved elastic modulus of treated C30B/PA12 composite when compared with neat PA12 and untreated C30B/PA12 composite. Moreover, the reduction in elongation at break for treated composite was less pronounced than for untreated composite.*

### **Section 4.2: Introduction**

Clay nanocomposites have gained much attention in recent decades. When made through melt-compounding processes, via extrusion or injection molding, enhancement of the properties of the melt compounded objects have been reported [1]–[3]. However, challenges involved in the fabrication of complex geometries have also been recorded [4]. Compared to the conventional techniques mentioned above, Laser Sintering (LS) can create highly complex geometrical parts and does not require any post-machining [5], [6]. Unlike other

methods, LS, as an additive manufacturing technique, uses 3D CAD from a computer connected to the machine, to form three-dimensional parts in a layer-by-layer process [7], [8]. In LS processing, laser power and powder bed temperature have to be carefully adjusted. The powder bed temperature is held below the powder melting temperature [6], and is used to preheat the powder, whereas the laser is used to fuse polymer particles together [5], [6], [9]. Preheating is essential to reduce the thermal gradient between the sintered and non-sintered powder and to reduce the laser power needed to melt the powder.

Although many studies on LS have focused on thermoplastic polymers, particularly semi-crystalline thermoplastics, due to their low melting temperature such as polyamides (nylons) [7], [8], [10], few studies have been conducted on the reinforcement of polymers with nanofillers for LS in order to improve the mechanical properties of neat polymers by creating polymer nanocomposites. Polymers have been filled with different types of nanomaterials such as carbon nanotubes [11], [12] or carbon nanofibers [13]. Among all the nanofillers, nanoclay (mostly montmorillonite) is the most commonly used because of the remarkable changes exhibited by the polymer after adding a small amount of nanoclay [5], [14].

Montmorillonite (MMT) is an inorganic, layered silicate and the hydrophilic clay interacts only weakly with organic polymers (typically hydrophobic ones); it tends to aggregate to form large agglomerations in the matrix. Therefore, very few studies have investigated polymers filled with pristine MMT (nontreated) [2], [15]. Chemical modification of the pristine MMT via surfactants is mostly used to change the hydrophilic MMT to organophilic by exchanging the interlayer cations with organic cations (different kinds of surfactants were used) [1], [2], [16], [17]. Although surface modification of the MMT has improved the interaction between clay and polymer, chemical modification has also been reported [15] to be expensive; hence, alternative processes are of interest.

Previously, very few attempts have been made to treat clays using a different method i.e. plasma treatment [18], [19] and there have been only a few attempts at using the plasma treated clay to prepare polymer nanocomposites[20], [21]. However, none of those studies used the treated nanoclay to prepare the polymer/nanoclay nanocomposite through a LS process.

Here we describe and employ a Downward Heat Sintering (DHS) process using a hot press to process small quantities of dry mixed C30B-nanoclay/Polyamide 12 (PA12) powders into tensile test specimens after optimisation attempts based on differential scanning calorimetry (DSC) and hot-stage microscopy (HSM) [22]. We also demonstrate that DHS results can be successfully applied to adjust the LS bed temperature to allow the fabrication of clay/PA12 nanacomposites.

Tensile tests were used to determine the strength, elastic modulus, and elongation at break [2]–[4], and some of the published results related to the current work, in comparison with our results, are summarized in *Table 4-1* and discussed in this paper.

**Table 4-1:** Summary of results from previous studies on PA12 and PA12/nanoclay composites (brackets relative values with regards to neat PA12)

	<i>Phang et al (2005) [17]</i> (Melt Compounding)	<i>Yan et al (2011) [14]</i> (Laser Sintering)	<i>Jain et al (2010) [5]<sup>a</sup></i> (Laser Sintering)	<i>Current study</i> <i>PT C30B Composite (DHS)</i>
<b>Clay %</b>	<b>Elastic Modulus, MPa</b>			
0%	1045±51.6	1420±250	736	853±28
1%	1110±25.8 (6.2±5.5%)	xxx	xxx	xxx
2%	1140±77.4 (9.1±8.9%)	xxx	xxx	xxx
3%	xxx <sup>a</sup>	1870±240 (31.7±25%)	808.7(9.9%)	1011.7±10 (18.6±3.54%)
5%	1480±100 (41.6±10.9%)	xxx	755.7(2.7%)	998±17 (17±3.9%)
<b>Clay %</b>	<b>Tensile strength, MPa</b>			
0%	33.56±0.18	38.3±2	49.15	39.58±0.68
1%	34.94±0.18 (4.1±0.75%)	xxx	xxx	xxx
2%	34.75±0.18 (3.5±0.75%)	xxx	xxx	xxx
3%	xxx	47.2±1.9 (23.2±7.3%)	48.42(-1.5%)	42.95±0.41 (8.5±2%)
5%	34.63±0.25 (3.2±0.91%)	xxx	36.5(-25.7%)	40.3±0.35 (1.8±1.9%)
<b>Clay %</b>	<b>Elongation at break, %</b>			
0%	xxx	20.8±2.8	27.82	24.17±1.27
1%	xxx	xxx	xxx	xxx
2%	xxx	xxx	xxx	xxx
3%	xxx	17.7±3 (-15±19.8%)	14.62 (-47.4±%)	18.44±2.02 (-23.7±9.9%)
5%	xxx	xxx	10.37 (-62.7±%)	9.17±1.34 (-62.1±8.3%)
<sup>a</sup> means no data is available				
<sup>b</sup> absolute values are available in				

## **Section 4.3: Materials, Preparation Methods, and Experimental Work**

### ***Section 4.3.1: Materials and Preparation Methods***

An organically modified layered silicate nanoclay used in the current study is known commercially as Cloisite 30B (C30B). It was obtained from Southern Clay Products. Virgin Polyamide 12 [trade name is Nylon 12 (N12)], the matrix, was purchased from EOS (e-Manufacturing Solution). However, the polymer used in this study was not virgin, it had previously been exposed to a high temperature in a LS, at least twice, but the powder was still good quality and the same batch was used for all trials to ensure consistency.

The materials (PA12 and C30B) were processed together to make nanocomposites using simple, easy and low-cost methods comprising three parts: clay treatment and modification, dry mixing and finally sample fabrication.

#### *(a) Clay treatment: Plasma treatment technique*

The C30B powder was treated for 30 min before being mixed with PA12 powder. Plasma treatment was carried out in a Plasma Cleaner Zepto (from Diener Electronic) with the following parameters: max power: 100 W, pressure: 0.2-0.4 mbar, time period: 1000 s for each session, and process gas: air.

#### *(b) Mixing: Dry mixing to obtain composite powder*

Treated and untreated C30B were added to the neat PA12 in small glass jars (50 ml) as per the concentrations (3 and 5 wt%) shown in **Table 4-2**. The composite powders were then stirred using a magnetic stirrer for 30 min at 800 rpm and sonicated for another 30 min using an ultrasonic bath. The resulting powder was stored in a sealed glass jar for less than 2 weeks.

**Table 4-2** Technical specifications of DHS

Materials	Lower plate		Upper Plate		Sample per session
	Time, min	Temp., °C	Time, min	Temp., °C	
Neat Polyamide 12 (PA12)	15	185	15	190	3
(3% Untreated C30B/PA12 composite)	15	188	15	192-195	3
(5% Untreated C30B/PA12 composite)	15	188	15	192-195	3
(3% Treated C30B/PA12 composite)	15	188	15	192	3
(5% Treated C30B/PA12 composite)	15	188	15	192	3

(c) Sample fabrication method: Downward Heat Sintering (DHS)

The composite powders and the neat powder were formed into tensile test specimens in a hot press, which was used to mirror the laser sintering process, and therefore no additional pressure was applied during the sample fabrication. A stainless steel hollow mold was used to make tensile test samples according to the British Standard (BS ISO 527) and it was closed from one side by a removable thick plate.

Neat PA12 and composite powders (weight ratios are given in **Table 4-2**), respectively, were placed in the mold and then the mold and the powder were placed in between the two parts of the hot press. The powders were preheated by the lower part only, which was at a temperature of 185 °C for the neat PA12, and 188 °C for PA12 composites, before the upper part (temperature is 190 °C for the neat PA12 and 192-195 °C for PA12 composites) was brought down. From the point at which the upper part comes into contact with the lower part, the preheated powder will be in a closed heated chamber similar to the laser sintering chamber. As a result, the powder temperature, will then rise to just above the melting temperature until being fully melted, after which, the two hot press parts will release. The temperatures of the upper and lower parts were adjusted by two digital electronic thermometers were attached on the hot press. Times and temperatures of DHS are shown

in *Table 4-2*. Finally, the parts are removed from the mold using a stainless steel spatula and left to cool to ambient temperature outside the hot press system. Natural cooling process were carried out outside the hot press without cooling chillers, therefore samples shrink to less than the mold standard dimensions. Therefore, dimensions of samples (tensile testing samples) released from molds were measured using digital calipers before tensile testing.

### ***Section 4.3.2: Experimental work***

#### *(a) X-Ray Diffraction (XRD) and Scanning Electron Microscopy (SEM)*

XRD of powder and solid samples was carried out on a Siemens D5000 (Cu, GAXRD). X-ray scans were obtained at room temperature from  $2\theta = 2^\circ$ - $27^\circ$  in steps of  $0.02^\circ$  with a dwell time of 1 s per step. The machine was operated at 40 KV and 40 mA. The obtained data were analyzed using the DIFFRAC.EVA application from Bruker.

Morphological investigations were conducted using a Nova NanoSEM (Low-Voltage SEM)). Two different detectors were used: a through-lens detector (TLD) for secondary electron imaging at low magnification and a concentric back-scatter detector (CBS) using back-scattered electrons to obtain high-magnification images. The TLD is normally used for topography imaging whereas the CBS is for chemical analysis [23].

#### *(b) DSC and HSM*

A DSC 8500 from Perkin Elmer and a HSM (BX50 light microscope from Olympus with temperature controlled stage from Linkam attached) were used to optimize the melting temperature of PA12 and its nanocomposites. In DSC, three samples of each powder were tested, and melting and cooling curves were collected using associated software (Pyris™). Samples for both DSC and HSM were heated from ambient to 250 °C with a rate of 10 °C/min.

#### *(c) FTIR and TGA*

TGA and FTIR were used to investigate the effect of plasma treatment on the nanoclay decomposition process. FTIR analysis was carried out by recording 10 scans at wavenumber of 400-4000  $\text{cm}^{-1}$  using a PerkinElmer Frontier spectrophotometer. TGA was conducted by Pyris from PerkinElmer.

#### *(d) Tensile Testing*

The tensile test was carried out to evaluate the mechanical properties of DHS samples using a Hounsfield Tensometer according to BS ISO 527. The test parameters used were: load cell was 10,000 N, the speed of test was 5 mm/min and a preload 5 N.

## **Section 4.4: Results and Discussion**

### ***Section 4.4.1: Optimisation of processing conditions by HSM***

To determine the most suitable process temperature for the fabrication of parts from the composite powder, it is necessary to use a technique that is most similar to the melting process during fabrication. Although, the DSC is commonly used to quantify the melting behavior of samples in both melt processing [1], [24], [25] and powder sintering [5], [7], [14], [26], we found that the melting temperatures obtained from the DSC did not result in fully melted powders in HSM (**Figure 4-1**). The DSC results showed a single endotherm peak for each sample with different intensities. The average melting temperature at peak points for all samples are almost the same (PA12:  $185.5 \pm 0.56$  °C, untreated composite:  $185.8 \pm 0.18$  °C, and plasma treated composite:  $185.3 \pm 0.19$  °C). An example of each sample is shown in **Figure 4-1**.

The single endotherm peak corresponds to the  $\gamma$  crystal form [7]. The peak positions were just above 185 °C with a variation less than 1 °C. However, the melting temperature observed during HSM was different, revealing a much larger variation between neat PA12 and the two different composite powders, as shown in **Figure 4-2(a-i)**.



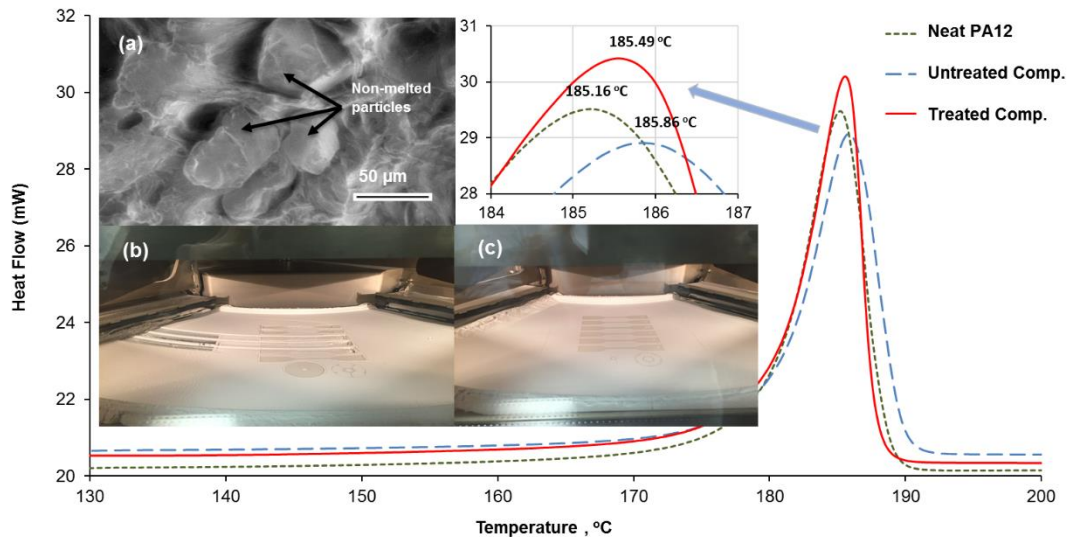


**Figure 4-1:** Melting temperature for PA12 and its composites measured by DSC showing no significant changes between peaks especially if the standard deviation mentioned in the text was considered. Inset (a) is a SEM image of a cross-section of a untreated composite tensile test sample with non-melted particles; sample was made with temperature suitable for neat PA12. Inset (b) unsuccessful LS attempt for printing untreated composite at neat PA powder bed temperature. Inset (c) successful LS attempted for treated composite at DHS adjusted powder bed temperature. A clear difference was observed between the mixtures, whereby the initial and final melting temperatures increased from neat PA12 to 3% untreated C30B/PA12 to 3% treated C30B/PA12. For these mixtures, respectively, melting began with micron-size particles at 185 °C, 192 °C and 190 °C (**Figure 4-2(a,d,g)**), larger particles were partially melted and necks were formed between adjacent particles at 190 °C, 195 °C and 192 °C (**Figure 4-2(b,e,h)**), and the melting process was completed at 192 °C, 200 °C and 195 °C (**Figure 4-2(c,f,i)**). This is in stark contrast to the DSC results that do not show such clear differences. Compared to untreated C30B, the treated C30B composite powder resembles more closely the processing conditions for neat PA12, whereas the untreated composite powder required substantially higher temperatures.

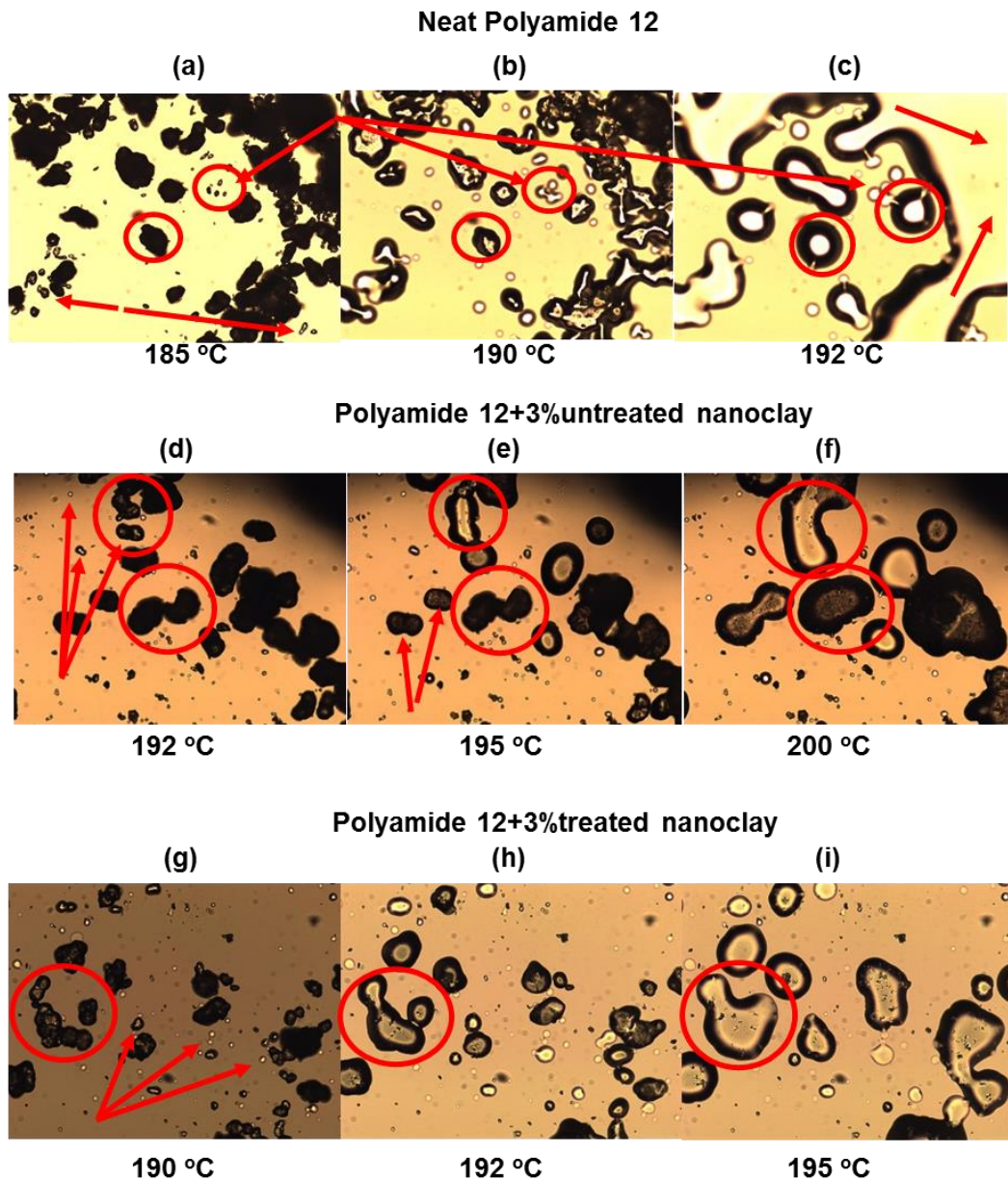


**Figure 4-2:** HSM results for PA12 and its composites under different temperatures (Neat PA12 at temperatures (a) 185 °C, (b) 190 °C, and (c) 192 °C, 3% untreated C30B/PA12 at temperatures (d) 192 °C, (e) 195 °C, and (f) 200 °C, and 3% treated C30B/PA12 at temperatures (g) 190 °C, (h) 192 °C, and (i) 195 °C)

As mentioned previously, the aim is to replicate the melt processing of powder in the hot press. In the HSM the powder is heated in an open environment, similar to the initial stages of DHS, whereas DSC takes place in a fully sealed environment. That the HSM delivered more reliable input for both the DHS process and the LS is evident in *Figure 4-1(inset c)*, which shows successful LS attempted for the treated composite when the powder bed temperature was increased by 2 °C compared to neat PA12.

#### ***Section 4.4.2: Effect of Plasma Treatment on the Nanoclay***

##### ***(Characterisation Techniques)***

The FTIR spectra shown in **Figure 4-3a** indicate the presence of structural changes resulting from subjecting C30B to 30 min of plasma treatment. A significant decrease of the stretching vibration of the Si-O-Si bonds ( $990\text{ cm}^{-1}$ ) and some reduction in Si-O bonds ( $1116\text{ cm}^{-1}$ ) are observed in treated C30B compared to untreated C30B. These reductions suggest the introduction of lamellae disorder [21], which can also explain some of the observed broadness of the XRD peak of treated C30B (**Figure 4-3b**) [21], [27]. The change in the chemical structure was not limited to the silicate band but also led to the formation of new hydroxyl groups, as evidenced by a small increase in intensity at  $3623\text{ cm}^{-1}$  in the treated C30B spectrum (**Figure 4-3a-ii**). These might be the reason for the new shoulder appearing in the XRD pattern of treated C30B in **Figure 4-3b**. The FTIR also showed a small decrease at the peak  $3360\text{ cm}^{-1}$  that revealed a reduction in the adsorbed water. The peaks associated with the organo-modifier were also changed. The peak at  $1640\text{ cm}^{-1}$  (the stretching of the quaternary ammonium salt) was slightly decreased, and a new peak was observed at wave angle  $1695\text{ cm}^{-1}$ . The interpretation of this change is the formation of carboxyl from the carbon of the organic modifier [21].

**Figure 4-3b** shows the XRD diffraction patterns for both plasma treated and untreated nanoclays. At high angles, the XRD spectra of untreated and treated clays exhibited two weak peaks at positions ( $2\theta$  of  $19.7^\circ$  and  $2\theta$  of  $19^\circ$ ). While at low angles, the XRD patterns of untreated and treated clays are different, although both exhibited the same characteristic basal diffraction at  $2\theta$  of  $4.8^\circ$  and the interlayer spacing (d-spacing) of those peaks was equal to 1.8 nm (001 crystal lattice). The peaks for untreated C30B are in good agreement with previous studies [5], [14], [28]. The pattern of treated C30B shows a much broader diffraction peak, consisting of a peak at  $4.8^\circ$  and shoulder ( $2\theta$  of  $6^\circ$ ). The formation of the

shoulder is probably attributable to a breakdown of Si-O-Si bonds and a formation of new hydroxyls (Si-OH) [19].

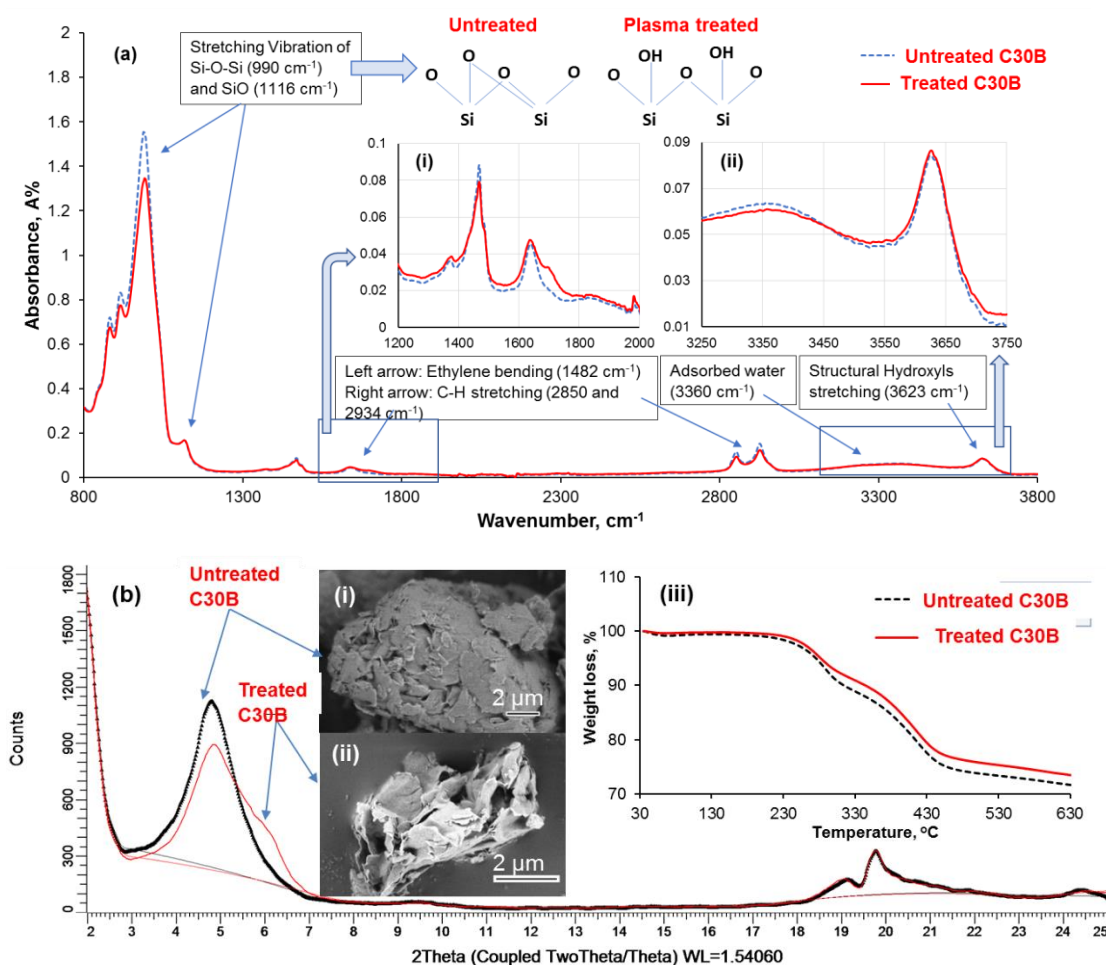


**Figure 4-3:** Influence of plasma treatment on the nanoclay using different characterization tests; (a) FTIR spectra and (b) XRD patterns, SEM images (inset i and ii) and TGA results (inset iii).

Moreover, the plasma treatment can induce oxidation of the octahedral iron leading to the release of interlayer cations [19]. The effect of the oxidation in plasma treated C30B can be observed by the colour change of the nanoclay particles from an off-white to gray colour. The formation of the oxidative layer on the treated C30B due to plasma treatment, might lead to less absorption of moisture, which could result in an improvement of the thermal stability, which can be tested by TGA. The TGA results (*Figure 4-3b-iii*) show that both treated and untreated clay are degraded in four stages, i.e. desorption of water, dehydration of hydrated cation, loss of surfactant, and dihydroxylation [16]. For a given temperature,

the weight loss of plasma treated clay is always smaller than in untreated. Hence, the plasma treated C30B is more stable than the untreated C30B, even at higher temperatures. In addition, TGA results corroborate our FTIR results, which indicated that plasma treatment releases some of the free water.

It is noted that the platelets of as received C30B nanoclay were conjoined in micron-size irregular shaped agglomerates. Some of the aggregated particles are relatively large, round or oval in shape as shown in the SEM image in *Figure 4-3b-i*. Full scale images are found in **Chapter 5**, in *Figure 5-3*. Such agglomerations reduce the surface contact area between the clay and polymers and can weaken the composite [5]. In contrast, the SEM image of the TC (*Figure 4-3b-ii*) reveals the separation into platelets resulting in a much increased surface area confirming the particles responded to the plasma treatment.

#### ***Section 4.4.3: Investigation of the properties of the treated nanoclay/polymer composites powders***

The composite powders that were made via dry mixing were investigated by XRD and SEM. The back-scattered (BSE) SEM images in *Figure 4-4(a&b)* show the incorporation of platelet shaped nanoclay in the circular or potato-shaped PA12 particles. SEM-BSE images reflect the average atomic number. As nanoclay is largely a mineral material, whereas PA12 is an organic material, the nanoclay appears bright.

For the untreated C30B we find stacks of clay platelets accumulated on the PA12 particle surface in some areas, resulting in a non-homogeneous nanoclay distribution. The treated C30B based composite exhibits less accumulation and a much more homogeneous clay distribution.

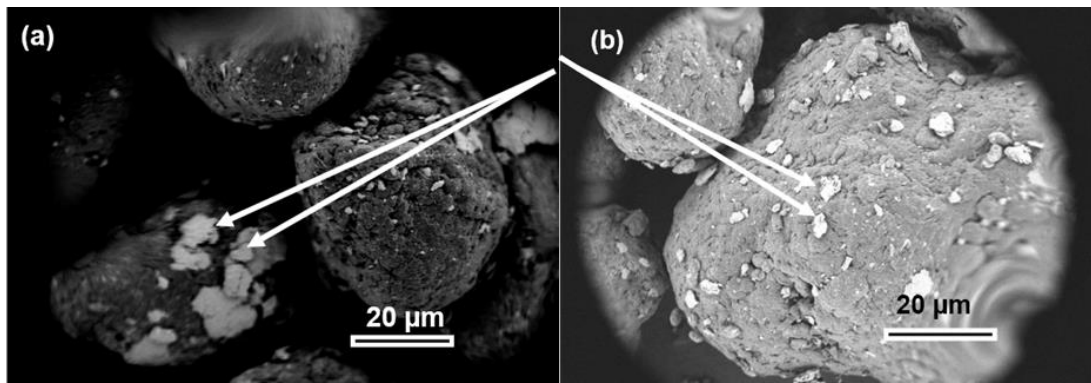


**Figure 4-4:** SEM images of 3% untreated C30B/PA12 mixed powders (a) and 3% treated/PA12 mixed powders (b)

#### **Section 4.4.4: Testing the mechanical properties**

Comparisons made between neat PA12, untreated composites, and treated composites are summarized in **Figure 4-5, Figure 4-6, and Table 4-3** and all data are accessible in [29]. Compared to neat PA12, an improvement of the elastic modulus and strength was found for both untreated and treated composites at clay concentrations of 3% and 5%, whereas at the same time a reduction in the elongation at break was measured. Ultimately, a combination of tensile modulus, tensile strength and elongation must be considered [30]. It was found, in the current study, that the best combination of these properties was obtained at 3% treated C30B/PA12. This reveals that the plasma treatment does not prevent the agglomeration of nanoclay at higher nanoclay loadings. As can be seen from the table in **Figure 4-5 and Table 4-3**, adding the TC at a concentration of 3% has increased, the elastic modulus and tensile strength by ~19% and ~9% respectively (compared with neat PA12), with a simultaneous reduction in the elongation at break by ~24%. Both exceed the performance of clay/PA12 laser sintered nanocomposites with the same clay loading reported in [5]. The elongation of treated composite that decreased by (~24%) is smaller than that obtained from the untreated, which is ~52% (see **Figure 4-7**).

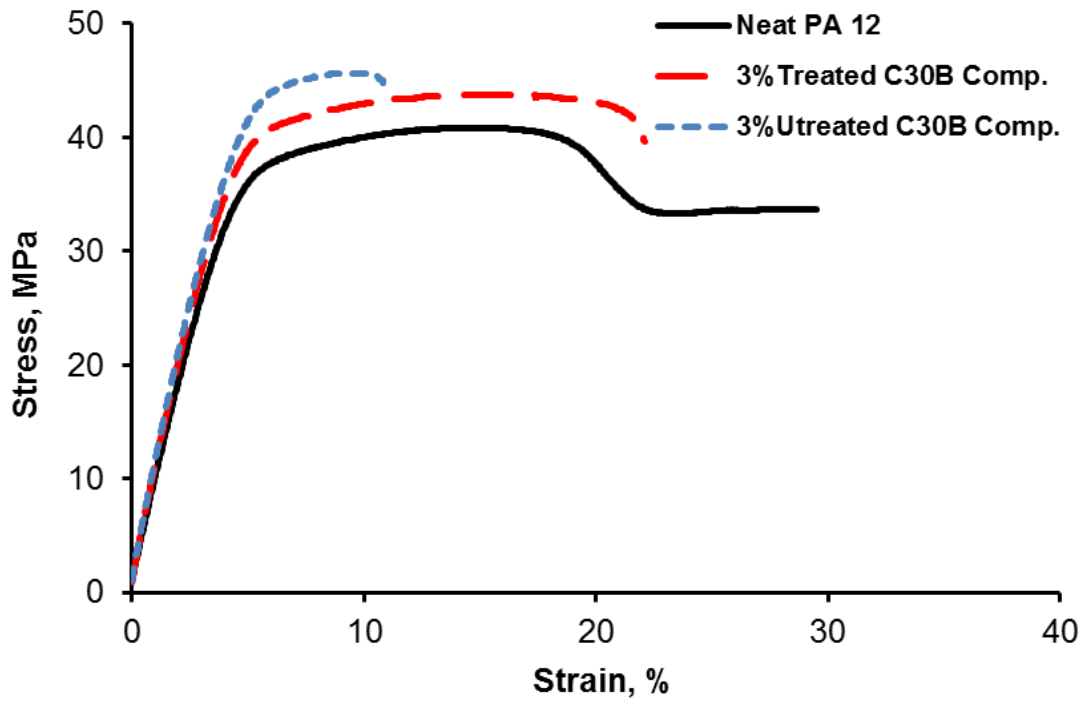


*Figure 4-5: Tensile test curves of PA12 and 3% C30B composites (treated and untreated). Each curve is almost the best in tensile strength.*

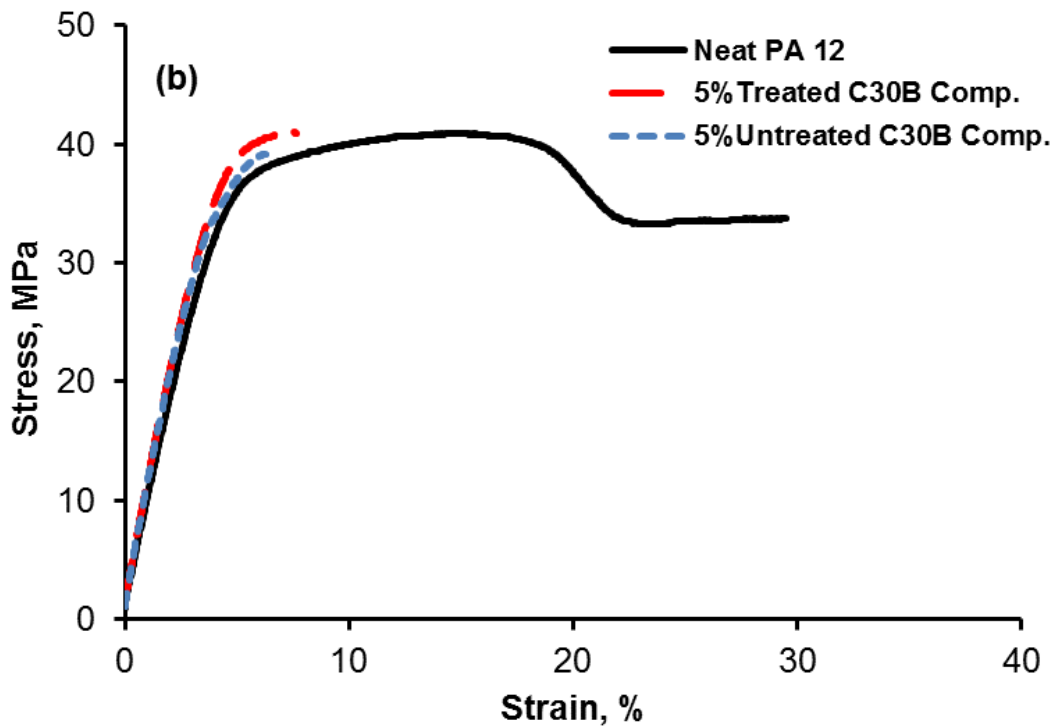


*Figure 4-6: Tensile test curves of PA12 and 5% C30B composites (treated and untreated). Each curve is almost the best in tensile strength.*

**Table 4-3:** Summary of the tensile test results of PA12 and composites (3% and 5% treated and untreated C30B).

<b>Material</b>	<b>Elastic Modulus, Mpa</b>	<b>Tensile Strength, MPa</b>	<b>Elongation at break, %</b>
<b>Neat PA12</b>	853.3±28	39.6±0.68	24.16±1.3
<b>3% Treated Comp.</b>	1011.7±10	43±0.41	18.4±2.02
<b>3% Untreated Comp.</b>	971.7±21.3	43.7±0.78	11.7±1.63
<b>Material</b>	<b>Elastic Modulus, MPa</b>	<b>Tensile Strength, MPa</b>	<b>Elongation at break, %</b>
<b>Neat PA12</b>	853.3±28	39.6±0.68	24.16±1.3
<b>5% Treated Comp.</b>	998.3±17	40.3±0.35	9.17±1.34
<b>5% Untreated Comp.</b>	967±24.2	41.2±1.5	8.06±1.19

The SEM gave further evidence of the ductile fracture for treated composite as shown in **Figure 4-7 (inset i)**. Incorporation of the rigid clay strengthens the matrix polymer but it also leads to a reduced ductility and brittle fracture, as expected [14]. In addition, the poor interaction between the nonorganic clay and organic polymer is not enough to resist the axial force. Micro-voids will be presented as a result of the bad dispersion [17]. The micro-voids may develop to initiate a micro crack and the propagated cracks will lead to a brittle fracture. Hence, our results suggest that the treated clay may have a stronger interaction with PA12 than the untreated clay.



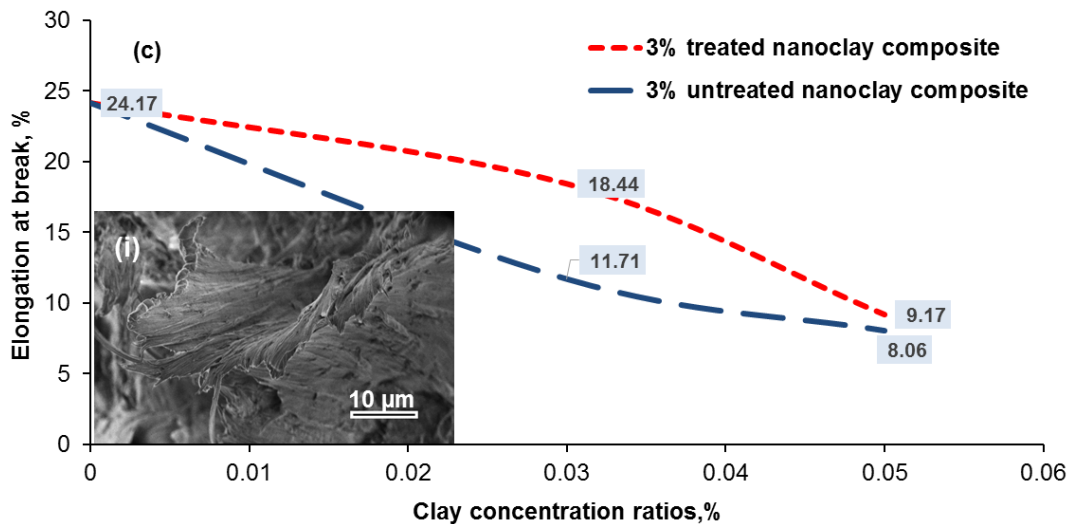


**Figure 4-7:** The elongation at break values of treated and untreated composites, and the SEM image of 3% treated C30B composite showing features of ductile fracture (Inset (i)).

A notable result from the tensile testing is the reduction in the variation of the elastic modulus results between different specimens, but only in the case of adding the treated clay to PA12, as shown in the tables of **Figure 4-5**. This is attributed to a more homogeneous distribution and better dispersion of the treated C30B within the PA12 powders and ultimately the composite (as evidenced by the SEM images of powders and fracture surfaces respectively).

The incorporation of clay at high concentration resulted in less strengthening [5] and reduced ductility [17]. Similarly, our results at 5% concentration showed that the strength and elastic modulus hardly improved. Moreover, the elongation at break was decreased dramatically by 62% treated composite compared with PA12.

**Figure 4-8(a&b)** (from supporting information) from the SEM images at low magnifications show the difference between two fracture surfaces: (1) the untreated C30B based composite exhibits brittle fracture areas, and (2) the treated C30B fracture surface (second fracture) shows a more ductile and uniform surface, presumably due to the avoidance of micron-sized agglomerates, which was the main aim of this work. The

presence of agglomerations may cause poor interfacial bonding and microcracks resulting in poor mechanical properties and brittle fractures. The effect of plasma treatment on nano-scale dispersion was not shown here in this study. Therefore, further optimisation of the plasma treatment should focus on the nano-scale dispersion (e.g., exfoliation and intercalation), which will be investigated in future work.

#### **Section 4.5: Conclusion**

The hot-stage microscopy has been used successfully to determine suitable processing temperatures to fabricate nanoclay-Polyamide 12 composites, while DSC has been shown to be less suited for process optimisation, as it did not reveal the difference in melting behavior for composite powders clearly.

The nanoclay/Polyamide 12 composites obtained with powders, made in a dry mixing process of plasma treated nano-clay with PA12, through downward heat sintering compare favourably to other mixing process, previously described in the literature, and are therefore encouraging for the use in Laser Sintering. Downward heat sintering was used to predict a suitable powder bed temperature, which was successfully applied to the Laser Sintering of the nanocomposite powders.

The current problem addressed is the avoidance of the micron scale aggregates, which has been achieved using a plasma treatment technique. It has been demonstrated that large clay aggregates can be avoided through the use of plasma treatment leading to smaller variations in mechanical properties between different test specimens.

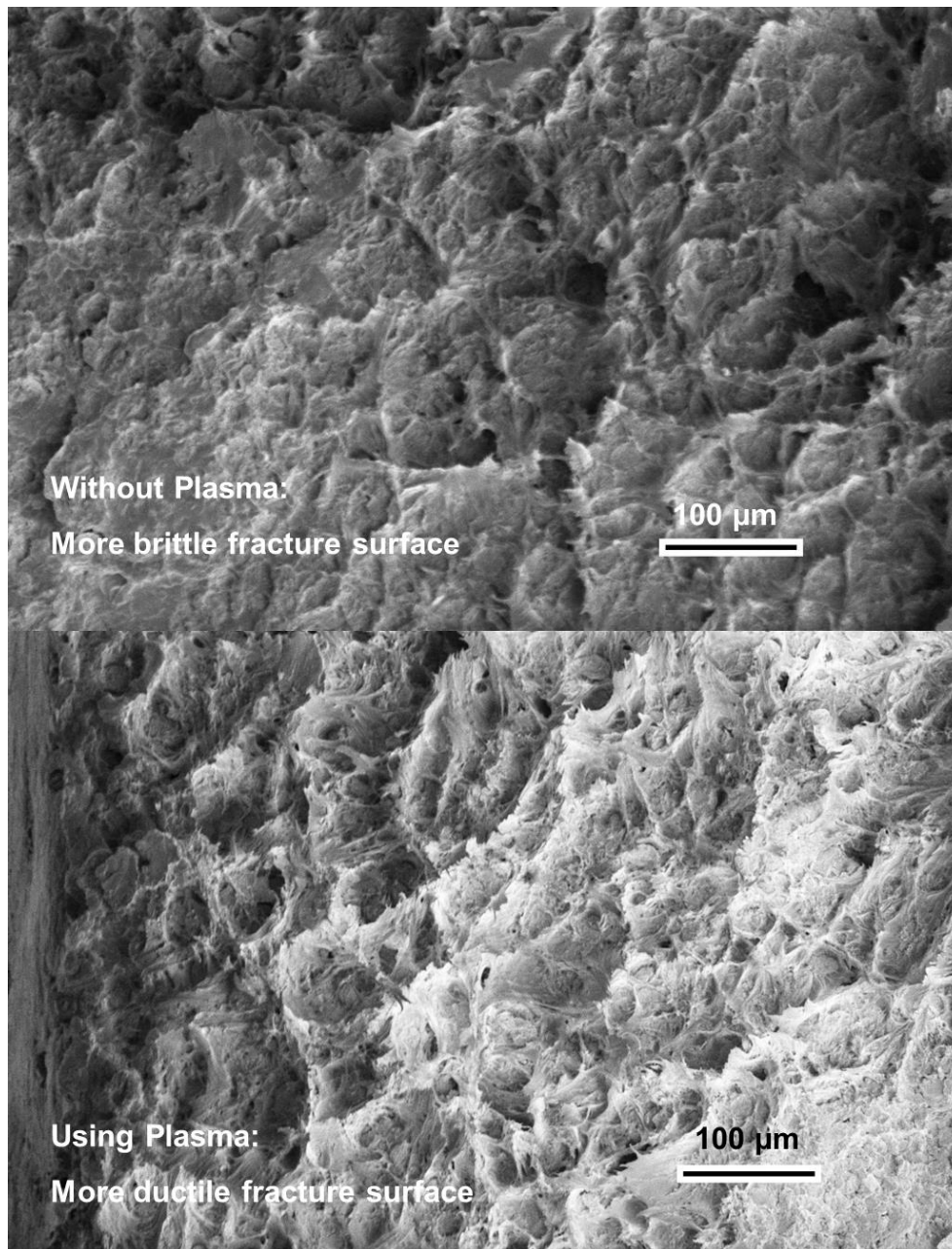


*Figure 4-8 Low magnification SEM images of the fracture surface of untreated 3% C30B composite in which more brittle fracture was occurred with no clear deformation before fracture (a) and 3% treated C30B composite indicating the sample was plastically deformed before fracture (b).*

#### **Section 4.6:References**

- [1] T. McNally, W. R. Murphy, C. Y. Lew, R. J. Turner, and G. P. Brennan, "Polyamide-12 layered silicate nanocomposites by melt blending," *Polymer (Guildf)*, vol. 44, no. 9, pp. 2761–2772, 2003.
- [2] C. Gunasingh, S. Soundararajan, and K. Palanivelu, "Studies on Mechanical,

- Thermal properties and Characterization of Nanocomposites of Nylon-6 – Thermoplastics Poly Urethane Rubber [TPUR] blend,” *IOSR J. Appl. Chem.*, vol. 4, no. 1, pp. 65–75, 2013.
- [3] J. W. Cho and D. R. Paul, “Nylon 6 nanocomposites by melt compounding,” *Polymer (Guildf)*, vol. 42, no. 3, pp. 1083–1094, 2001.
- [4] K. Kalaitzidou, S. Athreya, C. Chun, and S. Das, “Laser Sintering vs Melt Compounding: A New Approach For Functionally Graded Polymer Nanocomposites,” *17th Int. Conf. Compos. Mater.*, 2009.
- [5] P. K. Jain, P. M. Pandey, and P. V. M. Rao, “Selective laser sintering of clay-reinforced polyamide,” *Polym. Compos.*, vol. 31, no. 4, pp. 732–743, 2010.
- [6] D. L. Bourell, T. J. Watt, D. K. Leigh, and B. Fulcher, “Performance limitations in polymer laser sintering,” *Phys. Procedia*, vol. 56, no. C, pp. 147–156, 2014.
- [7] H. Zarringhalam, N. Hopkinson, N. F. Kamperman, and J. J. de Vlieger, “Effects of processing on microstructure and properties of SLS Nylon 12,” *Mater. Sci. Eng. A*, vol. 435–436, pp. 172–180, 2006.
- [8] C. E. Majewski, H. Zarringhalam, D. Toon, U. Ajoku, N. Hopkinson, and M. P. Caine, “The use of off-line part production to predict the tensile properties of parts produced by Selective Laser Sintering,” *J. Mater. Process. Technol.*, vol. 209, no. 6, pp. 2855–2863, Mar. 2009.
- [9] J. P. Kruth, X. Wang, T. Laoui, and L. Froyen, “Assembly Automation Lasers and materials in selective laser sintering Article information.”
- [10] H. Zarringhalam, C. Majewski, and N. Hopkinson, “Degree of particle melt in Nylon-12 selective laser-sintered parts,” *Rapid Prototyp. J.*, vol. 15, no. 2, pp. 126–132, 2009.
- [11] J. Bai, R. D. Goodridge, R. J. M. Hague, and M. Song, “Improving the mechanical properties of laser-sintered polyamide 12 through incorporation of carbon nanotubes,” *Polym. Eng. Sci.*, vol. 53, no. 9, pp. 1937–1946, Sep. 2013.
- [12] J. Bai, R. D. Goodridge, R. J. M. Hague, M. Song, and M. Okamoto, “Influence of carbon nanotubes on the rheology and dynamic mechanical properties of polyamide-12 for laser sintering,” *Polym. Test.*, vol. 36, pp. 95–100, 2014.

- [13] R. D. Goodridge *et al.*, “Processing of a Polyamide-12/carbon nanofibre composite by laser sintering,” *Polym. Test.*, vol. 30, no. 1, pp. 94–100, 2011.
- [14] C. Z. Yan, Y. S. Shi, J. S. Yang, and J. H. Liu, “An organically modified montmorillonite/nylon-12 composite powder for selective laser sintering,” *Rapid Prototyp. J.*, vol. 17, no. 1, pp. 28–36, 2011.
- [15] N. Fedullo, E. Sorlier, M. Sclavons, C. Bailly, J. M. Lefebvre, and J. Devaux, “Polymer-based nanocomposites: Overview, applications and perspectives,” *Prog. Org. Coatings*, vol. 58, no. 2–3, pp. 87–95, 2007.
- [16] P. Singla, R. Mehta, and S. N. Upadhyay, “Clay Modification by the Use of Organic Cations,” *Green Sustain. Chem.*, vol. 02, no. 01, pp. 21–25, 2012.
- [17] I. Y. Phang *et al.*, “Morphology, thermal and mechanical properties of nylon 12/organoclay nanocomposites prepared by melt compounding,” *Polym. Int.*, vol. 54, no. 2, pp. 456–464, 2005.
- [18] K. Fatyeyeva and F. Poncin-Epaillard, “Sulfur dioxide Plasma Treatment of the Clay (Laponite) Particles,” *Plasma Chem. Plasma Process.*, vol. 31, no. 3, pp. 449–464, Jun. 2011.
- [19] A. T. Djowe, S. Laminsi, D. Njopwouo, E. Acayanka, and E. M. Gaigneaux, “Surface Modification of Smectite Clay Induced by Non-thermal Gliding Arc Plasma at Atmospheric Pressure,” *Plasma Chem. Plasma Process.*, vol. 33, no. 4, pp. 707–723, Aug. 2013.
- [20] M. H. Shamsi, M. Luqman, F. Basarir, J. S. Kim, T. H. Yoon, and K. E. Geckeler, “Plasma-modified halloysite nanocomposites: Effect of plasma modification on the structure and dynamic mechanical properties of halloysite-polystyrene nanocomposites,” *Polym. Int.*, vol. 59, no. 11, pp. 1492–1498, 2010.
- [21] R. Scaffaro and A. Maio, “Enhancing the mechanical performance of polymer based nanocomposites by plasma-modification of nanoparticles,” *Polym. Test.*, vol. 31, no. 7, pp. 889–894, 2012.
- [22] G. M. Vasquez, C. E. Majewski, B. Haworth, and N. Hopkinson, “A targeted material selection process for polymers in laser sintering,” *Addit. Manuf.*, vol. 1, pp. 127–138, 2014.

- [23] Q. Wan *et al.*, “Angle selective backscattered electron contrast in the low-voltage scanning electron microscope: Simulation and experiment for polymers,” *Ultramicroscopy*, vol. 171, pp. 126–138, Dec. 2016.
- [24] R. R. Hegde, G. S. Bhat, and B. Deshpande, “Morphology and properties of nylon 6 blown films reinforced with different weight percentage of nanoclay additives,” *Int. J. Polym. Sci.*, vol. 2012, pp. 1–14, Jun. 2012.
- [25] T. D. Fornes and D. R. Paul, “Modeling properties of nylon 6/clay nanocomposites using composite theories,” *Polymer (Guildf)*, vol. 44, no. 17, pp. 4993–5013, 2003.
- [26] N. Hopkinson, C. E. Majewski, and H. Zarringhalam, “Quantifying the degree of particle melt in Selective Laser Sintering®,” *CIRP Ann. - Manuf. Technol.*, vol. 58, no. 1, pp. 197–200, 2009.
- [27] V. Skrockiene, K. Žukiene, and S. Tučkute, “Properties of Recycled Thermoplastic Polyurethane Filled with Plasma Treated Bentonite,” *Plasma Process. Polym.*, vol. 12, no. 11, pp. 1284–1292, 2015.
- [28] P. Bhagabati, T. K. Chaki, and D. Khastgir, “Panoptically exfoliated morphology of chlorinated polyethylene (CPE)/ethylene methacrylate copolymer (EMA)/layered silicate nanocomposites by novel in situ covalent modification using poly( $\epsilon$ -caprolactone),” *RSC Adv.*, vol. 5, no. 48, pp. 38209–38222, 2015.
- [29] A. Almansoori, C. Rodenburg, and C. Majewski, “Tensile test results of Nylon12 and its composites (3% and 5% of nanoclay), Figshare {<https://dx.doi.org/10.15131/shef.data.4063269.v1>},” 2016.
- [30] B. Chen and J. R. G. Evans, “Impact strength of polymer-clay nanocomposites,” *Soft Matter*, vol. 5, no. 19, p. 3572, Sep. 2009.

## **Chapter 5: Novel Plasma Treatment for Preparation of Laser Sintered Nanocomposite Parts**

### **Section 5.1: Abstract**

*Polymer Laser Sintering (LS) is a well-known Additive Manufacturing process, capable of producing highly complex geometries with little or no cost penalty. However, the restricted range of materials currently available for this process has limited its applications. Whilst it is common to modify the properties of standard LS polymers with the inclusion of fillers e.g. nanoclays, achieving effective dispersions can be difficult. The work presented here investigates the use of plasma treatment as a method of enhancing dispersion with an expectation of improving consistency and surface quality of laser sintered nanocomposite parts. To enable the preparation of polyamide 12 nanocomposite powder for applications in LS, plasma surface modification using Low Pressure Air Plasma Treatment was carried out on two nanoclays: Cloisite 30B (C30B) and Nanomer I.34TCN (I.34TCN). Plasma treatment strongly reduced the aggregation of the nanoclay (C30B and I.34TCN) particles, and powders displayed higher decomposition temperatures than those without plasma treatment. LS parts from neat polyamide 12, untreated I.34TCN and plasma treated I.34TCN composites were successfully produced with different complex shapes. The presence of well dispersed plasma treated nanoclays was observed and found to be essential for an improved surface quality of LS fabricated which was achieved only for plasma treated I.34TCN. Likewise, some mechanical properties could be improved above that of PA12 by incorporation of treated I.34TCN. For example, the elastic modulus of plasma treated composites was higher than that of polyamide 12 and the untreated composite. In the case of the ultimate strain, the plasma treated composite performed better than untreated and results had a reduced variation between samples. This illustrates the*

*feasibility of the use of plasma treatments on nanoclays to improve the properties of LS parts, even though further studies will be required to exploit the full potential.*

## **Section 5.2:Introduction**

This study explores the effect of the plasma treatment process on the physico-chemical properties of two organo-modified nanoclay surfaces (Cloisite 30B (C30) and Nanomer I.34 TCN (I.34TCN) and the consequences for their applications in laser sintering (LS) polymer nanocomposites. LS is designed to build 3-dimensional (3D) products with complex and accurate geometries from powdered materials without the need for moulds or patterns [1]–[3]. Firstly, polymeric powder is preheated to a temperature below its melting point for a certain time. Then, a CO<sub>2</sub>-laser selectively fuses the heated powder to produce products layer by layer. LS parameters such as laser power, scan speed, scan spacing and layer thickness can be varied for optimised properties [4]. However, a limited selection of materials and inconsistent mechanical properties are still challenges, restricting the overall potential of LS [5]–[8]. Porosity and surface quality also affect the functions of the end-use parts [9], [10]. Pore formation is highly affected by the melt flow and thermal stability and is also influenced by the powder particle shape, distribution and processing parameters (laser power and scan speed) [7], [11], [12].

The inclusion of nanomaterials into polymers has the potential to provide performance benefits improving part quality and offering new applications [8]. However, the dispersion of the nanomaterials still remains a critical issue for the preparation of Laser Sintered nanocomposites [13]. Poor interaction between polymers (organics) and nanofillers (e.g. nanoclays) leads to a nanoparticle micro-aggregation phenomenon and is a key issue for the mechanical properties [14]. Aggregated nanoclays can be expected to improve polymer



rigidity but reduce toughness and elongation [15]. Here, we exploit the potential of plasma treatment to address the poor dispersion of the nanoclay in the polymer matrix.

Layered silicate based nanomaterials have attracted great interest in the field of polymer nanocomposites due to their significant impact on the intrinsic properties of the polymer matrix. The smectite mineral clay group of phyllosilicates family has been widely used in industry since the mid-nineteenth century [16]. Montmorillonite (MMT), saponite (SP), and hectorite (HT) and other uncommon species are all listed in the smectite group, and montmorillonite ( $[Al_{1.67}Mg_{0.33}(Na_{0.33})]Si_4O_{10}(OH)_2$ ) [17] is the most widely used clay for reinforcing polymers. The mineral montmorillonite is composed of octahedral sheet (silica) sandwiched between two tetrahedral sheet (alumina) to form the most familiar 2:1 structure. The chemical structures, physical specifications and uses of the smectite group and other layered silicate clays are well-detailed in the literature [18]–[21]. Natural montmorillonite is a hydrous phyllosilicate with a negatively charged layer caused by the substitution of silicon with aluminum in the tetrahedral layer and the replacement of aluminum with magnesium in the octahedral layer. The negative charge is neutralised by mineral cations such as sodium, calcium or potassium resulting in a regular stack of tetrahedral-dioctahedral layers. The pristine montmorillonite clay is hydrophilic in nature and is consequently immiscible with hydrophobic polymers such polyamides [14]. A chemical surfactant is commonly used to increase the interlayer space (gallery) and render the hydrophilic into organophilic clay, in which the interlayer cations  $Na^+$  or  $Ca^{+2}$  are exchanged by an alkylammonium surfactant [22], [23]. This organomodification, however, is a time-consuming method [24]. In addition, organoclay platelets aggregate to form microscale tactoids, resulting in weak properties. Breaking up these aggregates into small sized tactoids or individual platelets requires further expensive or elaborate modifications. Montmorillonite can also be subjected to acid treatments with sulphuric acid ( $H_2SO_4$ ) [25]

or hydrochloric acid (HCl) leading to varying modifications [26]. Such treatments require special conditions to avoid any unacceptable increases of nanoclay acidity.

Therefore, this study aims to avoid the chemical techniques described previously, and to investigate a cheap, simple, and dry (chemical and water free) method for the modification of montmorillonite based nanoclays by Low Pressure Air Plasma Treatment (LP-PT) of composite powders in laser sintering applications. Although some studies on treating the clay/nanoclay (modified or nonmodified) for the reinforcement of polymers were previously carried out [27]–[29], plasma treatment in laser sintering applications is in its infancy [30]. Here we show for the first time that LP-PT of Nanomer (I.34TCN) clay can strongly improve the surface quality of clay/PA12 composite parts fabricated by LS. Thus, this is a unique study on the use of plasma treatment in LS applications, demonstrating for the first time that plasma treatment has the potential to provide crucial performance benefits for laser sintered nanocomposites.

## **Section 5.3: Materials and Materials Processing and Preparation**

### ***Section 5.3.1: Nanoclays***

Two different layered silicates clays were used: Cloisite 30B (C30B) (purchased from Southern Clay products, USA) and Nanomer (I.34TCN) (provided by Sigma Aldrich chemicals, UK). C30B and I.34TCN are montmorillonite-based nanoclays, organomodified with surfactants. The chemical structure and technical information of the surfactants are given in *Table 5-1*. C30B and I.34TCN were selected because they only differ in the structure of the surfactant. The alkyl ammonium salt of the C30B surfactant has a single alkyl tallow whereas two alkyl tallows are used to treat the I.34TCN [31]. However, both surfactants possess a hydroxyl group which may lead to the formation of a hydrogen bond between the hydroxyl group in the surfactant and the polyamide (possessing a polar nature) resulting in a strong interaction between the organic polyamide and organomodified clays

[32]. However, C30B and I.34TCN with the dihydroxyl-surfactant are more likely to suffer decomposition via the Hofmann elimination reaction [33], [34], catalysing the degradation of polymer matrix [14], [35].

**Table 5-1** Surfactants information and specification (according to the suppliers' technical sheets and Ref. [32], [36]).

Clay	Surfactant	Chemical Structure	Content
C30B	Methyl bis-2 hydroxyethyl tallow alkyl quaternary ammonium chloride: [(HE) <sub>2</sub> M <sub>1</sub> T <sub>1</sub> ] HE: Hydroxyethyl M: Methyl (T) Tallow: CH <sub>2</sub> (CH <sub>2</sub> ) <sub>11-15</sub> (CH=CH) <sub>0.5</sub> CH <sub>3</sub>	$  \begin{array}{c}  \text{CH}_2\text{CH}_2\text{OH} \\    \\  \text{CH}_3 - \text{N}^+ - \text{T} \\    \\  \text{CH}_2\text{CH}_2\text{OH}  \end{array}  $	25-30 %
I.34TCN	Methyl dihydroxyethyl hydrogenated tallow ammonium chloride: [(HE) <sub>2</sub> M <sub>1</sub> HT <sub>1</sub> ] HE: Hydroxyethyl M: Methyl (HT) Hydrogenated Tallow: CH <sub>2</sub> (CH <sub>2</sub> ) <sub>12-16</sub> CH <sub>3</sub>	$  \begin{array}{c}  \text{CH}_2\text{CH}_2\text{OH} \\    \\  \text{CH}_3 - \text{N}^+ - \text{HT} \\    \\  \text{CH}_2\text{CH}_2\text{OH}  \end{array}  $	25-30 %

The chemical composition of the Tallow (T) is: of 65% C18, 30% C16, and 5% C14.

N<sup>+</sup>: Quaternary ammonium salt

### Section 5.3.2: Low Pressure Air Plasma Treatment (LP-PT) technique

C30B and I.34TCN were subjected to a plasma treatment using a Low-Pressure Plasma Cleaner Zepto (from Diener Electronics) using ambient air as process gas. C30B was prepared for DHS, while I.34TCN for LS applications. A small quantity (<1 g) of the nanoclay powder was placed as a thin layer in a small glass petri dish. Three petri dishes were then placed inside a cylindrical glass vacuum chamber of the plasma instrument. After evacuating the chamber to a pressure of 0.3 mbar the plasma was generated using a power (100 W) for 1000 s. As only the top-layers of the powder bed in the petri dish are exposed to the plasma, the powder was then turned half way through the stated treatment time. This

procedure was repeated twice before the treated powder was then removed from the dishes and kept it in a sealed glass jar.

***Section 5.3.3: Materials preparation for Downward Heat Sintering (DHS) and laser sintering (LS) applications***

Polyamide 12 (PA12), used as a polymer matrix, were supplied by e-Manufacturing Solutions (EOS) with a trade name of (PA2200). As received PA12 is a thermoplastic and semicrystalline polymer and its chemical formula is  $(C_{12}H_{23}NO)_n$ . Powders (polymers and nanoclays) were mechanically mixed and ultrasonicated prior to sample production via melting (using DHS) or sintering (using LS) processes. Mixing, sonication conditions and material amounts for both processes are found in **Table 5-2**.

**Table 5-2 Laser and Heat Sintering processes parameters**

Clay	Materials weight <sup>1</sup>	Process	Parameters <sup>2</sup>
C30B	50-100g of PA12 3% and 5% plasma treated C30B and untreated C30B	Downward Heat Sintering (DHS) (30min. mixing and 30min. sonicating before sintering)	DHS carried out in a hot press under the following parameters**: PreT 185 °C for all DHS samples (15 min.) PA12: AppT 190 °C (15 min.) Plasma treated C30B/PA12 composite: AppT 192°C (15min.) Untreated C30B/PA12 composite: AppT 195°C (15min.)
I.34TCN	3kg of PA12 3% plasma treated I.34TCN and untreated I.34TCN	Laser Sintering (LS) (1hr. mixing and 30min. sonicating before sintering)	LS parameters are the same for all samples as follows: CO <sub>2</sub> laser with a wavelength of 10.6 μm; Bed temperature 172°C; laser power (energy density***) 13W (0.208 J/mm <sup>3</sup> ), 17W (0.272 J/mm <sup>3</sup> ) and 21W (0.336 J/mm <sup>3</sup> ); laser speed scan 2500mm/sec; layer thickness 0.1mm and scan spacing 0.25mm. Under Nitrogen environment.

\* Materials weight is a minimum one set of samples.

\*\* PreT-Preheating temperature (The hot press lower part temperature); and AppT-Applied temperature (The hot press upper Part Temperature).

\*\*\* The energy densities were determined according to equation developed by Kruth et al [37].

The composite materials of PA12 and C30B nanoclay (treated and untreated) were prepared for DHS method as described in [30]. Briefly, a simple, fast, low-cost and without any applied external pressure method was used to replicate the LS technique by means of a hot press. In the hot press, HS parts were fabricated by supplying heat from the top to powders (PA12 and C30B composites) which were preheated to below its melting temperature (temperatures and other parameters are listed in **Table 5-2**). HS parts left to cool at room temperature before collection. The processing parameters and temperatures described in [30] were optimised via our method through DSC-HSM.

Herein, the treated and untreated I.34TCN composites were prepared for LS applications. LS Parts from those materials (PA12 and I.34TCN composites) were produced horizontally (x and y are the layer directions) at three different laser powers (i.e. 13, 17, and 21 W) as shown in **Figure S5-1(a)** in **Appendix (Supplementary Information)**. Other LS parameters are mentioned in **Table 5-2**. The commercial LS system used for these purposes is Formiga P100 from EOS. PA12 and PA12/I.34TCN powder composites were tested to investigate the powder processing window and particle distribution as shown in **Tables S5- 1** in **Appendix (Supplementary Information)**. In summary, these investigations revealed no significant change in the morphological and thermal properties of the composite powders. Particle sizes of composite powder were slightly reduced at 10%, 50% and 90% compared to the PA12 powder due to the high-speed rotation mixing process used in this study. DSC results showed that the difference between melting and crystallisation temperatures of PA12 was only slightly changed after incorporation of untreated and treated I.34TCN nanoclay.

## **Section 5.4: Materials characterisation and testing**

### ***Section 5.4.1: Scanning electron microscopy (SEM) and Hot Stage***

#### ***Microscopy (HSM)***

A Low Voltage Scanning Electron Microscopy Nova NanoSEM was used for the morphological observation of the clays before and after plasma treatment and LS cross sections produced using PA12 composites with both the treated and untreated nanoclays. An electron beam with low landing energy (2.2 KeV) was used to reduce specimen surface charging and damage. Note that no metal coating was applied to the polymer surface. Secondary electron images were collected with a Through-Lens-Detector (TLD) and a Concentric Back Scatter (CBS) detector was used for higher magnification imaging and with some chemical contrast.

High resolution SEM imaging was performed using a Helios Nanolab G3 UC microscope specifically designed for ultrahigh resolution at low voltages (<1KV). Unlike ordinary SEM analysis, no conductive coating was deposited onto the samples. An accelerating voltage of 1.3 KV, typical vacuum pressure =  $10^{-6}$  mbar, current = 25 pA and a working distance of 4 mm was used. The design of the in-lens detector of this SEM allows the filtering of secondary electron (SE) energy ranges so that only SE below 6 eV are allowed to form the micrographs. This technique has been confirmed to remove the effects of topography [38] and allows the high-resolution imaging of the nanoclay within the composite.

HSM is a promising technique for visualising the coalescence of particles under heating for LS applications. Additionally, this technique allows the direct visualisation of nanoclay particles during the coalescence of the polymer particles. The HSM used here is composed of a BX50 light microscope from Olympus attached to a temperature controlled microscope stage from Linkam. Powders were melted from room temperature to 250 °C at a rate of 10°C/min in order to be comparable with DSC profiles.

#### ***Section 5.4.2: Fourier transform infrared spectroscopy (FTIR)***

To explore the clays' structural and chemical composition changes during the plasma treatments, FTIR spectra was obtained using PerkinElmer Frontier spectrophotometer equipped with a Golden Gate™-single reflection Diamond ATR accessory. FTIR measurements were carried out on nanoclay powders, C30B and I.34TCN (without KBr dilution) by recording 10 scans in the wavenumber range from 400 to 4000  $\text{cm}^{-1}$  at a spectral resolution of 4  $\text{cm}^{-1}$ . Before obtaining spectra from the samples, a background spectrum with no sample was taken as a control.

#### ***Section 5.4.3: Thermogravimetric analysis (TGA)***

The thermal stability and thermal decomposition temperatures of the treated and untreated clays were determined with a Thermogravimetric Analyser (Pyris 1 TGA from PerkinElmer). This is because the organoclay modified with alkylammonium can have two opposing effects on the polymer and composites, i) a barrier effect resulting in an improvement of the thermal stability, and ii) a catalytic effect on the decomposition of the polymer [14]. Thus, it is necessary to investigate the thermal properties of the nanoclay with and without plasma treatment before adding to the polymer matrix. The clay powder was heated, in a nitrogen environment, from 30 °C to 630 °C with a heating rate 10 °C/min.

#### ***Section 5.4.4: Tensile tests***

Tensile tests were carried out on LS samples, according the ASTM D638-02a, using a Tinius Olsen H5KS tensile testing machine fitted with a laser extensometer as shown in **Figure S5-1(b)**. Ultimate stress and strain, and elastic modulus were measured using the Horizon Software. The tensile tests were carried out under the conditions: speed 5mm/min, preload 5N and maximum load cell 5kN. **Figure S5-1c** shows a schematic illustration of a standard tensile test specimen based on the ASTM D638-02a standard.

## Section 5.5: Results and Discussion

### Section 5.5.1: Characterisation analysis and results

#### Section 5.5.1.1: SEM images

The SEM micrographs of the nanoclays C30B and I.34TCN before (as received) and after plasma treatment are shown in *Figure 5-1(a&b)* and *Figure 5-1(c&d)* respectively. C30B nanoclay exhibited a reduction in agglomeration due to the action of the plasma, as displayed in SEM images (using a high resolution CBS detector) in *Figure 5-1(a&b)*. *Figure 5-1a* shows the NT-C30B platelets aggregated to form large and round particles of several microns. In contrast, after LP-PT thin separate sheets of clay can be seen in *Figure 5-1b*.

As noted, *Figure 5-1c*, the untreated I.34TCN nano-platelets were conjoined in micron-size irregular shaped particles. Some of the aggregated particles are relatively large and round or oval in shape (highlighted by arrows in *Figure 5-1d* and thus, a poor micro and nano dispersion within the polymer matrix is expected [39], [40]. LP-PT of clay I.34TCN (*Figure 5-1d*) tended to reduce the agglomerate size to form more open, smaller agglomerates (highlighted by arrows) with visible small holes, confirming the particles responded to the plasma treatment.

These observations were also confirmed by the HSM images in *Figure S5-2* (a and b) during heating of PA12 particles. After PA12 powder coalescence, the untreated I.34TCN particles were aggregated in relatively large nonuniform particles (examples highlighted by red arrows) reducing the contact area which may ultimately adversely affect the properties of the final parts. However, a few dispersed untreated clay particles can also be seen in *Figure S5-2a* which are highlighted by light green arrows. Whilst, the treated I.34TCN particles were well-dispersed (highlighted by light green arrows in *Figure S5-2b*) and reduced agglomerations, and this resulted in an increase of the contact area and improved



the interaction between the clay and polymer matrix. Ultimately, this effect is expected to improve the properties of the final products. Some small aggregated treated clay particles were observed and highlighted by red arrows.

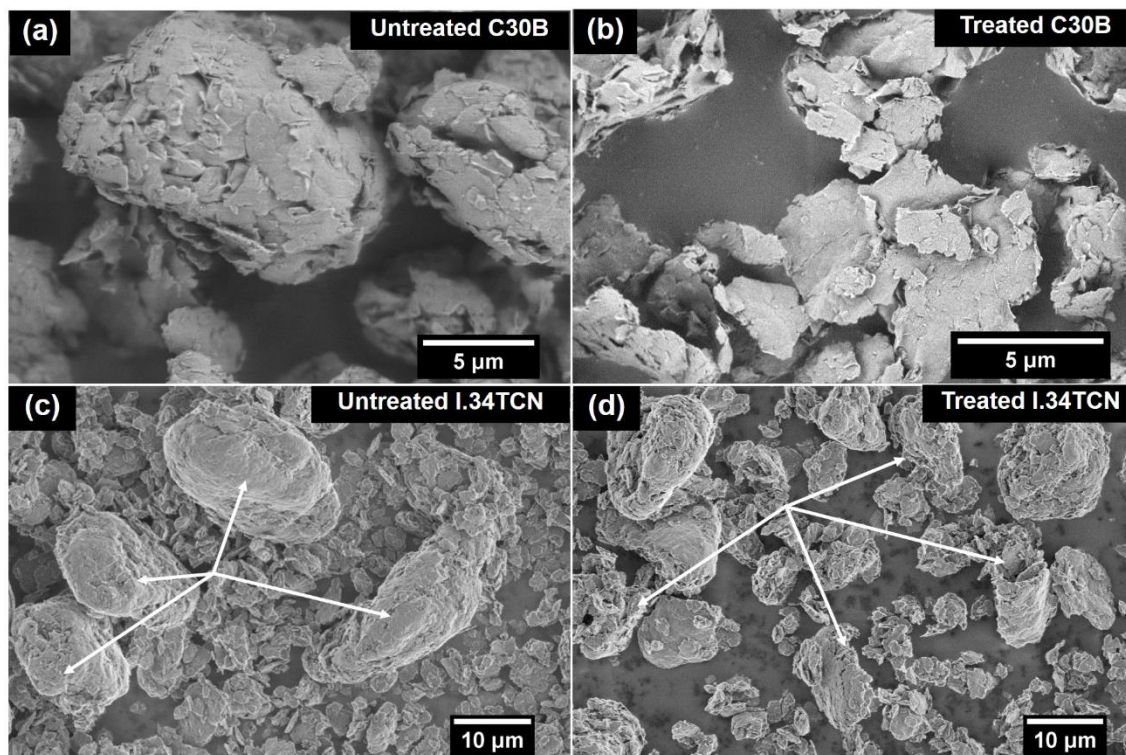


**Figure 5-1** Micrographs of the nanoclays before (as received) and after plasma treatment (a) untreated C30B which are reproduced from [30] under CC-BY-4, (b) treated C30B, (c) untreated I.34TCN, and (d) treated I.34TCN. Arrows in (c) refer to the large, round untreated particles, whereas in (d) they refer to particles were broken in to smaller particles during plasma treatment.

#### Section 5.5.1.2: FTIR Analysis

**Figure 5-2(a&b)** shows the FTIR spectra of untreated and plasma treated nanoclays C30B and I.34TCN respectively, with the major absorption bands positions outlined in four regions. It can be observed that the untreated C30B and untreated I.34TCN nanoclays displayed similar patterns and the intensity of the peaks were approximately the same. The FTIR spectra of C30B and I.34TCN in **Figure 5-2(a&b)** display inorganic montmorillonite peaks at wavenumbers  $\sim 990\text{ cm}^{-1}$  and  $\sim 1116\text{ cm}^{-1}$  which are related to the stretching vibrations of Si-O-Si and Si-O respectively,  $\sim 1640\text{ cm}^{-1}$  is assigned to O-H bending, and

$\sim 3360\text{ cm}^{-1}$  and  $\sim 3626\text{ cm}^{-1}$  correspond to O-H stretching for the adsorbed water and the silicate [33]–[41].

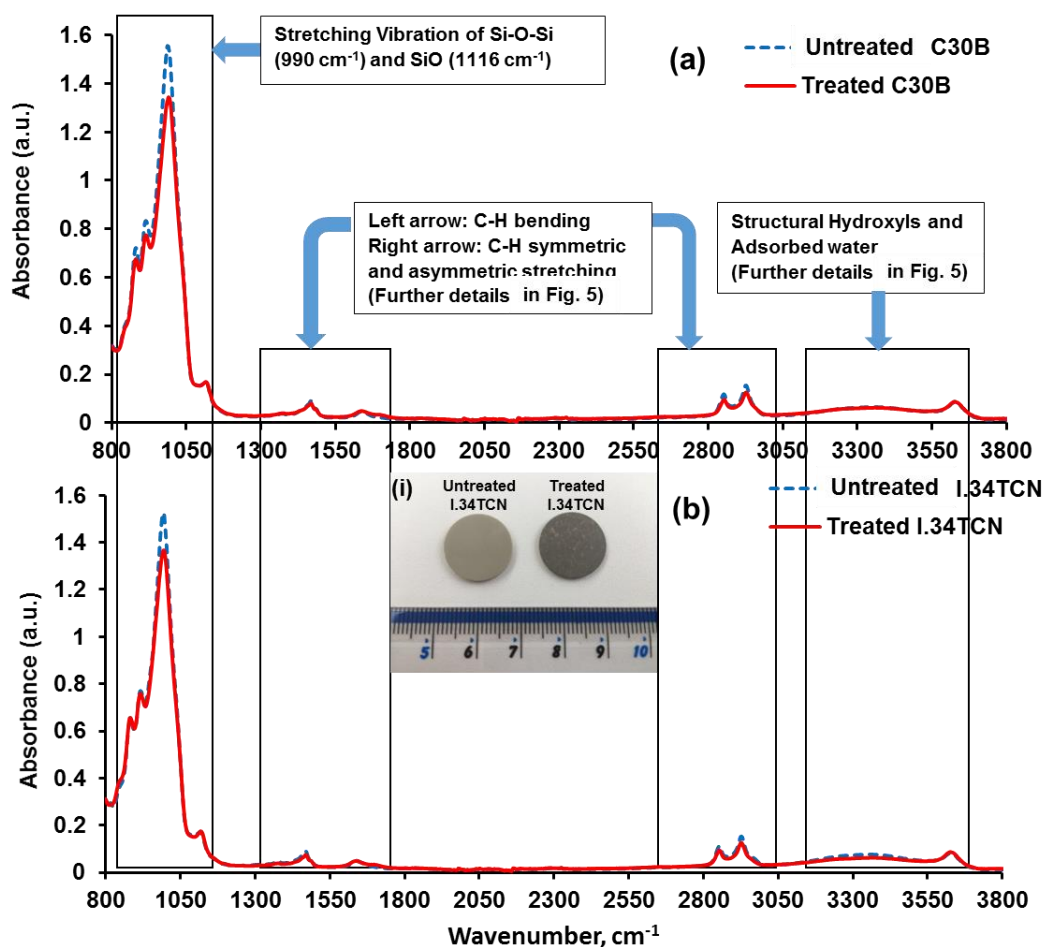


**Figure 5-2** FTIR spectra of untreated and plasma treated nanoclays (a) C30B, (b) I.34TCN; Pressed discs of the untreated and treated I.34TCN powders pictured in inset (i) shows a clear change in colour after air plasma.

In addition, the organic surfactant has displayed peaks attributed to the C-H vibration at  $\sim 1470\text{ cm}^{-1}$  (bending) and two adjacent peaks at  $\sim 2852\text{ cm}^{-1}$  and  $\sim 2926\text{ cm}^{-1}$  (symmetric and asymmetric stretching) [33]–[41]. The wide wavenumber range in **Figure 5-2** reveals that the strongest peak appeared at  $990\text{ cm}^{-1}$ . Further changes can be seen in the range of ( $1200\text{--}2000\text{ cm}^{-1}$  and  $3250\text{--}3750\text{ cm}^{-1}$ ) as shown in **Figure 5-3**.

As observed, a reduction in the intensity of the Si-O-Si peak related to the spectra of C30B and I.34TCN (**Figure 5-3(a&d)**) which is coupled with an intensity change of the peak

located at  $\sim 3626\text{ cm}^{-1}$  (hydroxyl stretching) in *Figure 5-3(c&f)* confirmed that the LP-PT has made structural changes in the mineral portion (MMT) of the organoclays. It is suggested that the chemical change is attributed to a partial breakdown of the surface silicate with a formation of a new hydroxyl [28]. The broad peak centred at about  $\sim 3360\text{ cm}^{-1}$  corresponding obtained from adsorbed water was also with adsorbed water also decreased in the C30B and I.34TCN spectra, as shown in *Figure 5-3(c&f)*, this could be due to the increased temperature within the plasma chamber. The influence of the plasma on the nanoclays' organic surfactants is observed as the peak associated with C-H bending ( $\sim 1470\text{ cm}^{-1}$ ) decreased and a peak at  $\sim 1695\text{ cm}^{-1}$  owing to the carboxylic acid [33] has become more intense [42]. In addition, the two adjacent peaks at  $\sim 2852\text{ cm}^{-1}$  and  $\sim 2926\text{ cm}^{-1}$  assigned to symmetric and asymmetric C-H stretching of the organic surfactant of C30B and I.34TCN also decreased as shown in *Figure 5-3(b&e)*.

*Figure 5-4(a&b)* shows the TGA thermograms of the untreated and plasma treated C30B and I.34TCN, respectively. Generally, the organic modified nanoclays decompose in four steps: (i) desorption of water (loss of free water) below  $200\text{ }^{\circ}\text{C}$ , and dehydration of hydrated cations (loss of the interlayer hydration water only if there is some unexchanged  $\text{Na}^+$  ions); (ii) decomposition of the organic surfactant, in the range  $200\text{ }^{\circ}\text{C}$  to  $500\text{ }^{\circ}\text{C}$ ; (iii) dihydroxylation of MMT (structural water) in the temperature range  $500\text{-}800\text{ }^{\circ}\text{C}$  and finally (iv) organic carbon reactions above  $800\text{ }^{\circ}\text{C}$  [22], [43], [44]. As shown in *Figure 5-4*, the decomposition patterns of the untreated and plasma treated nanoclays (treated C30B and treated I.34TCN) are similar. However, the plasma treated C30B and I.34TCN exhibited higher decomposition temperature than the untreated ones at all the degradation steps.

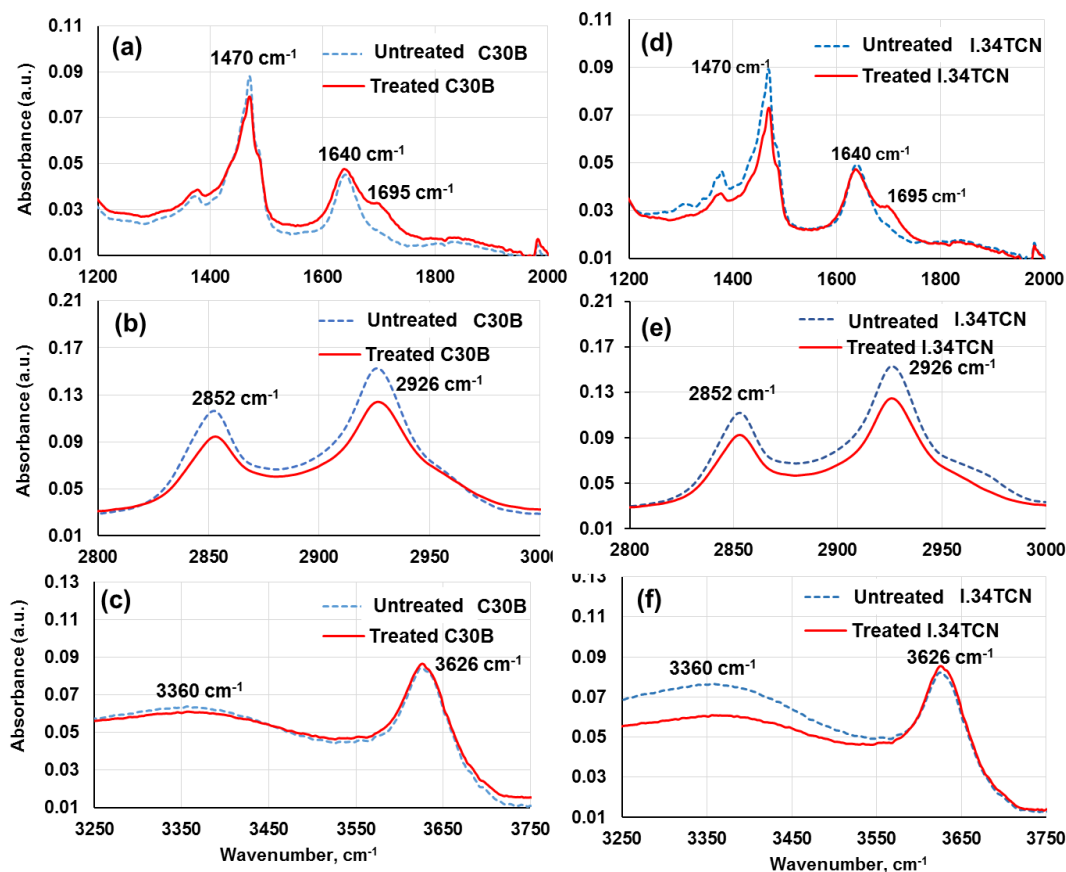


**Figure 5-3** FTIR spectra of untreated and treated nanoclays (a-c) C30B and (d-f) I.34TCN.

### Section 5.5.1.3: Thermogravimetric analysis (TGA) Results

For a deeper insight, the decomposition temperatures at onset point (5%) and 10% and of the untreated and plasma treated C30B and I.34TCN obtained from **Figure 5-4** are summarised in *inset Tables i and ii*. The first observation is that, at the early stage degradation (below 200 °C), the difference in the decomposition temperature between the untreated C30B and I.34TCN is limited (5 °C at 5% weight loss) compared to the degradation at higher temperatures (such as at 10% the difference 20.9 °C) of the untreated nanoclays' degradation patterns. It is attributed to the fact that the region at the temperature below 200 °C is assigned mostly to the free water (and possibly interlayer water loss) in which the organoclays are expected to have a similar water content [44]. In contrast, above 200 °C the organic surfactant is the main degraded substance [44] and, as mentioned earlier in this study, the organic surfactants of C30B and Nanomer I.34TCN are not the same since

C30B surfactant has a single alkyl tallow whereas I.34TCN has two alkyl tallows. Thus, as can be seen in *inset Tables* in **Figure 5-4**, the decomposition temperature of I.34TCN is higher than those of C30B at the temperature where the organic substance is involved. In addition, the plasma shifts the decomposition temperatures of C30B and I.34TCN to higher values at all steps as shown in **Figure 5-4** and *inset Tables*. This plays a critical role in maintaining the thermal stabilisation of the composite powder at higher temperature or laser power for the LS fabricated parts and even to the surrounding powder for the recovering process.

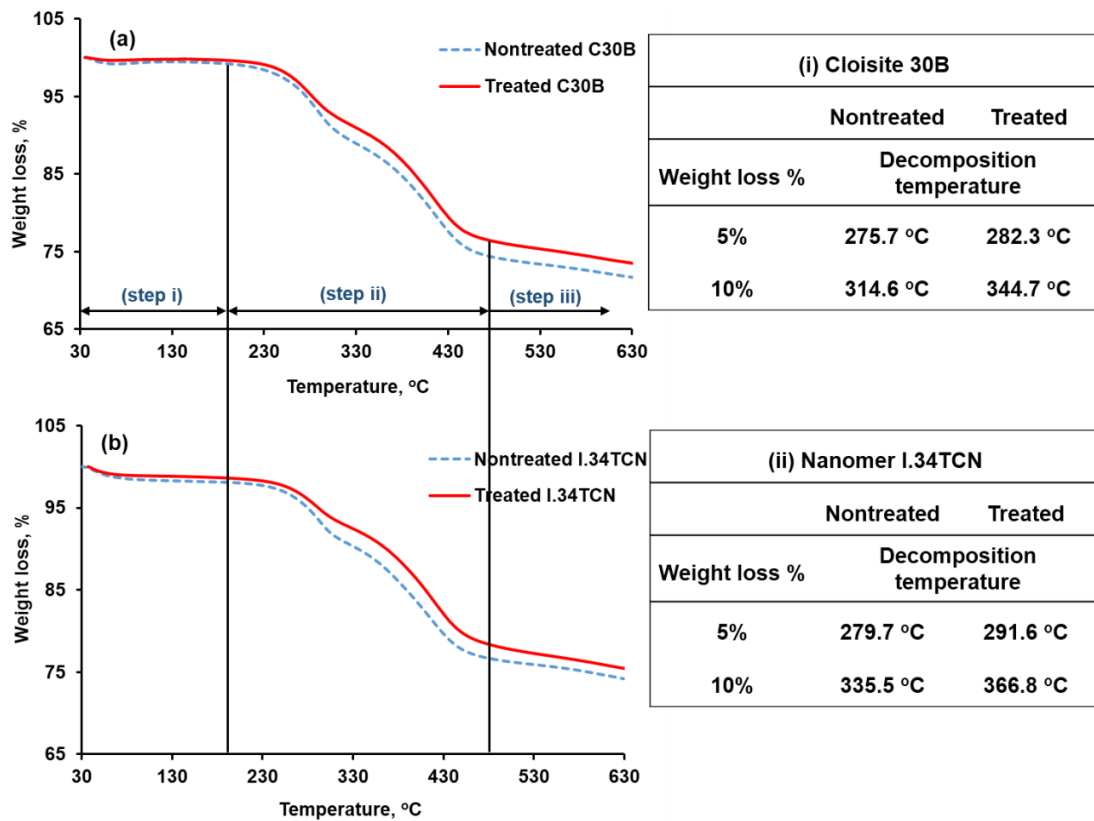


**Figure 5-4** TGA thermograms of untreated and plasma treated nanoclays (a) C30B, (b) I.34TCN. Inset Tables (i) and (ii) are the decomposition temperatures of untreated and plasma treated C30B and I.34TCN.

We suggest that the above TGA results coupled with the FTIR analysis shows that the plasma results in two actions i) the thermal stability of C30B and I.34TCN was improved although some volatiles were lost during plasma exposure and ii) the formation of a new

hydroxyl at the surface of the MMT converting carbons from the alkylic tail to carboxyl [42].

### ***Section 5.5.2: Influence of plasma treatment on the quality of Laser sintered parts***

In our previous works [30], [45], the organonano clay C30B (treated and untreated) was used to reinforce the PA12 using a new, simple and cheap fabrication method: Downward Heating Sintering (DHS). Previous work [30] aimed to replicate the laser sintering process whilst minimising powder waste as DHS method requires 50-100 grams compared to the typical 3 kg required by LS. As noted earlier, both C30B and I.34TCN are almost similar since both are MMT-based nanoclays modified by dihydroxyl alkyl ammonium organic surfactant. Moreover, these thermal investigations showed that the I.34TCN are more thermally stable than C30B. Hence, I.34TCN was the only nano-clay used for the following used for LS investigations.

DHS was used to determine LS parameters [30], which were then used to fabricate the PA12 and composites (3% untreated I.34TCN and 3% treated I.34TCN). Different samples with different shapes and complexities were built successfully by LS as shown in **Figure 5-5**. Visual inspection showed that there was no shrinkage or failed complex shapes for all of the built objects. The colour of LS samples is as follows: neat PA12 -white; untreated I.34TCN composite -light beige and treated I.34TCN composite -light grey. The colour differences imply that the plasma treatment of nanoclay affects the nanocomposite formation during LS.

The microstructure of cross-sectioned LS parts (bed temperature 172 °C and laser power 21W) built from neat PA12, untreated and treated I.34TCN composites obtained by SEM are shown in **Figure 5-6**. The surface morphology of two different areas of each specimen were investigated: top left and middle sections of neat PA12 (**Figure 5-6(a)**) and

*Figure 5-6b*), untreated I.34TCN composite (*Figure 5-6c* and *Figure 5-6d*) and treated I.34TCN composite (*Figure 5-6e*), and *Figure 5-6f*). The fracture surface of the PA12 sample displays various irregular pores. Enlarged internal pores are surrounded by unmelted or partially melted particles on the edges of the part. Heterogeneous rough and porous surfaces are also observed in areas far from the edges of the part as shown in *Figure 5-6b*, with the elongated shape of the pores potentially demonstrating some ductile fracture.

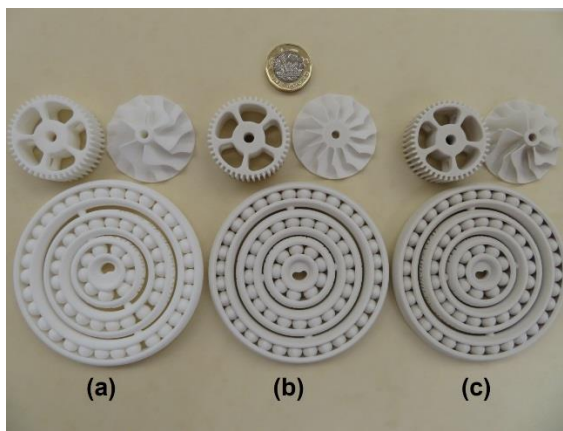


*Figure 5-5* Different shaped-LS samples (a) Neat PA12, (b) 3% untreated I.34TCN composite and (c) 3% plasma treated I.34TCN composite

The incorporation of nanoclay (untreated and treated I.34TCN) has altered the surface morphologies (see *Figure 5-6(c-f)*) where relatively flat and uniform cross sections are observed. Micro-holes and cracks were also observed in *Figure 5-6(c-f)* (marked by arrows) which are attributed to the interlayer spaces or voids generated by adjacent particles that did not fuse completely [46]. However, the composite containing the treated I.34TCN (*Figure 5-6e*) reveals a more uniform surface than the untreated I.34TCN composite shown in *Figure 5-6c*. Moreover, the former fracture surface has smaller sized micro-pores and fewer unmelted/partly melted particles than the fracture surface of the composite containing the untreated I.34TCN (*Figure 5-6c*). Furthermore, larger cracks were observed in the untreated I.34TCN composite specimen (*Figure 5-6d*) whilst the treated I.34TCN

composite (*Figure 5-6f*) has relatively few pores compared to the untreated one in parallel zones.

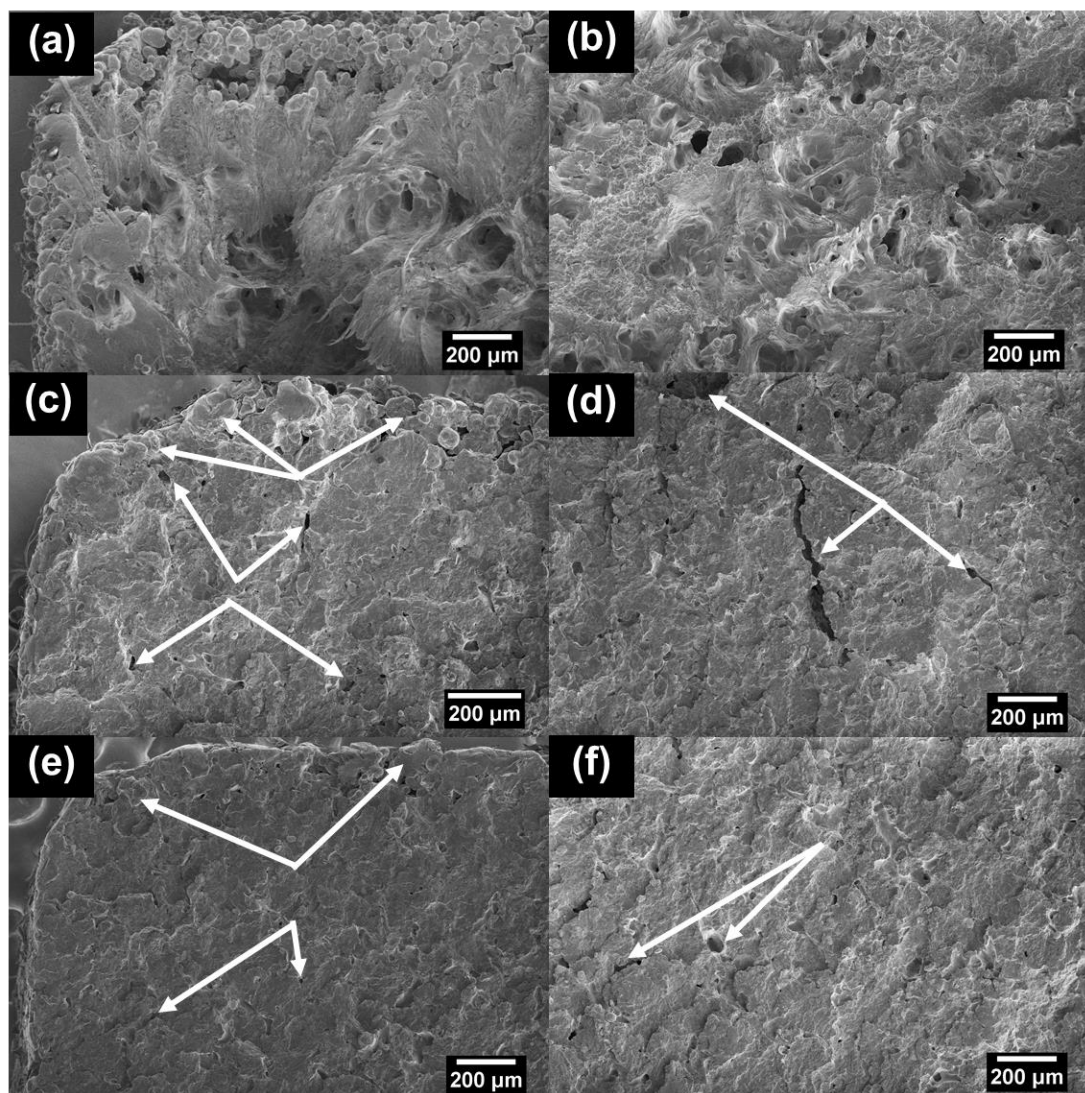


*Figure 5-6* Cross-sectional SEM images of the LS specimen (a-b) neat PA12, (c-d) untreated I.34TCN composite (e-f) treated I.34TCN composite. Images on the left display the top left region of the composites whilst the images on the right are of the middle regions. The white arrows highlight cracks and pores. PA12 fractures (a-b) are more ductile but more porous, while Figures (c-f) from the composite materials are more brittle fractures.

This suggests that the interaction between the LP-PT treated nanoclay (treated I.34TCN) and polymer (PA12) (reflected by the color change of the composite parts) may facilitate the flowability of the nanocomposite powders. In addition, the well-dispersed plasma



treated I.34TCN particles in PA12 could potentially enhance laser energy absorption during sintering.

Cross-sectional SEM images near edges in *Figure S5-3a* in *Appendix (Supplementary Information)* (untreated I.34TCN composite) and *Figure S5-3b* (treated I.34TCN composite) show the following main features: unmelted particles (rougher surface); partially melted particles (smooth surface and neck formation); micro-pores and sintered regions (similar observations were also reported [7], [46]).

As the LS is a mould-less powder casting system, it is possible the particles at the boundaries have not received sufficient energy for sintering resulting in non or partially melted particles at the part edges. Similarly, to the inhomogeneity in the untreated composite powder before sintering [30], untreated I.34TCN aggregated particles can be easily seen on the non-melted PA12 particles (highlighted by circles in *Figure S5-3a*) whereas the absence of visible clay aggregates in *Figure S5-3b* suggest efficient incorporation of clay into the polymer matrix. High resolution images at high magnification (scale bar 1  $\mu\text{m}$  or similar) were collected to discuss the nanoclay dispersion in the polymer matrix in next section.

The well dispersed clay has been shown to influence melt and crystallisation [47] which is consistent with improved melt behaviour here as evidenced by the smooth surface in *Figure S5-3b*. The uniformly dispersed plasma treated nanoclay could act as a nucleation centre during the crystallisation of the polymer matrix [48]. In contrast, untreated nanoclay shows island-like aggregations [13] as shown in *Figure S5-3a*. However, a further investigation on the exact mechanism of nanoclay incorporation on the surface morphology of the LS parts is required if this effect is to be exploited for improved surface quality or mechanical properties of LS produced parts.

### ***Section 5.5.3: Dispersion of I.34TCN (untreated and plasma treated) in***

#### ***PA12***

***Figure 5-7*** shows the SEM micrographs illustrating the morphologies of PA12 (***Figure 5-7(a&d)***), untreated I.34TCN composite (***Figure 5-7b&e***) and treated I.34TCN composite (***Figure 5-7c&f***) cross sections. TiO<sub>2</sub> nanoparticles were observed on PA12 polymeric surface as shown in ***Figure 5-7a*** and ***Figure 5-7d*** (were added to increase flowability and powder whiteness) which has been discussed in our previous study [49] and ***Chapter 3 (Section 3.1.1)***. Further analysis about these observations are inserted in ***Appendix (Supplementary Information), Figure S5-4*** The inhomogeneity of the untreated nanoclay can be easily observed in ***Figure 5-7b*** and ***Figure 5-7e*** (Full-scale SEM images of ***Figure 5-7b*** and ***Figure 5-7e*** are available in ***Appendix (Supplementary Information), Figure S5-5a*** and ***Figure S5-5b*** respectively). The nanoclay particles were aggregated on the micro-scale in a flat surface area like in ***Figure 5-7b*** and nanoscale aggregates were observed in a plastically deformed area such as in ***Figure 5-7e***. Some of the islands of untreated I.34TCN, found on nonmelted particles in ***Figure S5-3a***, are observed to have broken-up under tension to smaller aggregates of a few microns in size or less on the PA12 surface, for example ***Figure S5-6*** in ***Appendix (Supplementary Information)***.

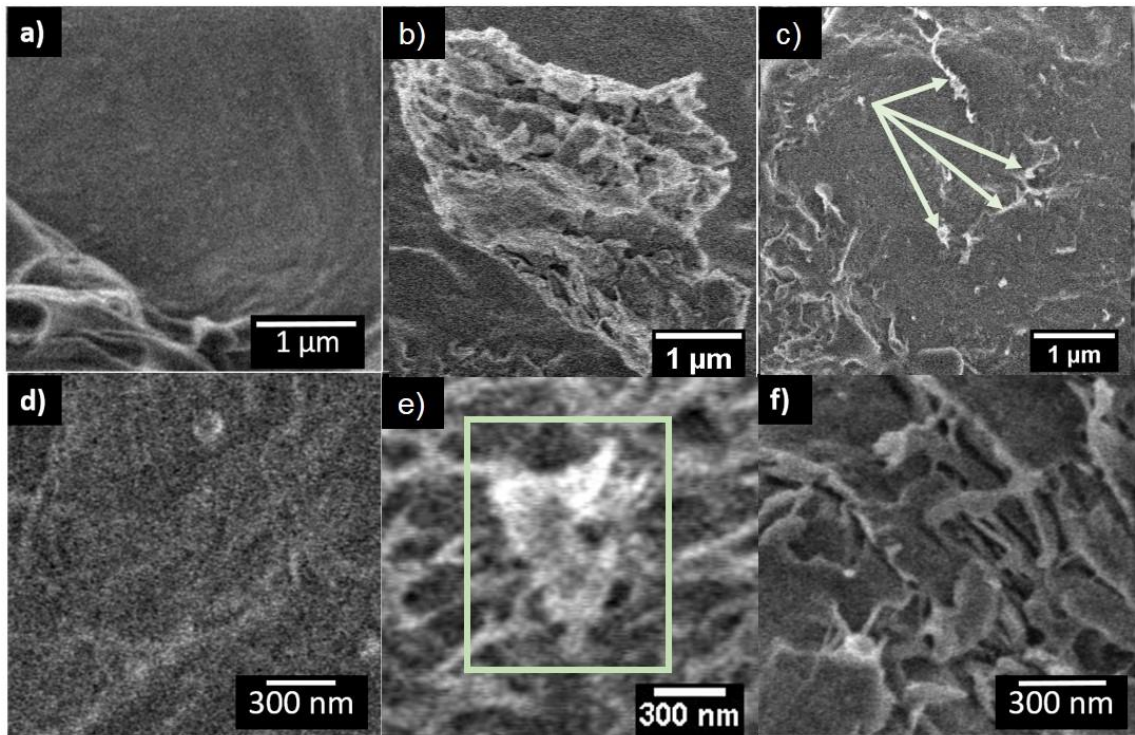


**Figure 5-7** High resolution low voltage SEM imaging of fractured surfaces of a) PA12, b) untreated I.34TCN composite, and c) treated I.34TCN composite on the micron scale and d) PA12, e) untreated I.34TCN composite, and f) treated I.34TCN composite on the nanoscale.

An area is more likely to promote a brittle fracture shown **Figure S5-7** in the Appendix (Supplementary Information), displayed a relatively flat and aggregated nanoclay platelets. On the other hand, the advantageous effect of the LP-PT is shown by the improvement in dispersion of the nanoclay into PA12 was observed in **Figure 5-7c** and **Figure 5-7f** (Full-scale SEM image of **Figure 5-7c** and **Figure 5-7f** are available in Appendix (Supplementary Information), **Figure S5-5c** and **Figure S5-5d** respectively). The plasma treated nanoclay platelets (**Figure 5-7c**) are randomly distributed and less aggregated than the untreated ones (**Figure 5-7b**) even though the region was flat. The treated particle sizes were remarkably reduced (highlighted by arrows in **Figure 5-7c**) and were dispersed more efficiently than untreated particles shown in **Figure 5-7b**. The nanoscale SEM image in **Figure 5-7e** was taken on a plastically deformed region, reveals that the treated nanoclay was dispersed in-between the PA12 layers as nanosized thin sheets and oriented toward the cross section.

However, some of these nanosheets had a poor interfacial bonding with PA12 in one side of these sheets as observed in *Figure 5-7f*. This poor cohesion in parts of the composite structure may limit the advantageous effect of the nanoclay [50]. Hence, a further optimisation of the plasma treatment is required for a better interfacial bonding. These SEM observations and results are linked to the mechanical behaviour of the PA12 composites in the next section.

To conclude the SEM observations, the plasma treatment reduced the micro-aggregation and improved the dispersion of the nanoclay leading, to some extent, to a partially exfoliated structure in some regions and partially intercalated structure in other regions. This confirms the critical role of the plasma treatment for successful nanocomposite formation.

#### ***Section 5.5.4: Mechanical properties***

The tensile test (Ultimate Stress, Ultimate Strain and Elastic Modulus) results obtained from the LS samples of the PA12 and its composites (untreated I.34TCN composite and treated I.34TCN composite) are shown in *Figure 5-8*, *Figure 5-9* and *Figure 5-10*. Data shown in those figures represented the average values and standard deviation from 6 samples of each material. The ultimate stress of PA12 linearly increased with increasing laser power from  $40.49 \pm 1.99$  MPa at 13W to  $42.40 \pm 0.49$  MPa at 17W and then to  $43.30 \pm 0.44$  MPa at 21W. Whilst the measured ultimate strain increased from  $11.36\% \pm 0.87$  reaching maximum values of  $14.13 \pm 0.58\%$  at 17W and then decreased to  $13.02 \pm 0.13\%$  at 21W.

The ultimate stress and strain of the PA12 composites (untreated and treated) both demonstrated a different trend compared to that of neat PA12. The ultimate stress of the untreated I.34TCN composite and treated I.34TCN composite has remarkably increased from  $26.83 \pm 0.35$  MPa and  $25.62 \pm 1.05$  MPa at 13W to  $34.88 \pm 0.22$  MPa and  $34.37 \pm 0.26$  MPa at 17W and a limited increase to  $35 \pm 3.7$  MPa and  $35.45 \pm 0.40$  MPa with increasing the laser power to 21W. The ultimate strain, on the other hand, of untreated I.34TCN composite and

treated I.34TCN composite increased from  $4.71 \pm 0.13 \text{MPa}$  and  $5.6 \pm 0.32 \text{MPa}$  at 13W to  $6.27 \pm 0.13 \text{MPa}$  and  $7.76 \pm 0.36 \text{MPa}$  at 17W and then to  $6.66 \pm 0.25 \text{MPa}$  and  $8.23 \pm 0.32 \text{MPa}$  at 21W.

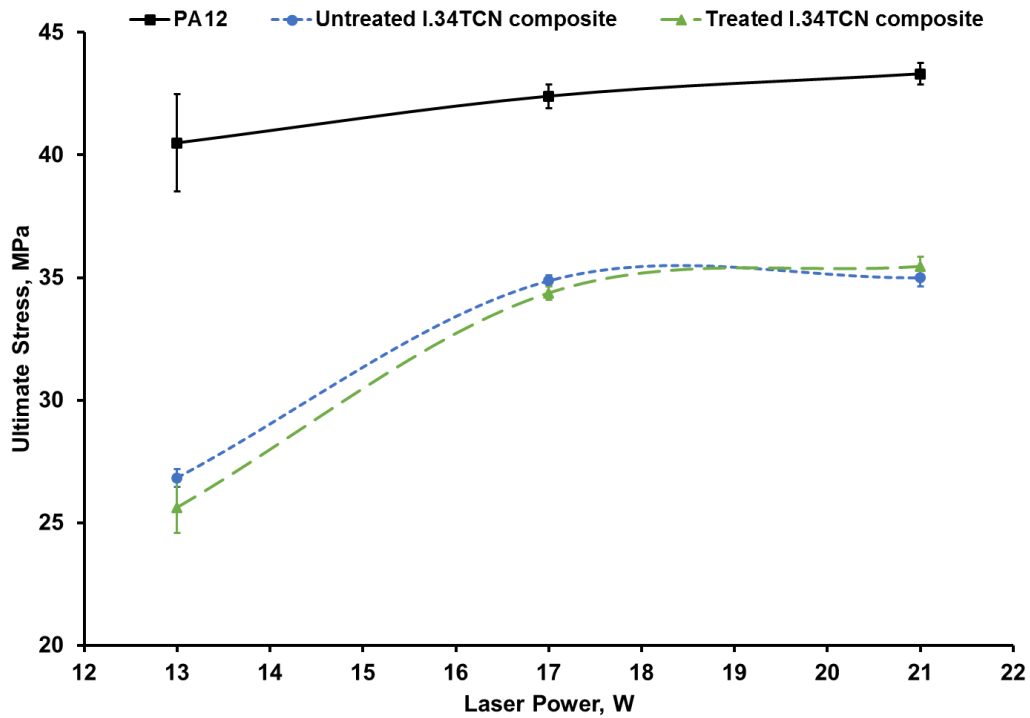


**Figure 5-8** Ultimate stress results obtained from PA12, untreated I.34TCN and treated I.34TCN composites at three different laser powers: 13, 17, and 21W.

As can be seen, in each case the UT-Stress of plasma treated, and untreated composites were lower than that for PA12, and more dramatically so at lower laser powers (**Figure 5-8**). Also treated vs untreated showed no effect. As expected, the UT-Strain of the untreated I.34TCN composite and treated I.34TCN composite, shown above, are substantially lower than that of the PA12 due to the addition of rigid nanoclays [51].

However, the treated I.34TCN composite show a better elongation than that obtained from the untreated I.34TCN composite samples as shown in **Figure 5-9**. The variation in the

ultimate stress values for low laser powers of the treated I.34TCN composite was smaller than that for PA12 and untreated I.34TCN composite.

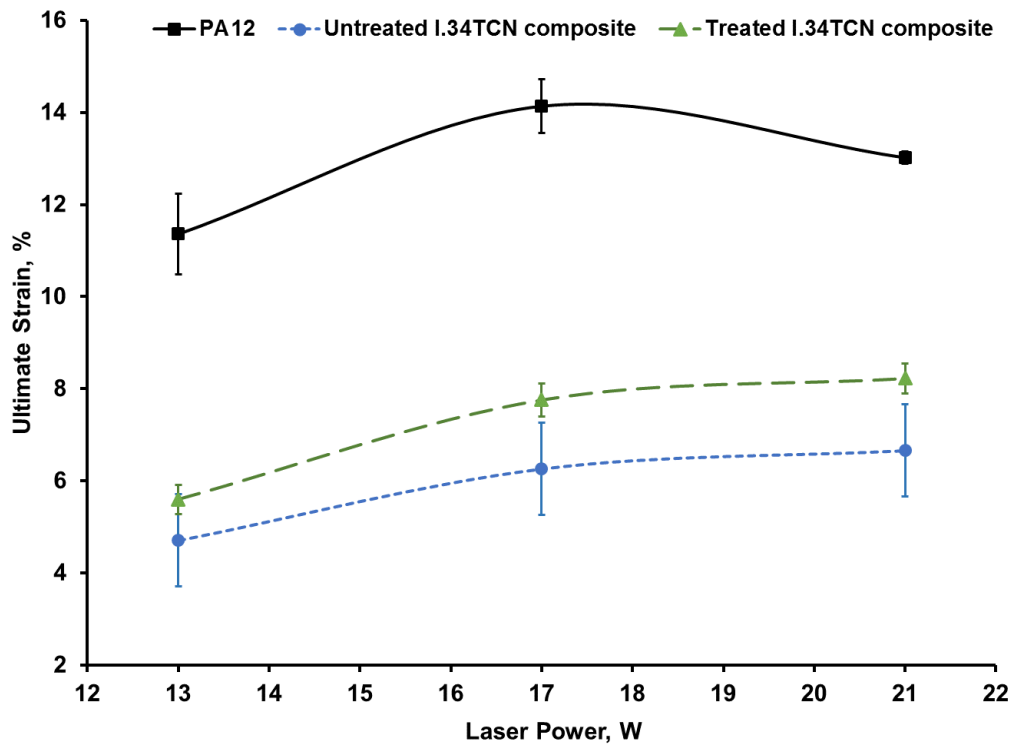


**Figure 5-9** Ultimate strain results obtained from PA12, untreated I.34TCN composite and treated I.34TCN composite at three different laser powers: 13, 17, and 21W.

All the elastic modulus results obtained from PA12, untreated I.34TCN composite, and treated I.34TCN composite started from lowest values at 13W:  $1412 \pm 150.7$ MPa,  $1190 \pm 101.4$ MPa, and  $1265 \pm 72$ MPa respectively. Then, these values increased reaching maximum values at 17W:  $1460 \pm 162.9$ MPa,  $1346.7 \pm 99.5$ MPa, and  $1618 \pm 118.2$ MPa, before decreasing at 21W to:  $1446 \pm 107.1$ MPa,  $1320 \pm 71.3$ MPa, and  $1486.7 \pm 89.6$ MPa respectively. As can be observed, at 17W and 21W laser powers, the elastic moduli of the treated composite exhibited higher values than those obtained from PA12 and untreated composite and the best value was obtained at laser power 17W. In addition, the spread of data of the elastic modulus is relatively large compared to the ultimate stress and strain data at all laser power inputs in line with previous literature [1], [6].

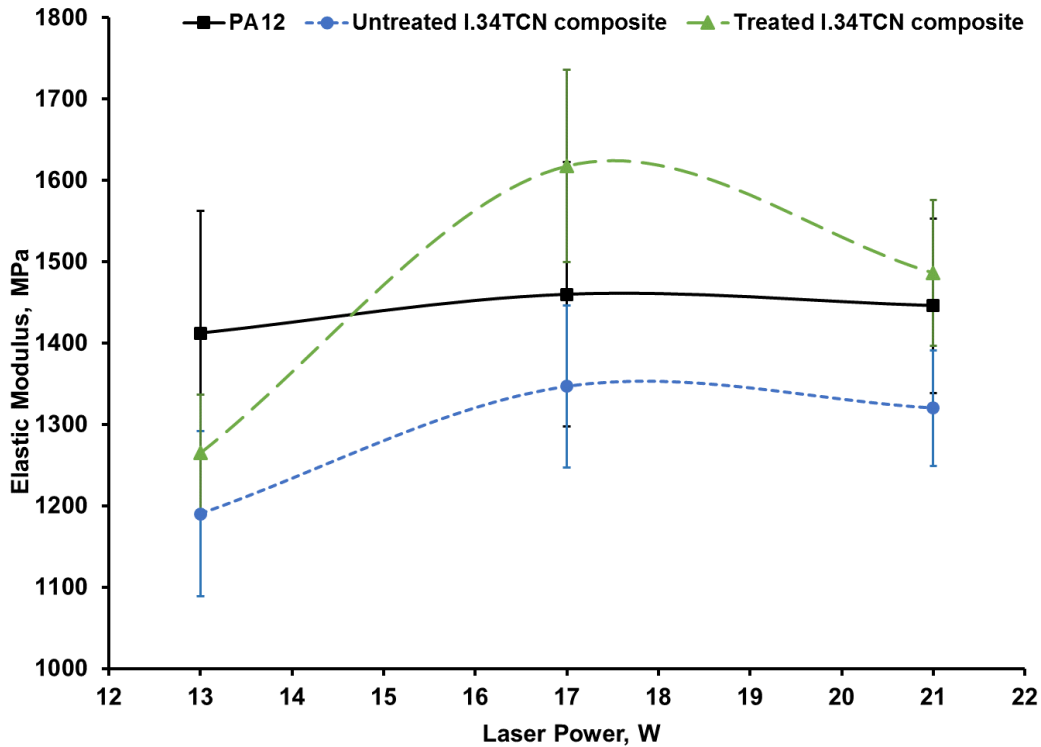


*Figure 5-10 Elastic modulus results obtained from PA12, untreated I.34TCN composite and treated I.34TCN composite at three different laser power: 13, 17, and 21W.*

In conclusion, as expected, the poorer tensile test results of untreated I.34TCN composite *Figure 5-9* and *Figure 5-10* coupled with the non-uniform surface showed by SEM images in *Figure 5-6c*, *Figure S5-3a* and *Figure 5-7b* suggest that the untreated nanoclay agglomerations absorbed higher energy causing large local variations of temperature. Therefore, some particles with poorly distributed untreated nanoclays were mostly partially melted which resulted in weak mechanical properties as reported in previous studies [14], [22]. On the other hand, no signs of large agglomerations but smooth surface melt area (*Figure S5-3a*) and better dispersion (*Figure 5-7d* and *Figure 5-7f*) were obtained in treated I.34TCN composite. As a result, the elastic modulus of treated I.34TCN composite was significantly improved and higher than that of PA12 and untreated I.34TCN composite at a laser power of 17 and 21W. Although, for most materials improving stiffness are accompanied by reduction in ductility [1], the LP-PT has a beneficial effect on stiffness

whilst also promoting a less brittle fracture of treated I.34TCN composite. On the other hand, the reduction in the composites toughness, shown in *Figure 5-8*, can be attributed to the fact that a fully exfoliated structure was not achieved [52] even though, the PT composite exhibited well-dispersed nanoclay as previously discussed. This is because some region showed poor-adhesion between the plasma treated I.34TCN and PA12 (*Figure 5-7f*) could lead to less interfacial reinforcing area and less resistance to nanoclay slippage. We observed that the same particle showed good adhesion one side but a poor adhesion on the other, suggesting uneven exposure to the plasma. Therefore, further work is required to optimise the processing parameters of the LS PA12 composites including the powder mixing parameters but most importantly, the plasma treatment geometry and duration.

### **Section 5.6: Conclusion**

We conclude that surface modification by air plasma exposure can be used to improve the nanoclay thermo-chemical properties and enhance the compatibility between the organic and nonorganic materials, ultimately, resulting in good processibility of complex LS composite parts, and most notably, improving the surface quality. We found, the plasma treatment could improve the affinity between the nanoclay and PA12 and therefore it reduced significantly the nanoclay aggregates and improved the dispersion quality. Furthermore, LP-PT can increase stiffness and promote a reduced brittleness when plasma treated nanoclays are added instead of untreated nanoclay. Therefore, it is feasible to establish a link between plasma and laser sintering techniques to modify the end-use part properties, however, a further optimisation of the plasma treatment is required to fully exploit the potential of this method.

### **Section 5.7: References**

- [1] G. M. Vasquez, C. E. Majewski, B. Haworth, and N. Hopkinson, "A targeted material selection process for polymers in laser sintering," *Addit. Manuf.*, vol. 1, pp. 127–138, 2014.



- [2] D. Bourell *et al.*, “Materials for additive manufacturing,” *CIRP Ann. - Manuf. Technol.*, vol. 66, no. 2, pp. 659–681, 2017.
- [3] S. Berretta, K. Evans, and O. Ghita, “Additive manufacture of PEEK cranial implants: Manufacturing considerations versus accuracy and mechanical performance,” *Mater. Des.*, vol. 139, pp. 141–152, 2018.
- [4] M. M. Savalani, L. Hao, P. M. Dickens, Y. Zhang, K. E. Tanner, R. A. Harris, “The effects and interactions of fabrication parameters on the properties of selective laser sintered hydroxyapatite polyamide composite biomaterials”, *Rapid Prototyping Journal*, Vol. 18 Issue: 1, pp.16-27, 2012.
- [5] S. Berretta, O. Ghita, and K. E. Evans, “Morphology of polymeric powders in Laser Sintering (LS): From Polyamide to new PEEK powders,” *Eur. Polym. J.*, vol. 59, pp. 218–229, 2014.
- [6] C. E. Majewski, H. Zarringhalam, D. Toon, U. Ajoku, N. Hopkinson, and M. P. Caine, “The use of off-line part production to predict the tensile properties of parts produced by Selective Laser Sintering,” *J. Mater. Process. Technol.*, vol. 209, no. 6, pp. 2855–2863, Mar. 2009.
- [7] D. L. Bourell, T. J. Watt, D. K. Leigh, and B. Fulcher, “Performance limitations in polymer laser sintering,” *Phys. Procedia*, vol. 56, no. C, pp. 147–156, 2014.
- [8] A. Wegner, “New polymer materials for the laser sintering process: Polypropylene and others,” *Phys. Procedia*, vol. 83, pp. 1003–1012, 2016.
- [9] S. C. Ligon, R. Liska, J. Stampfl, M. Gurr, and R. Mülhaupt, “Polymers for 3D Printing and Customized Additive Manufacturing,” *Chem. Rev.*, vol. 117, no. 15, pp. 10212–10290, 2017.
- [10] S. A. M. Tofail, E. P. Koumoulos, A. Bandyopadhyay, S. Bose, L. O’Donoghue, and C. Charitidis, “Additive manufacturing: scientific and technological challenges, market uptake and opportunities,” *Mater. Today*, vol. 21, no. 1, pp. 22–37, 2018.
- [11] L. Hao, M. M. Savalani, Y. Zhang, K. E. Tanner, and R. A. Harris, “Effects of material morphology and processing conditions on the characteristics of hydroxyapatite and high-density polyethylene biocomposites by selective laser sintering,” *Proc. Inst. Mech. Eng. Part L J. Mater. Des. Appl.*, vol. 220, no. 3, pp. 125–137, 2006.
- [12] G. V. Salmoria, J. L. Leite, and R. A. Paggi, “The microstructural characterization of PA6/PA12 blend specimens fabricated by selective laser sintering,” *Polym. Test.*, vol. 28, no. 7, pp. 746–751, 2009.

- [13] P. K. Jain, P. M. Pandey, and P. V. M. Rao, "Selective laser sintering of clay-reinforced polyamide," *Polym. Compos.*, vol. 31, no. 4, pp. 732–743, 2010.
- [14] S. Pavlidou and C. D. Papaspyrides, "A review on polymer-layered silicate nanocomposites," *Prog. Polym. Sci.*, vol. 33, no. 12, pp. 1119–1198, 2008.
- [15] P. C. Lebaron, Z. Wang, and T. J. Pinnavaia, "Polymer-layered silicate nanocomposites: An overview," *Appl. Clay Sci.*, vol. 15, no. 1–2, pp. 11–29, 1999.
- [16] I. E. Odom, "Smectite clay Minerals: Properties and Uses," *Philos. Trans. R. Soc. A Math. Phys. Eng. Sci.*, vol. 311, no. 1517, pp. 391–409, 1984.
- [17] L. A. Utracki, "Clay-containing polymeric nanocomposites and their properties," *IEEE Electr. Insul. Mag.*, vol. 26, no. 4, pp. 6–15, 2010.
- [18] S. Sinha Ray and M. Okamoto, "Polymer/layered silicate nanocomposites: A review from preparation to processing," *Prog. Polym. Sci.*, vol. 28, no. 11, pp. 1539–1641, 2003.
- [19] G. Brown, "Crystal Structures of Clay Minerals and Related Phyllosilicates," *Philos. Trans. R. Soc. London*, vol. 311, no. 1517, pp. 221–240, 1984.
- [20] H. H. Murray, "Traditional and new applications for kaolin, smectite and polygorskite: A general overview," *Appl. Clay Sci.*, vol. 17, pp. 207–221, 2000.
- [21] J. Madejová, "FTIR techniques in clay mineral studies," *Vib. Spectrosc.*, vol. 31, no. 1, pp. 1–10, 2003.
- [22] Y. Xi, Z. Ding, H. He, and R. L. Frost, "Structure of organoclays - An X-ray diffraction and thermogravimetric analysis study," *J. Colloid Interface Sci.*, vol. 277, no. 1, pp. 116–120, 2004.
- [23] H. He, Y. Ma, J. Zhu, P. Yuan, and Y. Qing, "Organoclays prepared from montmorillonites with different cation exchange capacity and surfactant configuration," *Appl. Clay Sci.*, vol. 48, no. 1–2, pp. 67–72, 2010.
- [24] A. Vazquez, M. López, G. Kortaberria, L. Martín, and I. Mondragon, "Modification of montmorillonite with cationic surfactants. Thermal and chemical analysis including CEC determination," *Appl. Clay Sci.*, vol. 41, no. 1–2, pp. 24–36, 2008.
- [25] B. Tyagi, C. D. Chudasama, and R. V. Jasra, "Determination of structural modification in acid activated montmorillonite clay by FT-IR spectroscopy," *Spectrochim. Acta - Part A Mol. Biomol. Spectrosc.*, vol. 64, no. 2, pp. 273–278, May 2006.
- [26] J. Madejová, J. Bujdák, M. Janek, and P. Komadel, "Comparative FT-IR study of structural modifications during acid treatment of dioctahedral smectites and

- hectorite,” *Spectrochim. Acta - Part A Mol. Biomol. Spectrosc.*, vol. 54, no. 10, pp. 1397–1406, 1998.
- [27] K. Fatyeyeva and F. Poncin-Epaillard, “Sulfur dioxide Plasma Treatment of the Clay (Laponite) Particles,” *Plasma Chem. Plasma Process.*, vol. 31, no. 3, pp. 449–464, Jun. 2011.
- [28] A. T. Djowe, S. Laminsi, D. Njopwouo, E. Acayanka, and E. M. Gaigneaux, “Surface Modification of Smectite Clay Induced by Non-thermal Gliding Arc Plasma at Atmospheric Pressure,” *Plasma Chem. Plasma Process.*, vol. 33, no. 4, pp. 707–723, Aug. 2013.
- [29] V. Skrockiene, K. Žukiene, and S. Tučkute, “Properties of Recycled Thermoplastic Polyurethane Filled with Plasma Treated Bentonite,” *Plasma Process. Polym.*, vol. 12, no. 11, pp. 1284–1292, 2015.
- [30] A. Almansoori, C. Majewski, and C. Rodenburg, “Nanoclay/Polymer Composite Powders for Use in Laser Sintering Applications: Effects of Nanoclay Plasma Treatment,” *JOM*, vol. 69, no. 11, 2017.
- [31] I. K. Yang and P. H. Tsai, “Preparation and characterization of polyether-block-amide copolymer/clay nanocomposites,” *Polym. Eng. Sci.*, vol. 47, no. 3, pp. 235–243, Mar. 2007.
- [32] Z. Zhang, J. H. Lee, S. H. Lee, S. B. Heo, and C. U. Pittman, “Morphology, thermal stability and rheology of poly(propylene carbonate)/organoclay nanocomposites with different pillaring agents,” *Polymer (Guildf.)*, vol. 49, no. 12, pp. 2947–2956, 2008.
- [33] J. M. Cervantes-Uc, J. V. Cauich-Rodríguez, H. Vázquez-Torres, L. F. Garfias-Mesías, and D. R. Paul, “Thermal degradation of commercially available organoclays studied by TGA-FTIR,” *Thermochim. Acta*, vol. 457, no. 1–2, pp. 92–102, 2007.
- [34] C. Zhao, H. Qin, F. Gong, M. Feng, S. Zhang, and M. Yang, “Mechanical, thermal and flammability properties of polyethylene/clay nanocomposites,” *Polym. Degrad. Stab.*, vol. 87, no. 1, pp. 183–189, 2005.
- [35] A. S. Hadj-Hamou, S. Matassi, H. Abderrahmane, and F. Yahiaoui, “Effect of cloisite 30B on the thermal and tensile behavior of poly(butylene adipate-co-terephthalate)/poly(vinyl chloride) nanoblends,” *Polym. Bull.*, vol. 71, no. 6, pp. 1483–1503, 2014.
- [36] E. Pérez, C. J. Pérez, V. A. Alvarez, and C. Bernal, “Fracture behavior of a

- commercial starch/polycaprolactone blend reinforced with different layered silicates,” *Carbohydr. Polym.*, vol. 97, no. 2, pp. 269–276, 2013.
- [37] J. P. Kruth, B. Vadenbroucke, J. V. Vaerenbergh, Naert I; “Digital manufacturing of biocompatible metal frameworks for complex dental prostheses by means of SLS/SLM”, In: Proceedings of the 2nd International Conference on Advanced Research and Rapid Prototyping, Leiria, Portugal, pp. 139-45, (2005).
- [38] V. Kumar *et al.*, “Nanoscale Mapping of Bromide Segregation on the Cross Sections of Complex Hybrid Perovskite Photovoltaic Films Using Secondary Electron Hyperspectral Imaging in a Scanning Electron Microscope,” *ACS Omega*, vol. 2, pp. 2126–2133, 2017.
- [39] D. R. Paul and L. M. Robeson, “Polymer nanotechnology : Nanocomposites,” *Polym. with aligned carbon Nanotub. Act. Compos. Mater.*, vol. 49, no. 15, pp. 3187–3204, 2008.
- [40] E. Sancaktar and J. Kuznicki, “International Journal of Adhesion & Adhesives Nanocomposite adhesives : Mechanical behavior with nanoclay,” *Int. J. Adhes. Adhes.*, vol. 31, no. 5, pp. 286–300, 2011.
- [41] R. Gu *et al.*, “Characteristics of wood – plastic composites reinforced with organo-nanoclays,” *J. Reinf. Plast. Compos.*, vol. 29, no. 24, pp. 3566–3586, 2010.
- [42] R. Scaffaro and A. Maio, “Enhancing the mechanical performance of polymer based nanocomposites by plasma-modification of nanoparticles,” *Polym. Test.*, vol. 31, no. 7, pp. 889–894, 2012.
- [43] G. Edwards, P. Halley, G. Kerven, and D. Martin, “Thermal stability analysis of organo-silicates, using solid phase microextraction techniques,” *Thermochim. Acta*, vol. 429, no. 1, pp. 13–18, 2005.
- [44] W. Xie, Z. Gao, K. Liu, W. Pan, and R. Vaia, “Thermal characterization of organically modified montmorillonite,” vol. 368, pp. 0–11, 2001.
- [45] A. Almansoori, R. Seabright, C. Majewski, and C. Rodenburg, “Feasibility of Plasma Treated Clay in Clay/Polymer Nanocomposites Powders for use Laser Sintering (LS),” in *IOP Conference Series: Materials Science and Engineering*, 2017, vol. 195, no. 1.
- [46] H. C. H. Ho, W. L. Cheung, and I. Gibson, “Morphology and properties of selective laser sintered bisphenol a polycarbonate,” *Ind. Eng. Chem. Res.*, vol. 42, no. 9, pp. 1850–1862, 2003.
- [47] T. G. Mofokeng, S. S. Ray, and V. Ojijo, “Influence of selectively localised nanoclay

- particles on non-isothermal crystallisation and degradation behaviour of PP/LDPE blend composites,” *Polymers (Basel)*., vol. 10, no. 3, 2018.
- [48] B. Chen, S. Berretta, K. Evans, K. Smith, and O. Ghita, “A primary study into graphene/polyether ether ketone (PEEK) nanocomposite for laser sintering,” *Appl. Surf. Sci.*, vol. 428, pp. 1018–1028, 2018.
- [49] A. Almansoori *et al.*, “Surface modification of the laser sintering standard powder polyamide 12 by plasma treatments,” *Plasma Process. Polym.*, vol. 15, no. 7, p. 1800032, Jul. 2018.
- [50] S. G. Lei, S. V. Hoa, and M. T. Ton-That, “Effect of clay types on the processing and properties of polypropylene nanocomposites,” *Compos. Sci. Technol.*, vol. 66, no. 10, pp. 1274–1279, 2006.
- [51] C. Z. Yan, Y. S. Shi, J. S. Yang, and J. H. Liu, “An organically modified montmorillonite/nylon-12 composite powder for selective laser sintering,” *Rapid Prototyp. J.*, vol. 17, no. 1, pp. 28–36, 2011.
- [52] K. Masenelli-Varlot, E. Reynaud, G. Vigier, and J. Varlet, “Mechanical properties of clay-reinforced polyamide,” *J. Polym. Sci. Part B Polym. Phys.*, vol. 40, no. 3, pp. 272–283, 2002.

## Section 5.8: Appendix (Supplementary Information)

*Tables S5- 1 PA12, and I.34TCN composites (untreated and treated) powders particle distribution and thermal properties.*

Powder	Thermal Properties from DSC*		Particle Distribution from Mastersizer**		
	Melting Temperature, °C	Crystallisation Temperature, °C	Dv (10)	Dv (50)	Dv (90)
PA12	184.8±0.186	147.72±1.26	35.7 µm	57.2 µm	86.8 µm
Untreated Composite	185.04±0.042	148.54±0.514	33.8 µm	55.8 µm	85.3 µm
Treated Composite	185.34±0.093	149.84±1.131	34.1 µm	56.0 µm	85.3 µm

\* DSC was used in this study is DSC6 from Perkin Almer, and powder was heated from room temperature to 250 °C, before cooling back to the original point in a rate of 10 °C/min. Results shown are the average ± standard deviation of three samples from each material.

\*\* Particle size analysis was carried out using Mastersizer 2000 Particle Size Analyser from Malvern Instruments. Each sample was tested ten times and data were analysed using software Mastersizer v3.4.

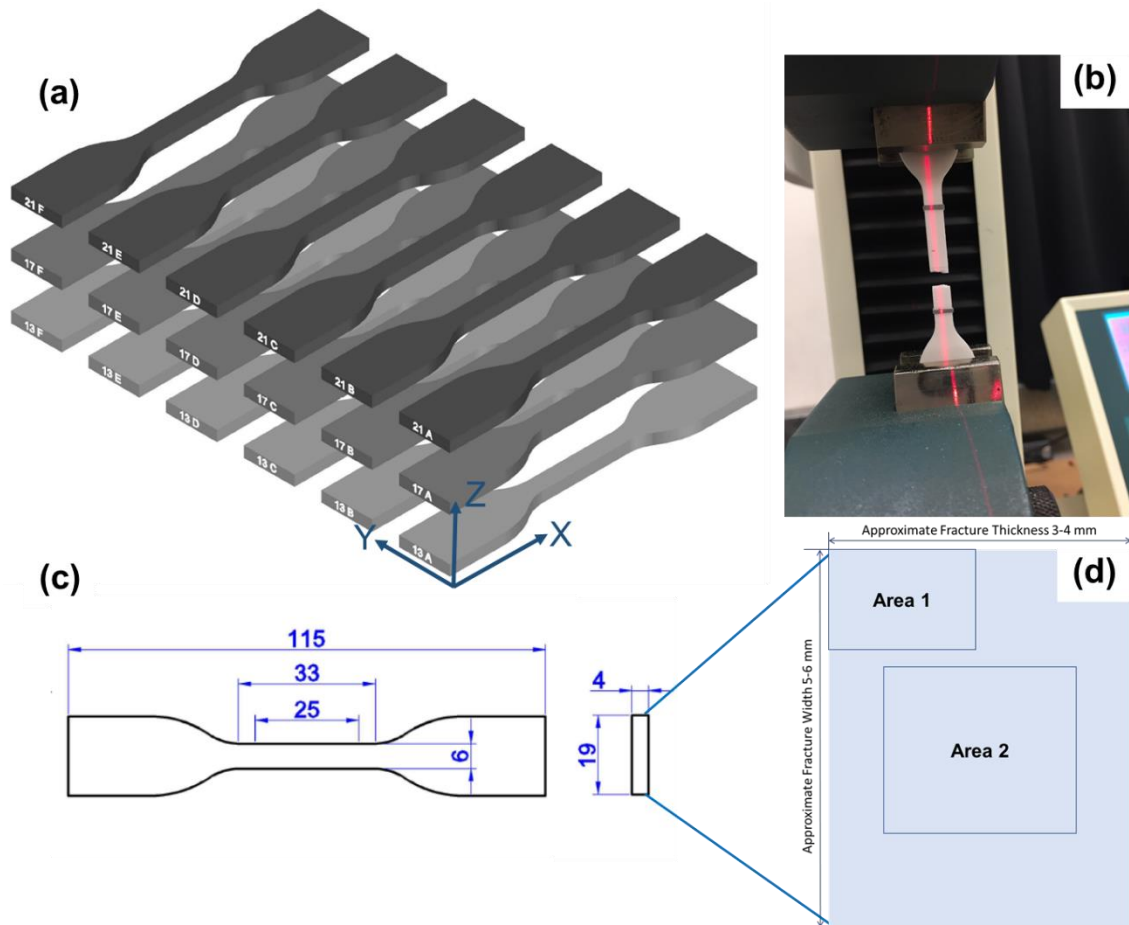


**Figure S5-1**(a) LS specimen design and build layout oriented parallel to the  $xy$ -plane, (b) Tensile test and laser extensometer setup, (c) standard dimensions (in mm) of a single tensile test specimen according to the ASTM D638-02A, and (d) A diagram represents the fracture area after tensile testing, showing the SEM scanned areas, Area 1 and Area 2 in Figure 5-6. figures

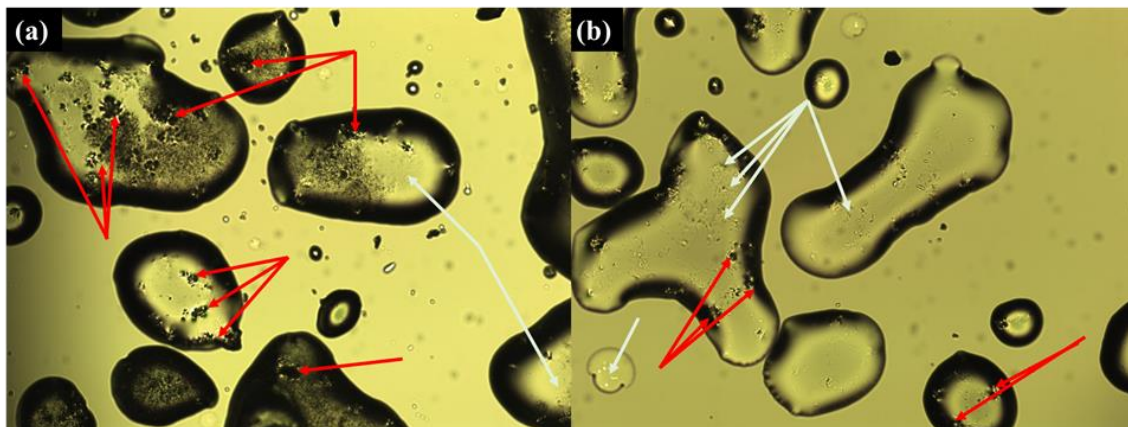


**Figure S5-2** HSM images of (a) Untreated PA12/I.34TCN composite (b) Plasma treated PA12/I.34TCN composite.

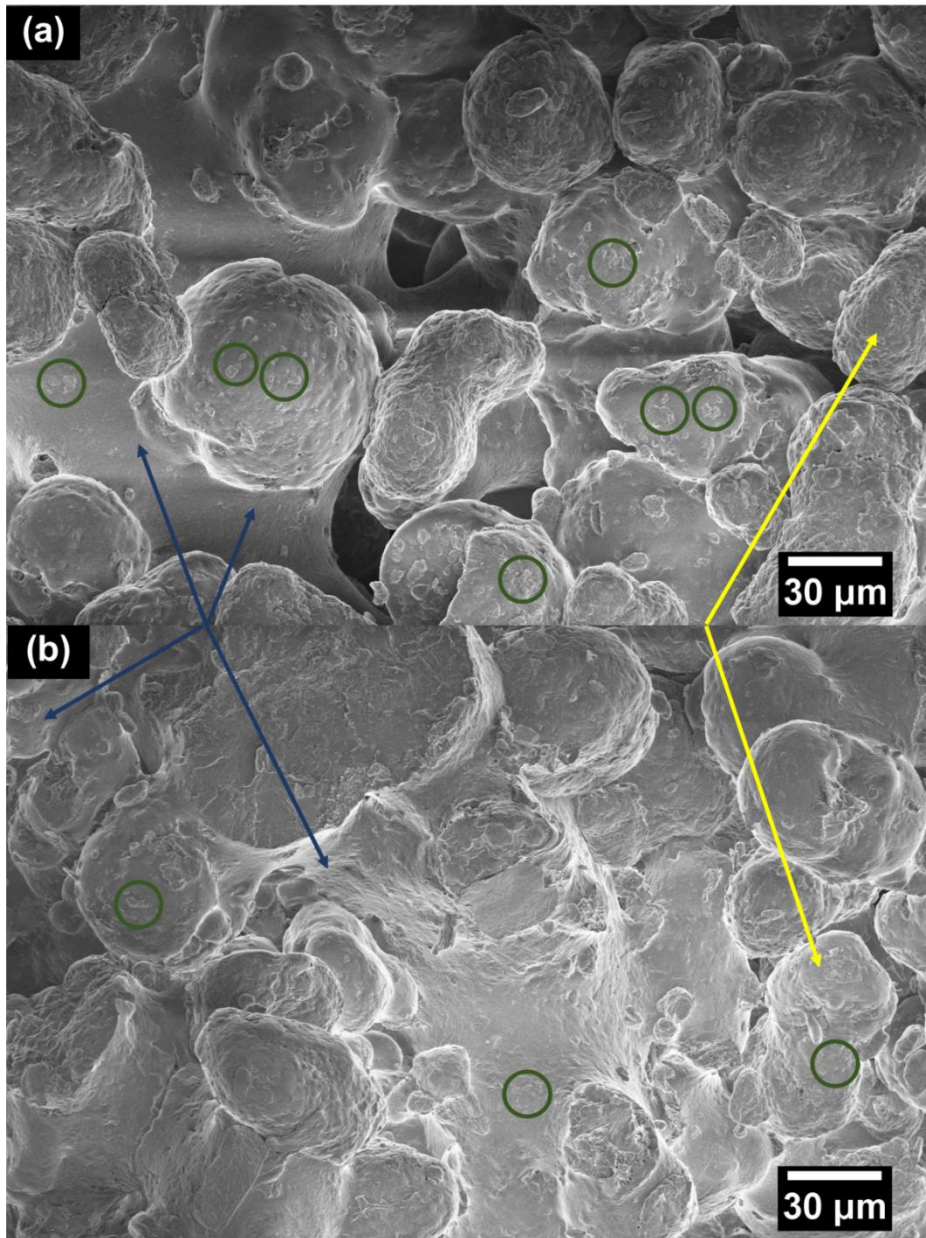


**Figure S5-3** Cross section of the LS specimens of the untreated I.34TCN composite (a) and treated I.34TCN composite (b). Examples of aggregated untreated clay particles in (a) and smaller size of treated clay particles in (b) are highlighted with green circles. Yellow and blue arrows in (a) and (b) are found to highlight rough and smooth areas respectively.



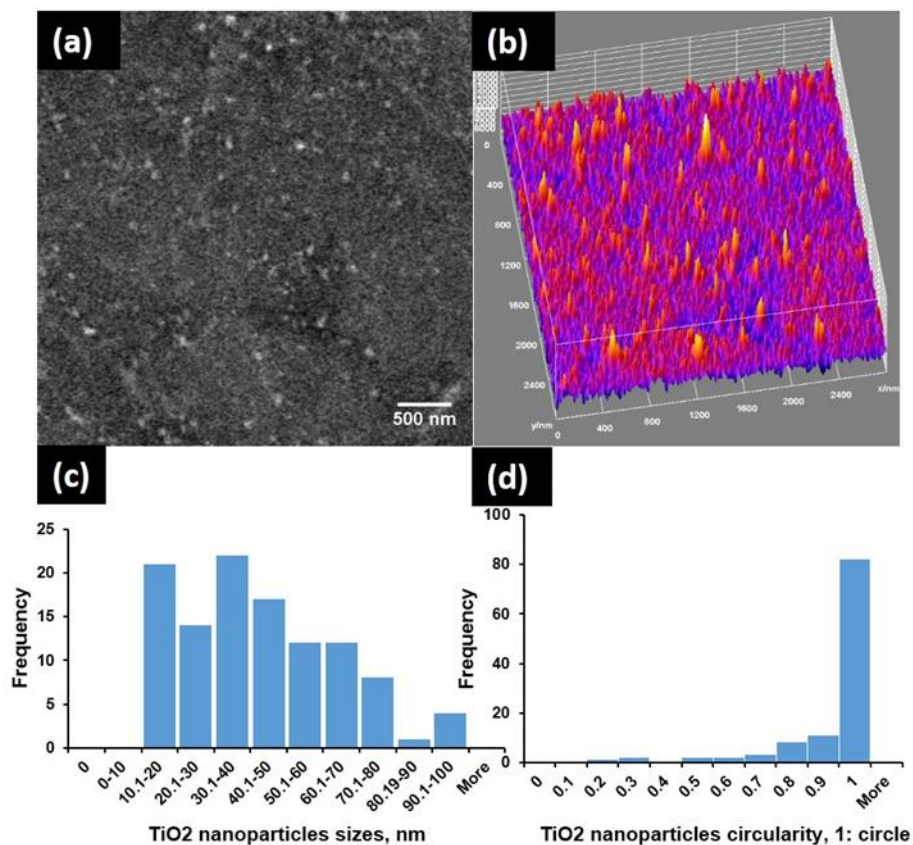


**Figure S5-4** SEM micrograph of the PA12 cross section shows the presence of TiO<sub>2</sub> nanoparticles (a), 3D surface plot of the PA12 surface displays the distribution of the TiO<sub>2</sub> nanoparticles (b), TiO<sub>2</sub> particle size statistics using ImageJ shows the range of the particles size and (c). The presence of TiO<sub>2</sub> can be evidenced by the intense peaks in ImageJ 3D surface plot shown in (b). Histogram of the TiO<sub>2</sub> particles shows a range of the particle sizes (c) but about 80% of these particles has a full circularity as shown in circularity (d).

More explanation about the effect of plasma on the distribution of TiO<sub>2</sub> nanoparticles on PA12 particles is found in Chapter 6.

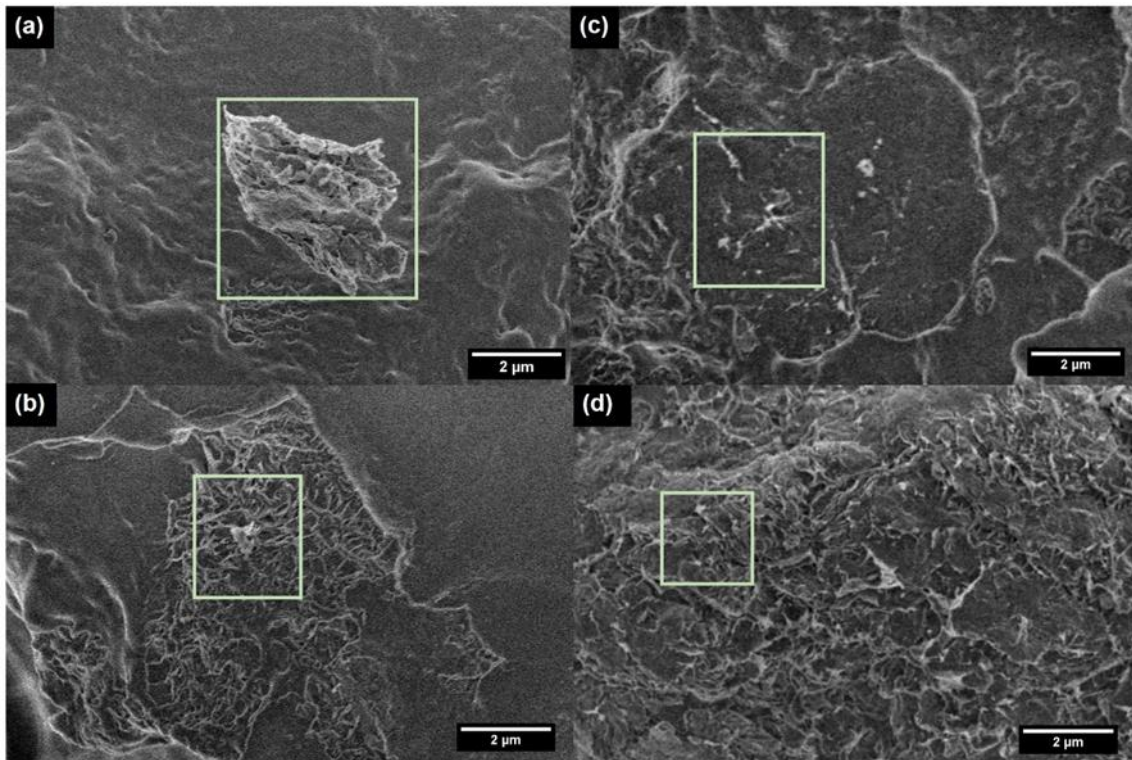


*Figure S5-5 Panels a-d are the large-scale SEM images of Figure 5-7b, Figure 5-7e, Figure 5-7d and Figure 5-7f respectively in the main document.*

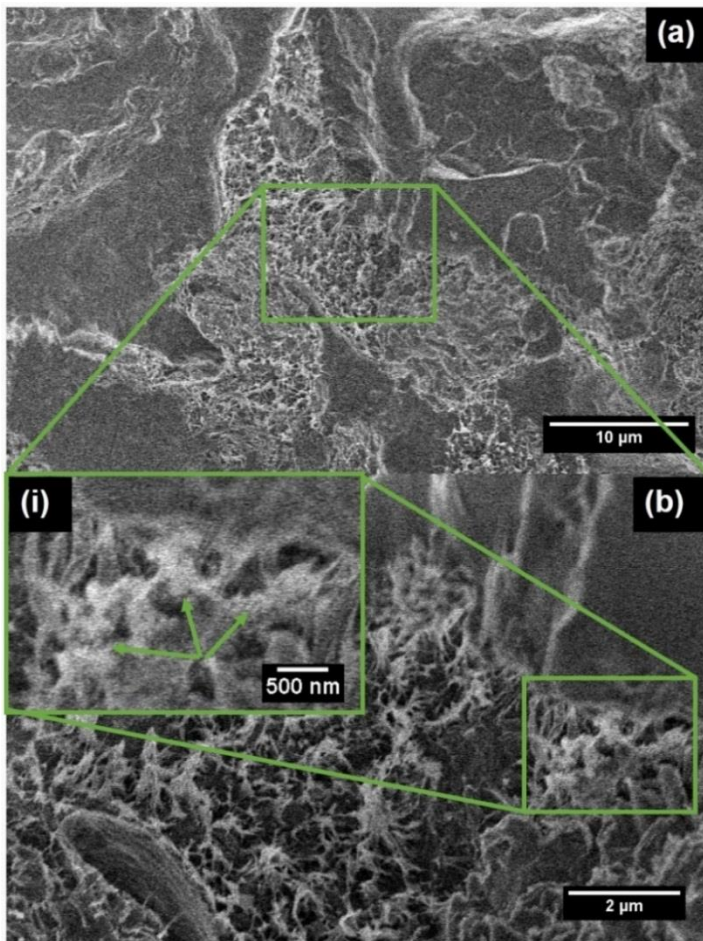


*Figure S5-6 SEM micrographs of untreated I.34TCN composite surface at different magnifications (a) low magnification image (b) high magnification image, and (i) nanoscale image shows the aggregation of untreated clay.*

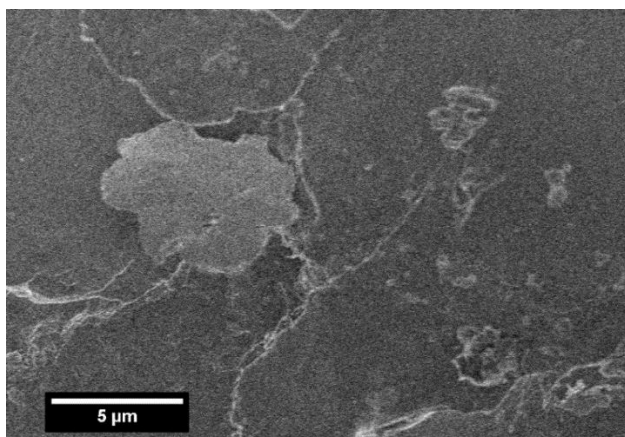


*Figure S5-7 SEM micrographs shows a large aggregated untreated I.34TCN on PA12 surface.*



## Chapter 6: Surface Modification of the Laser Sintering Standard

### Powder Polyamide 12 by Plasma Treatments

#### Section 6.1: Abstract

*Polyamide 12 (PA12) powder was exposed for up to 3 hours to low pressure air plasma treatment (LP-PT) and several minutes by two different atmospheric pressure plasma jets (PJ) i.e. KinPen (K-APJ) and Hairline (H-APJ).*

*The chemical and physical changes resulting from LP-PT were observed by a combination of Scanning Electron Microscopy (SEM), Hot Stage Microscopy (HSM) and Fourier transform infrared spectroscopy (FTIR), which demonstrated significant changes between the plasma treated and untreated PA12 powders.*

*PA12 exposed to LP-PT showed an increase in wettability, was relatively porous, and possessed a higher density, which resulted from the surface functionalisation and materials removal during the plasma exposure. However, it showed poor melt behaviour under heating conditions typical for Laser Sintering. In contrast, brief PJ treatments demonstrated similar changes in porosity, but crucially, retained the favourable melt characteristics of PA12 powder.*

#### Section 6.2: Introduction

During the last decade, laser sintering (LS) has become one of the most promising polymer Additive Manufacturing techniques, capable of manufacturing 3-dimensional (3D) products with complex and accurate geometries from powdered materials. However, the range and reliability of materials for this process is currently a limiting factor; the ultimate aim of this research is to address this issue [1]–[5].

Polyamide 12 (PA12) powder is frequently selected for LS applications due to its easy processability (i.e. ease of sintering), large processing windows, high laser energy

absorption, and good mechanical properties [5]–[7]. Despite this potential, however, the consistency of mechanical performance of LS parts made from PA12 powder needs to be improved by the inclusion of fillers. Nano-materials such as nanoclays have potential in this area, but their dispersion can be difficult. Plasma etching has been used to improve dispersion and therefore make these nano-materials more viable [8], [9].

LS-PA12 parts with many other polymers have also restricted applications where adhesive bonding of polymers with other materials, wettability or printability are required, due to their poor hydrophilic properties [10]. PA12 powder tends to have the lowest swelling and solubility in polar solvents like water due to its longer methylene chain and strong hydrogen bonds between the amide groups of the PA12 [11]. Consequently, different surface modification techniques, for instance, wet chemical and/or plasma treatment have been frequently used to modify the polymeric surfaces for such applications [12].

Plasma-based surface modification has been used extensively in the past decade due to its favourable properties, such as lack of toxic chemicals or waste products; therefore, it is considered as an environmentally friendly method [12]. Plasma surface modification is used mainly to tailor the surface chemistry by enhancing the polymeric surface energy.

Plasma- a reactive medium containing free electrons, excited and ionised atoms and molecules, radicals and metastables and VIS-UV radiation is widely applied also for chemically modification of polymer surfaces [10], [13]–[15], e.g. ultrafine cleaning [16], [17], functionalisation [18], etching [19] or thin film deposition [20]. Plasma jet (PJ) at atmospheric pressure is used to improve the wettability and adhesion, [10], [21]–[23] as is low pressure plasma [13], [24], [25]. Both of these techniques are investigated in this work, although the plasma jet, can be expected to have an advantage that it is more economical than the low pressure ones requiring a vacuum chamber [10], [26]. An optimal use of plasma treatment promotes the surface functionality and dampens structural degradation of

original material. For this purpose, an advanced characterisation of chemical properties is required in correlation to plasma process settings (gas, pressure, excitation frequency, power). Different gases or gas mixtures for example, Argon or Fluorine based plasmas such as CF<sub>4</sub> and oxygen gas plasma, are used for the surface hydrophilisation or hydrophobisation of polymers [23]–[25]. Plasma based technique is a common way but not the only method, other types of methods like grafting or electron beam irradiation can also be used to manipulate the surface properties of materials [27]–[29].

Several attempts have been carried out to modify a wide range of polymers using plasma for different purposes [13], [30]–[32]. Studies focused on the plasma treatment of PA12 are concentrated on the bulk material, thin films [10], [22], [33]–[35] or fibres [36]. A significant plasma effect on solid materials is limited to the topmost surface layer, the thickness of which depends on the plasma power and exposure time [37]. Within this surface layer, the chemical structure and properties (e. g. mechanical properties) differ significantly from those of pristine materials or from the bulk [10], [32], [33]. Hence, a phase separation in the region between the surface and bulk materials can occur [38]. Ageing and degradation of the plasma-assisted active sites after exposure to the ambient environment is another common issue which is caused by the interaction between the surfaces free radicals and environmental oxygen [32], [39].

Further, the practical application of plasma treatments to complex-shaped laser sintered parts is challenging. As a solution to these issues, we suggest using plasma treatment on polymer powders (PA12 is the target material) before sintering. Laser Sintering of plasma treated powder is in its infancy, and studies in this field are very rare. In a recent work, LS-PA12 powder was plasma treated to observe whether the plasma treatment changes the powder surface tension. [40] This study was aimed to present a correlation between the

measured and estimated surface tension of the powder and melt for understanding the LS processes and additional qualifying new materials.

Here, we conduct a comprehensive study of the usability of plasma treated PA12 powder in laser sintering for applications which require high hydrophilicity. Surface chemical reactions and microstructure development were considered in this paper towards a better understanding of the plasma treatment mechanisms and benefits. Downward heat sintering (DHS) was used as a casting method to mirror the technology of laser sintering but on smaller powder quantities to reduce cost and waste products for Additive Manufacturing. DHS was used only to cast the nontreated and LP-PT treated PA12 powder as the PJ treated powder has shown its meltability during plasma exposure. PA12 particles were rapidly responded to PJ at shorter exposure time (1-3min.) contrary to the LP-PT. This study is a part of a series of works linking plasma treatment and its advantages on polymers or polymer composites for laser sintering applications [8], [9].

## **Section 6.3: Materials and Experimental**

### ***Section 6.3.1: Materials***

Polyamide 12 (PA12) (often named as Nylon12) supplied by e-Manufacturing Solution (EOS) is a white, odourless, thermoplastic and semicrystalline polymer. PA12 is selected for this study as, by far, it is the most established and commonly used laser sintering powder. PA12 is an aliphatic polymer with structure as displayed in *Figure S6-1* in *Section 6.9: Appendix (Supplementary Information)*. The powder batch used in this paper comprised 50% recovered powder from previous Laser Sintering builds, blended with 50% virgin powder, as is standard in industry.

PA12 particles, as shown in *Figure S6-1a*, often have rounded or potato shape with an average size of 60-80  $\mu\text{m}$  particles which is the standard specification of the LS powder. In *Figure S6-1b*, higher magnification Scanning Electron Microscopy (SEM) image of a



single PA12 particle before treatment, shows a non-porous solid surface. In SEM image in **Figure S6-1b**, we observe that the PA12 particles were covered by white nanosized particles which are assumed to be TiO<sub>2</sub> which are added to improve the powder whiteness [41]. These nanoparticles look whiter due to their higher refractive index, which means the TiO<sub>2</sub> has a higher scattering light affinity than the PA12 particles [42], [43].

### ***Section 6.3.2: Plasma Treatment Technologies***

#### *(e) Low pressure air plasma treatment (LP-PT)*

As polymers are heat-sensitive materials, a cold plasma treatment was required to provide low temperature surface modification. A Zepto plasma cleaner from Diener Electronics was used in this study.

PA12 powder (~3g) was placed in thin layers in a glass petri dishes in the plasma cleaner chamber (glass cylindrical chamber), exposing only the surface of the powder layer to the plasma. Thus, the powder was turned half way through the stated treatment time as shown in **Figure S6-2** to increase the homogeneity of the treatment.

After placing powder in the plasma chamber, that was evacuated before running the plasma. Air gas plasma (ambient air is the process gas) generated inside a glass cylindrical chamber was applied by a strong electric field in between two electrodes. Oxygen molecules are activated and dissociated into reactive species, atoms, radicals, ions and electrons. The plasma generator is switched on when working pressure has been achieved (3 mbar or less). However, this pressure changes slightly after generating the plasma. Then, plasma system receives continuously fresh gas while the contaminated gas is evacuated. PA12 powders were treated at 100 W power for 1, 2, and 3 hours respectively, the treated powder was then removed and stored in a sealed glass jars.

#### *(f) Atmospheric pressure plasma jet (PJ)*

The direct treatment of PA12 powder was conducted using two different cold atmospheric pressure plasma jets i.e. kINPen (K-APJ) and Hairline (H-APJ) the differences between the two pen sources are shown in the table in **Figure S6-3** but essentially the K-APJ has a higher power than H-APJ. The operating gas mixture here is Argon. PA12 powder was treated at atmospheric pressure for 1, 3 and 6 minutes. A thin layer of PA12 powder was placed on a small metal stub with a distance ~1 cm between the plasma pen and the powder.

### ***Section 6.3.3: Sample Fabrication Methods***

LP-PT and non-treated PA12 samples were produced via Downward Heat Sintering method (DHS) to mirror the laser sintering as described in [9]. PA12 powders were placed in a hollow mould in between the upper and lower parts of the hot press for thirty minutes in two stages. First, the powder was preheated in the lower part at a temperature 185 °C for 15 minutes before the upper part at a temperature 190 °C was brought down for another 15 minutes. Thus, samples and parts were cast without applied external pressure with a downward supplied heat energy, therefore the DHS was considered as a good indicator for the laser sintering. In the laser sintering process, parts were produced by laser energy layer-by-layer supplied on a preheated powder bed. The main parameters of laser sintering process are: part bed preheating temperature- 170-172 °C; laser power-13-21 W; laser speed scan 2500 mm/sec; layer thickness- 0.1mm and scan spacing- 0.25 mm.

## **Section 6.4: Characterisation and Testing**

### ***Section 6.4.1: Morphology Investigations by SEM***

Low Voltage Scanning Electron Microscopy (NovaSEM) was used to analyse the morphology. An electron beam with a low landing energy (2.2 KeV) was used to reduce the specimen surface charging and damage. Note no metal coating was applied to the polymer surface. In addition, two different detectors were used to image the powder and bulk samples; a Through-lens-detector (TLD) for secondary electron (SE) imaging at low

magnification and concentric back scatter detector (CBS) using back-scattered electrons (BSE) to obtain high magnification images. A Low Voltage FEI Sirion (FEGSEM) was used for imaging the 1 and 3 minute K-APJ treated PA12 at low voltage up to 1kV primary beam and 4.8-4.9 mm working distance, with SE collected using the immersion-lens TLD. A Low Voltage FEI Helios SEM specifically designed for high resolution imaging at low voltages <1kV and working distance of 4 mm was used to probe the nontreated and H-APJ treated PA12 powders. All micrographs were processed to enhance contrast.

#### ***Section 6.4.2: Wettability and density measurements***

As a solid and flat surface is commonly required in the contact angle measurements, a simple experiment was developed in this study to investigate the plasma effect of the wettability of polymer powders. Nontreated and 1hour LP-PT treated PA12 powders were mixed with tap water and stirred gently using a magnetic stirrer for 15 minutes in glass jars. Then the glass jars were left in ambient temperature and images recorded before stirring and after every hour for up to 72 hours.

The densities of PA12 (nontreated, one hour and two hours treated) were measured using Gas Pycnometer (Accupyc II 1340) from micromeritics.

#### ***Section 6.4.3: Fourier Transform Infrared Spectroscopy (FTIR) and Hot Stage Microscopy (HSM)***

FTIR analysis was performed using a PerkinElmer Frontier spectrophotometer equipped by Golden Gate™-single reflection Diamond ATR accessory. FTIR measurements were carried on LP-PT treated and nontreated PA12 powders (without KBr dilution) by recording 10 scans of the wavenumber range from 500 to 4000  $\text{cm}^{-1}$  with a spectral resolution of 4  $\text{cm}^{-1}$ . Before obtaining spectra from the samples, a background spectrum with no sample was taken as a control. HSM was performed on BX50 light microscope from Olympus attached to a temperature-controlled microscope stage from Linkam.

## Section 6.5: Results and Discussion

### *Section 6.5.1: Visual observation and chemical reactions description*

The reactive plasma species attack the polymer surface leading to physical and chemical changes on the exposed polymer surface, e.g. changes of crystalline forms, macroradical generation and splitting of the macromolecules into fragments. One of the most frequently occurring reactions is polymer oxidation, particularly when oxygen-containing plasma is used in the treatment process. As can be clearly seen in *Figure 6-1a*, a dramatic change in the colour of the PA12 powder was observed as the pristine PA12 powder is white and becomes light brown after a 1 hour exposure, and a darker brown after 2 hours. The treated and nontreated powders were also pressed into solid discs with the disc surface displaying a uniform colour which reveals that only fewer powder particles were not well-exposed (see *Figure 6-1b*). Activated atoms and molecules in the electric field during plasma exposure react with the modified surface, creating new oxygenated groups and new chemical functionalities [13]–[36].

Polymer oxidation can therefore occur when the oxygen atoms attack the activated surface leading to hydrogen abstraction (separation) from the polymeric chain, and forming free radicals, which can react to the oxygen in the plasma field. PA12 has a weak resistance to UV radiation and exposure weakens the C-C and C-H bonds. As described earlier, the PA12 particles were covered by TiO<sub>2</sub> nanoparticles (see inset image in *Error! Reference source not found.b*), and the inclusion of photoactive particles could play a critical role in enhancing the production of radical species [43]. In an environment rich with oxygen and radicals (see *Figure 6-1c*), this enables chemical reactions that produce volatile products like CO and CO<sub>2</sub>, new functional groups, i.e. –OH and –COOH [13] and physical changes like the discolouration [44]. Volatile molecules created were subsequently boiled off and swept away by the vacuum pump leading to the formation of pores and holes. Besides the

formation of new chemical functionalities, powder surface etching and powder discolouration, surface activation by oxygen plasma often leads to increased surface energy and roughness, morphological changes, and enhanced wettability.

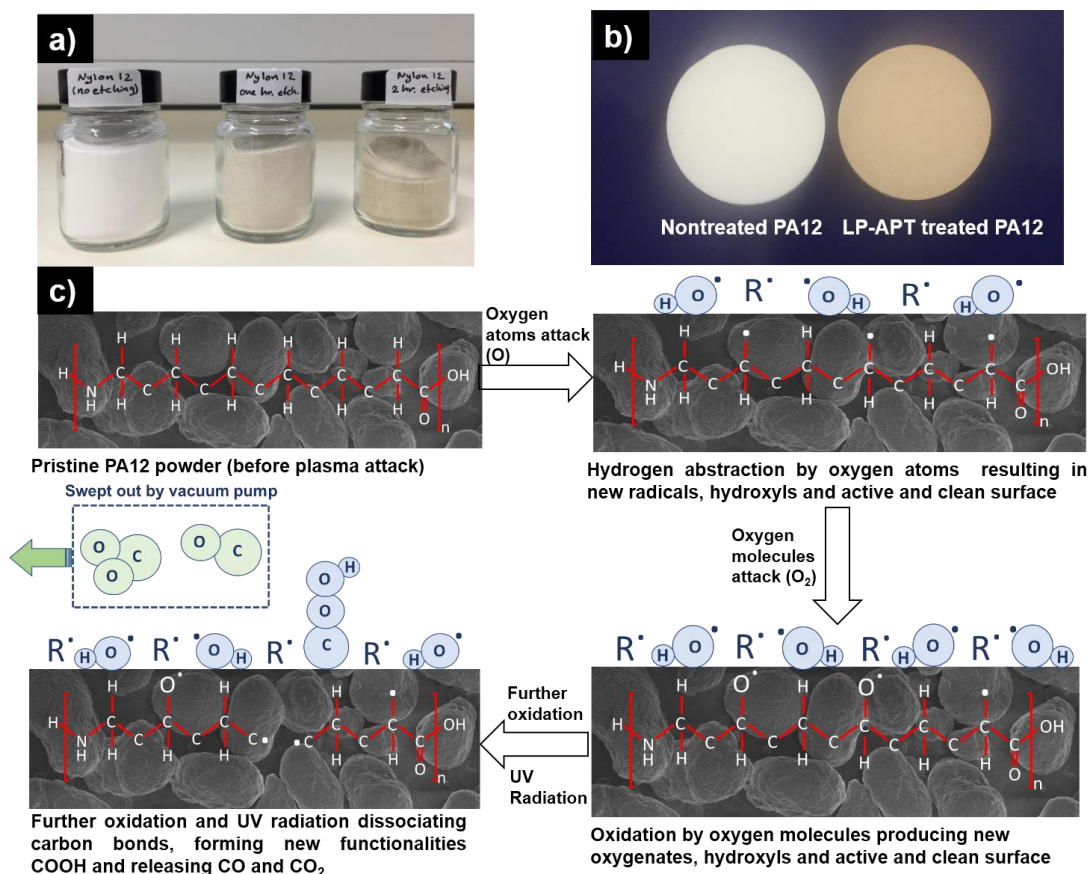


**Figure 6-1** (a) A photograph of nontreated PA12, 1 hour and 2 hour treated PA12 reveals that the PA12 colour change with the plasma treatment. (b) Cold pressed discs of nontreated and 1 hour treated PA12 show the treated pellet has a uniform coloured surface after 1 hour LP-PT exposure. (c) Schemes of the chemical reactions resulting from plasma exposure.

Surface energy is increased by the formation of immobilised free radicals through the generation of dangling bonds [37]. Immobilised free radicals are reactive and unstable, however have higher kinetic stability and longer lifetimes than mobile, free radicals [37]. It is also worthy to note, although oxygen is the most active gas in the air plasma treatment, nitrogen N<sub>2</sub> gas (ions or atoms) also interacts with the polymeric surfaces and chemical abstraction leading to the formation of volatile products like NO and NO<sub>2</sub> [26].

### ***Section 6.5.2: Surface morphology investigations by SEM***

The morphological surface changes of the plasma-exposed particles can be observed in the SEM micrographs in **Figure 6-2**.

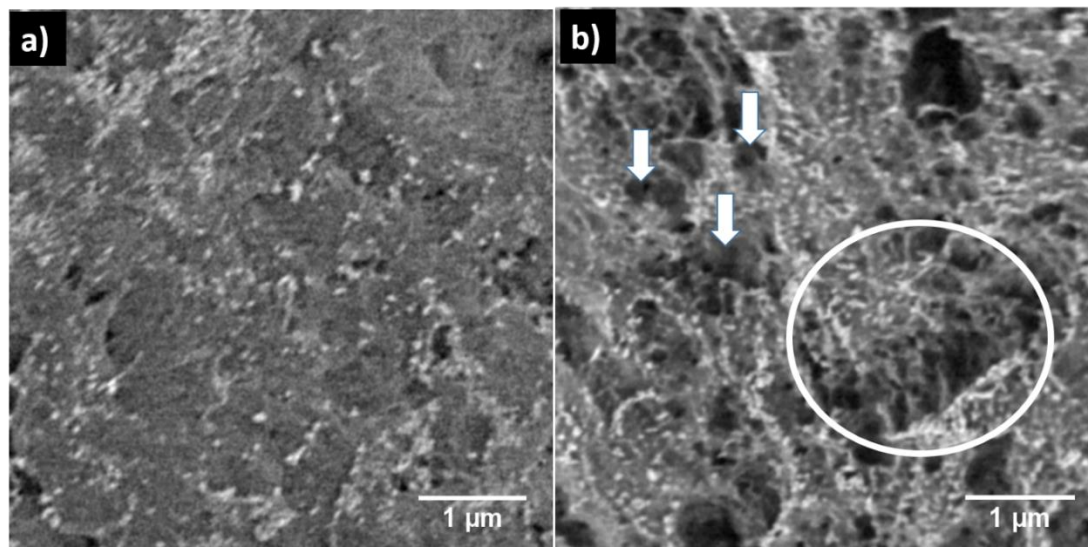


**Figure 6-2** SEM micrographs of the PA12 particles surfaces (a) without LP-PT plasma treatment, (b) 1hr LP-PT plasma treated PA12 (porosity examples marked with circle and arrows)

Distinct differences between nontreated (**Figure 6-2a**) and treated PA12 (**Figure 6-2b**) particles are observed in the BSE-SEM images. Both exhibit dark areas, which are pores or cracks [45] and very bright nanostructures which we assume are the TiO<sub>2</sub> nanoparticles present in the nontreated PA12 powder [41]. The nontreated powder exhibits few nanopores, while the LP-PT powder contains micron size pores. Less obvious is the change in distribution of the bright nano-structures with visible accumulations of the latter at the pores edges (examples are marked with arrows and circle in **Figure 6-2b**). This contrast reveals a heterogeneity in the molecular weight and topography of the treated particle surface due to the plasma species coupled with the UV radiations.

The heterogeneous surface morphology is attributed, as mentioned above, to the dissociation of carbon bonds and conversion to CO and CO<sub>2</sub> gases and other volatile chemical compounds, resulting in surface etching and material loss [25], [26]. The

formation of pores in this section (shown in **Figure 6-2b**) especially those with a size of a few hundred  $\mu\text{m}$ , was possibly due to the chemical changes induced by the plasma species and UV radiation. The chemistry of the etch products is discussed in the FTIR analysis sections.

### ***Section 6.5.3: Powder wettability and density results***

The polymer-water interaction significantly changed after plasma exposure as shown in **Figure S6-4**, **Figure S6-5** and **Figure 6-3**. As can be observed in **Figure S6-4** the LP-PT treated PA12 powder was easily spread over the water surface just before penetrating the water surface, suggesting that the plasma treated powder was rendered wettable (hydrophilic). On the other hand, the nontreated PA12 powder aggregated on top and revealed poor wettability as shown in Error! Reference source not found.. For a deeper insight, photographs were taken of the LP-PT treated and nontreated PA12 powders, at 1 minute and 1 hour intervals after mixing and stirring with water (**Figure 6-3(a-c)** and **Figure S6-5**).

As can be observed in **Figure 6-3a**, the LP-PT plasma-treated PA12 powders tended to spread and disperse within water before stirring while the nontreated PA12 powder remained on the top. During stirring, the treated powder became well-dispersed in the water changing the colour of the treated powder-water mixture to that of the treated powder, whilst the nontreated powder was suspended in the stirred water leading to a “milky” appearance of the powder-water suspension as seen in **Figure 6-3b**. After stirring, some of the treated powder particles began to settle at the bottom, whilst others floated either at the top or within the jar space (see **Figure S6-5** in supporting information). In a photograph taken after 72 hours, all the powder either settles at the bottom (wetted), or floats to the top with some of suspended particles remaining stable in between as observed in **Figure 6-3c**. In contrast, all the nontreated powder accumulated at the top as shown in **Figure 6-3c** and

**Figure S6-5.** This experiment reveals that the PA12 powder becomes wettable upon plasma exposure.

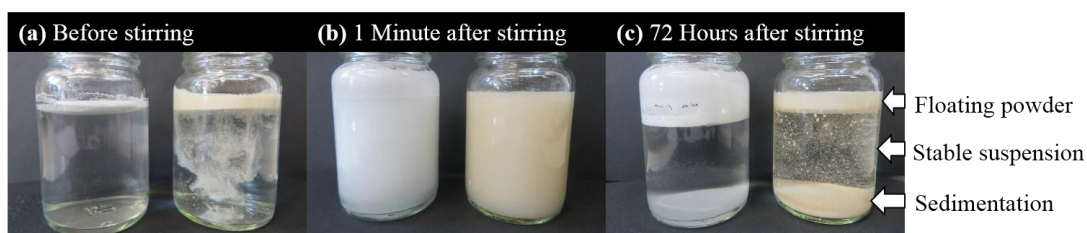


**Figure 6-3** Photographs of PA12 powders (untreated and 1 hour treated LP-PT) immersed and stirred in water (untreated is white and treated is darker): (a) before stirring, (b) 1 minute (c) 72 hours after stirring respectively.

After exposure to atmospheric air plasma (rich in oxygen), the hydrogen bonding with water becomes easier and polar components are increased on the PA12 particles, which facilitate the PA12 powder wettability [10], [34], [46], [47]. However, as seen in **Figure 6-3c**, only a part of the powder was fully dispersed which is possibly because of density heterogeneity, as shown in **Table 6-1**, which summarises the density and volume changes of PA12 caused by plasma treatments. It is noted that the density of PA12 powder was increased by 3% and 3.2% due to 1 hour and 2 hours' plasma treatment respectively.

As previously mentioned, the exposure of the powder to plasma releases etched products, and material removal from the amorphous regions and results in an increase in the polymer density. However, this density increase was probably not the same for all the particles, therefore some of the particles were heavier than the others and settled down at the glass jar bottom (**Figure 6-3**).

**Table 6-1** Change percentage of density of PA 12 powder with the time of treatment.

Weight of each sample: 0.3 gram	Untreated PA12	1hr. treated PA12	Change %	2hr. treated PA12	Change %
Density g/cm <sup>3</sup>	1.0366 g/cm <sup>3</sup>	1.0677 g/cm <sup>3</sup>	+3.00	1.0694 g/cm <sup>3</sup>	+3.164
Standard deviation (Density)	0.0050 g/cm <sup>3</sup>	0.0027 g/cm <sup>3</sup>		0.0023 g/cm <sup>3</sup>	



Volume cm <sup>3</sup>	0.2894 cm <sup>3</sup>	0.2810 cm <sup>3</sup>	-2.903	0.2805 cm <sup>3</sup>	-3.075
Standard deviation (Volume)	0.0014 cm <sup>3</sup>	0.0007 cm <sup>3</sup>		0.0006 cm <sup>3</sup>	

It is also believed that the LP-PT treated powder was better packed than the nontreated as the Pycnometer measured the true density from a measured volume and, as observed by **Table 6-1**, the measured volume treated powder was less than that of nontreated powder for the same mass.

#### Section 6.5.4: Chemical analysis using FTIR

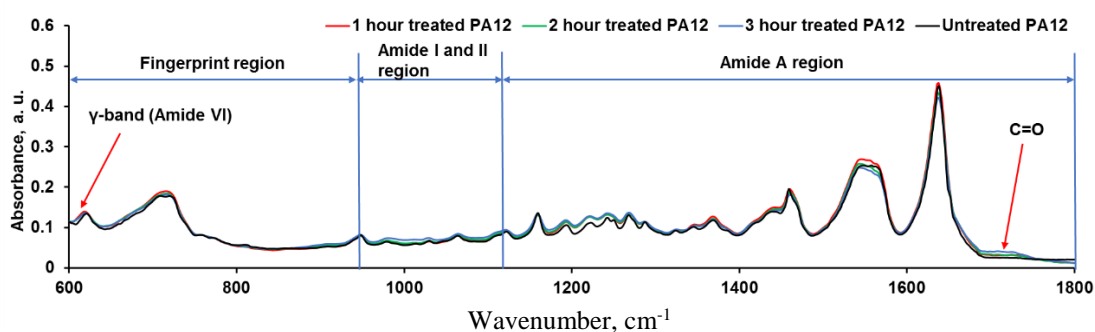


**Figure 6-4** FTIR spectra of nontreated PA12 and 1 hr, 2hr, and 3hr LP-PT treated PA12 powder.

FTIR was used to analyse chemical changes during the plasma exposure. **Figure 6-4** shows one FTIR spectrum of each sample of the tested materials: untreated PA12 powder and the treated ones (1, 2 and 3 hr. exposures) in the range between 600-1800 cm<sup>-1</sup>. Full range spectra are available in **Figure S6-6** in **Section 6.9: Appendix** and the major absorption bands appeared in the FTIR spectra of the PA12 samples as listed in **Table 6-2**. All of these bonds and their assignments are based on previous studies [10], [33], [48]–[54]. As noted in **Table 6-2** and **Figure 6-4**, the main functional groups are N-H groups (bending and stretching), carbonyl groups (carbon-oxygen double bonded), single bonded carbon-carbon groups and alkane groups (CH<sub>2</sub>).

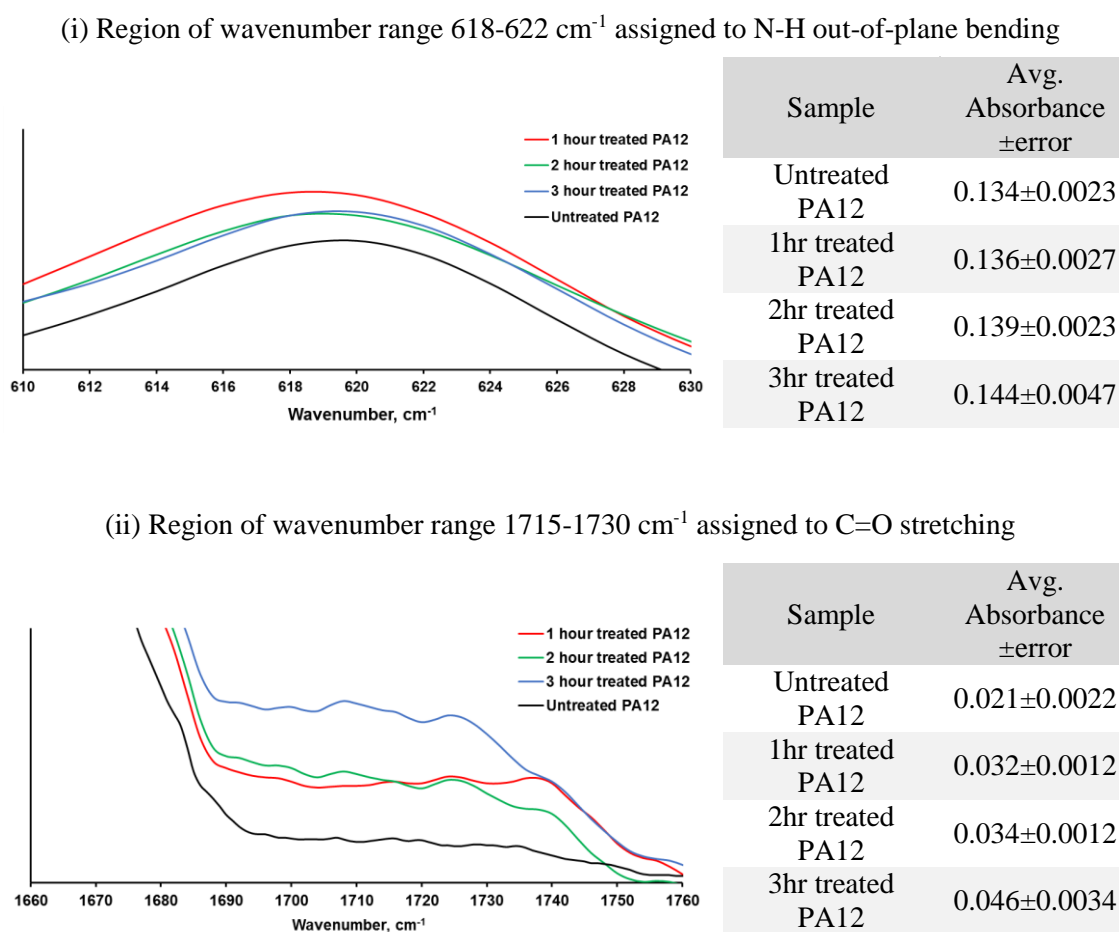
**Table 6-2 Major FTIR absorption bands and their assignments of PA12.**

Approximate wavenumber (cm <sup>-1</sup> )	Assignments	Region
576	N-H out-of-plane bending [48], [49]	Amide VI ( $\alpha$ -form)
622	N-H out-of-plane bending [48]–[50]	Amide VI ( $\gamma$ -form)
683	C=O out of plane bending[48], [50]	Amide V ( $\alpha$ -form)
719	CH <sub>2</sub> rocking [10], [33], [49]	Alkanes
770	N-H bending [51]	
925	C-CO stretching [52]	
950	CONH in plane [49]	
1124	C-C skeletal [10], [49]	
1161	CH <sub>2</sub> and CONH vibration [10], [49]	
1170	N-C-O stretching [53]	
1270	C–N stretching + C=O in plane bending [10], [49]	Amide III
1372	CH <sub>2</sub> wagging [10], [49], [51]	
1460	CH <sub>2</sub> scissoring vibration [10], [49]	Alkanes
1545	N-H bending + C-N stretching [10], [33], [48]–[50]	Amide II ( $\gamma$ -form)
1638	C=O stretching + C-N stretching [10], [33], [48]–[50], [54]	Amide I
1715-1730	C=O stretching [10], [33]	
2850	CH <sub>2</sub> symmetric stretching [10], [49]	Alkanes
2919	CH <sub>2</sub> asymmetric stretching, [10], [49]	Alkanes
3093	N–H stretching, [10], [49]	Amide II
3291	Hydrogen-bonded N–H stretching [10], [49], [50]	

Further, two bands representing the  $\alpha$ -phase of PA12 were observed at wavenumber of 576 and 683 cm<sup>-1</sup> belonging to N-H and C=O respectively [48]. These two bands, however, were not clearly distinguished, as the N-H band showed very low intensity and the C=O band was observed as a shoulder of the band of CH<sub>2</sub> at 719 cm<sup>-1</sup>.  $\gamma$ -phase was also observed at two absorption lines of 622 cm<sup>-1</sup> (N-H) and 1545 cm<sup>-1</sup> (N-H bending + C-N stretching) [48]. The entire FTIR spectral range in **Figure S6-6** displays all the fingerprint and Amide regions.

Limited spectral changes between the treated and nontreated PA12 samples were found in FTIR data as displayed in **Figure 6-4**. The main reason for this, is that the depth of the chemical changes during plasma exposure is mostly limited to the topmost few atomic layers of the surface whereas the FTIR probes 1  $\mu\text{m}$  beneath the tested surface [10]. Moisture may also affect the FTIR signal during specimen analysis [10], [33]. Hence, all the PA12 samples were examined three times, mean values were calculated and shown in **Table 6-3**.

**Table 6-3** FTIR absorption bands of PA12.



The FTIR results in **Table 6-3** reveals spectral changes in two absorption bands (618-622  $\text{cm}^{-1}$  and 1715-1730  $\text{cm}^{-1}$ ), confirming that surface chemical changes occurred on plasma treated surfaces. The intensity of the absorption bond at 618-622  $\text{cm}^{-1}$  in Table 3(i)

increased with the plasma exposure time indicating the proportion of  $\gamma$  crystalline phase increased [33], [50]. As increased  $\gamma$  crystalline phase results in toughened PA12, this suggests that the LP-PT can lead to enhanced toughness in PA12 sintered parts. The FTIR data in Table 3(ii) also confirms that absorption in the range of 1715-1730  $\text{cm}^{-1}$ , belonging to carbonyl groups, was increased to 0.032, 0.034 and 0.046 after plasma exposure of 1, 2 and 3 hours respectively. Increased carbonyl (C=O) absorption indicates the presence of oxygenic species on the treated surfaces, confirming the earlier hypothesis of regarding the creation of oxygen species during plasma treatment [33].

***Section 6.5.5: Pores formation in powder due to LP-PT (SEM and HSM analyses)***

A comparison between the nontreated PA12 and treated PA12 (1, 2 and 3 hours) was made using SEM, images shown in ***Figure 6-5(a-d)***. No significant changes were observed between powders from nontreated PA12 and 1hour treated PA12 except small holes appeared in the 1 hour etched PA12 without any visible cracks (see ***Figure 6-5a*** and ***Figure 6-5b***).

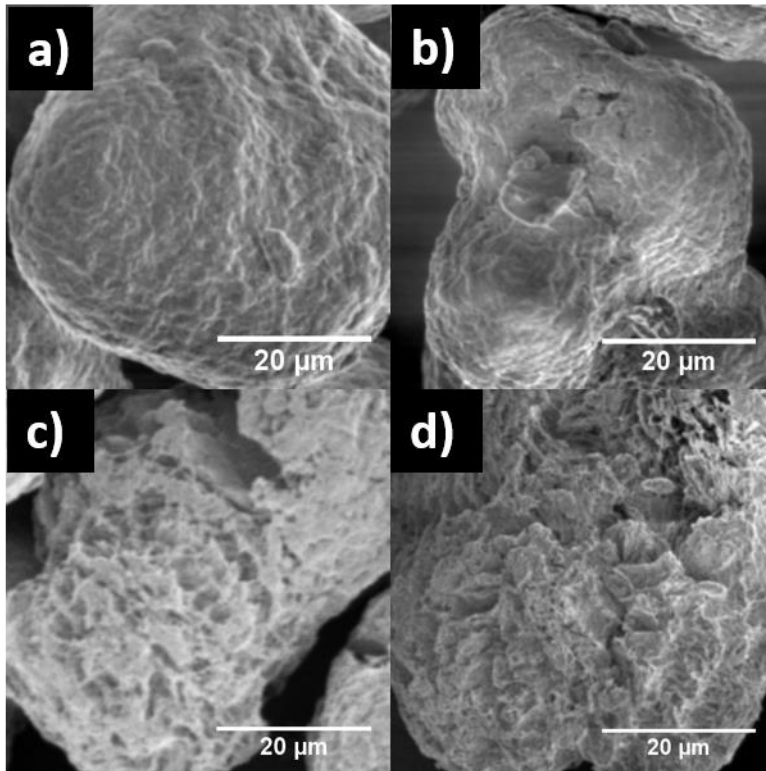


**Figure 6-5** High magnification SEM images of (a) PA12 without LP-PT plasma treatment (b) 1hr LP-PT treated PA12, (c) 2hr LP-PT treated PA12, and (d) 3hr LP-PT treated PA12.

After 2 hours of plasma treatment however, visible cracks and pores were easily observed in the particles, as shown in **Figure 6-5c**. These effects extended with prolonged plasma exposure of 3 hours, as can be seen in **Figure 6-5d**, in which the particles are strongly affected by the plasma treatment leading to a more porous structure. Longer plasma treatments (2 and 3 hours) have shown another beneficial effect of splitting the large agglomerates (non-sintered particles stuck to each other) into smaller particles as shown in **Figure S6-7**. It is believed that this effect is a result of chemical effect catalysed by a low intensity ion bombardment causing atoms and molecules to be ejected from the particle surface [55].

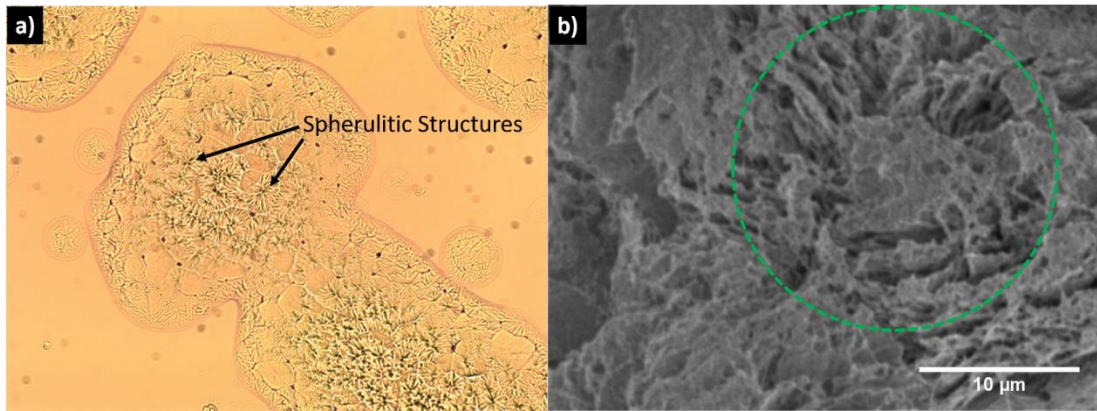


**Figure 6-6** (a) HSM image of PA12 particles taken during crystallisation from melting. (b) High magnification SEM micrograph of 3hr LP-PT treated PA12 particle revealing holes on surface where the amorphous component has been removed (highlighted by the green circle)

For a better understanding of the dual effect of LP-PT on the PA12 powder, hot stage microscopy (HSM) was used in which the powders were cooled followed by heating to 250 °C. Images taken during crystallisation (cooling process) in HSM of 3 hours' plasma treated PA12 powder, showed a spherulitic structure consisting of stacks of parallel lamellae embedded in amorphous regions (examples marked by arrows in **Figure 6-6a**). The lamellar morphology shown by HSM can be linked to SEM images after a prolonged plasma process, shown in **Figure 6-6b**. The region of interest marked in **Figure 6-6a** and **Figure 6-6b** shows that the material loss which was predominantly from the intermediate (amorphous regions) [56]. This phenomenon can be observed in many particles as shown in **Figure 6-5c** and **Figure 6-5d**. Thus, it confirms that there is a greater ratio of crystalline to amorphous material in the etched powder in comparison to the unprocessed powder, which is also suggested by density and FTIR measurements ( $\gamma$ -phase).

### **Section 6.6: Parts Fabricated from Plasma Treated**

Parts Fabricated from Plasma Treated (1 and 2 hour) and nontreated powders were fabricated into parts via a Downward Heat Sintering method (DHS) which was shown in previous work to be a good indicator of Laser Sintering [8]. DHS is used here to determine the optimal parameters (temperature and time) for establishing the printability of PA12

powders. SEM micrographs of the cross section and top surface morphologies are displayed in *Figure 6-7(a-c)*. The nontreated powders were entirely molten, showing a smooth top surface and homogeneous fracture in the range of temperature 185-195 °C as shown in *Figure 6-7a*. The treated powders (1 and 2 hour), on the other hand, showed a heterogeneity on the top surface, as well as unmelted particles, as observed in *Figure 6-7b* and *Figure 6-7c*. This may be attributed to the incorporation of new functionalities at the particles surface due to the plasma and UV radiation exposure, which was confirmed by the FTIR analysis in the previous sections. This suggests that the LP-PT had succeeded in altering the physical and chemical properties of PA12 by creating new functional groups, a wettable powder and a porous structure. However, the problem of the unmelted particles increases when the treated powder is subjected to melting conditions replicating those of laser sintering. The LS technique failed to fuse all the particles from the nontreated powders [57] (see *Figure 6-7d*) especially with aged powder (recovered powder) which was thermally degraded during subsequent LS processes [58].

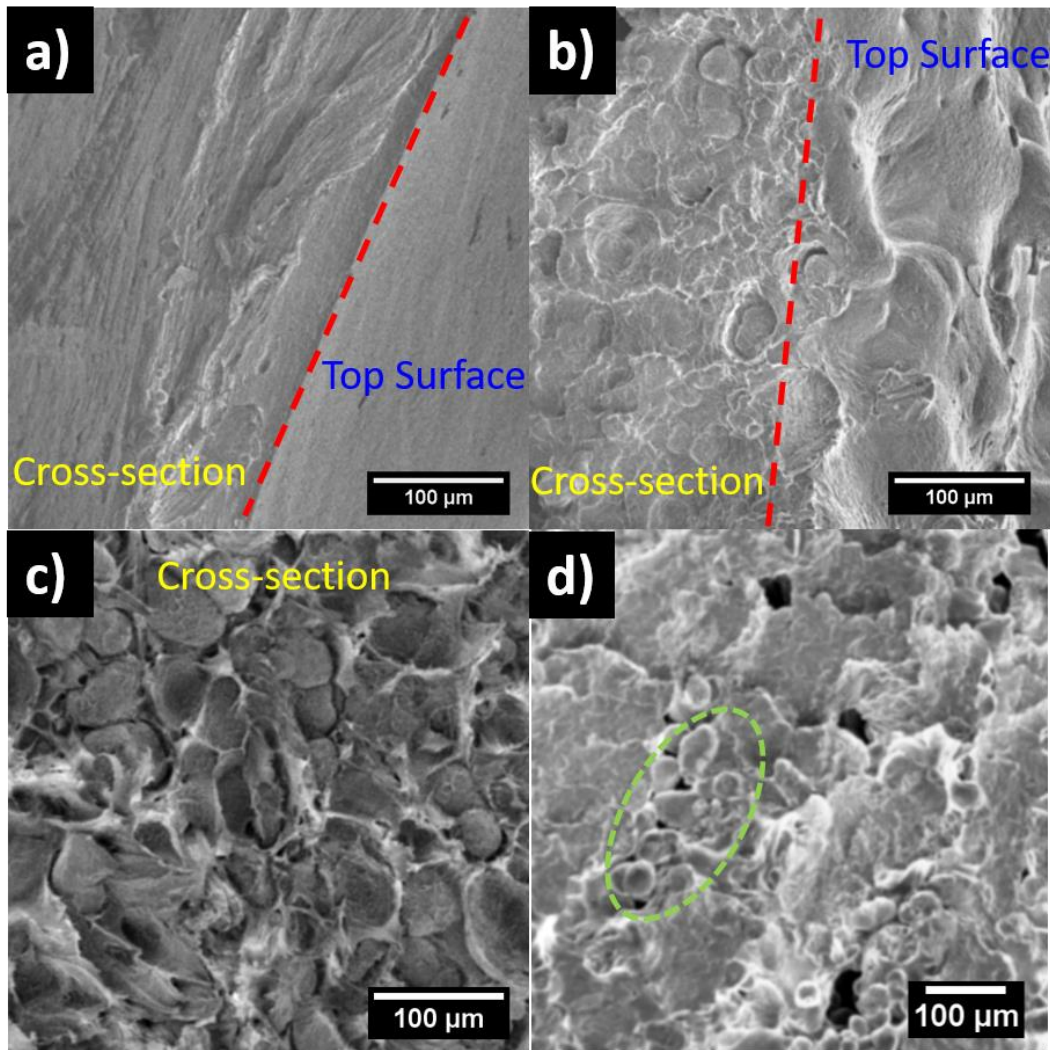


**Figure 6-7** (a) Top surface and cross section of the nontreated PA12 part, (b) Top surface and cross section of 1 hr treated PA12 part, (c) Cross section of the 2hr treated PA12 part and (d) Cross section of LS PA12 part sample ( green circle highlight unmelted powder).

Hence, to obtain any benefit from plasma treatment in Laser sintered parts, a shorter exposure time is required. Therefore, the same batch of powder was subjected to two types of PJ higher power –K-APJ for 1 and 3 minutes and lower power H-APJ for 6 minutes. SEM was used to study the morphological changes on these particle surfaces as shown in **Figure 6-8(a-f)**. The SEM showed that at 1minute duration with the K-APJ has made few micro-holes and porous structure as can be seen in **Figure 6-8a** and **Figure 6-8b** respectively of similar size to that of LP-PT for 1 hour. For a 3 minute exposure to K-APJ, many of the particles became fused together creating one sintered part (see green circle in



**Figure 6-8c)** and while the small pores within particles became bigger and similar in size to 2-3 hour of LP-PT. **Figure 6-8(e-f)** shows the lower power H-APJ 6 minutes treatment and shows no particle fusing, and a nano-porous structure. **Figure S6-8** additionally compares the morphology of the LP-PT and H-APJ for 6 minutes. It can be clearly seen that the LP-PT for 6 minutes hardly changes the PA12 surface whilst the H-APJ 6 minute treatment induces the above-mentioned porosity.

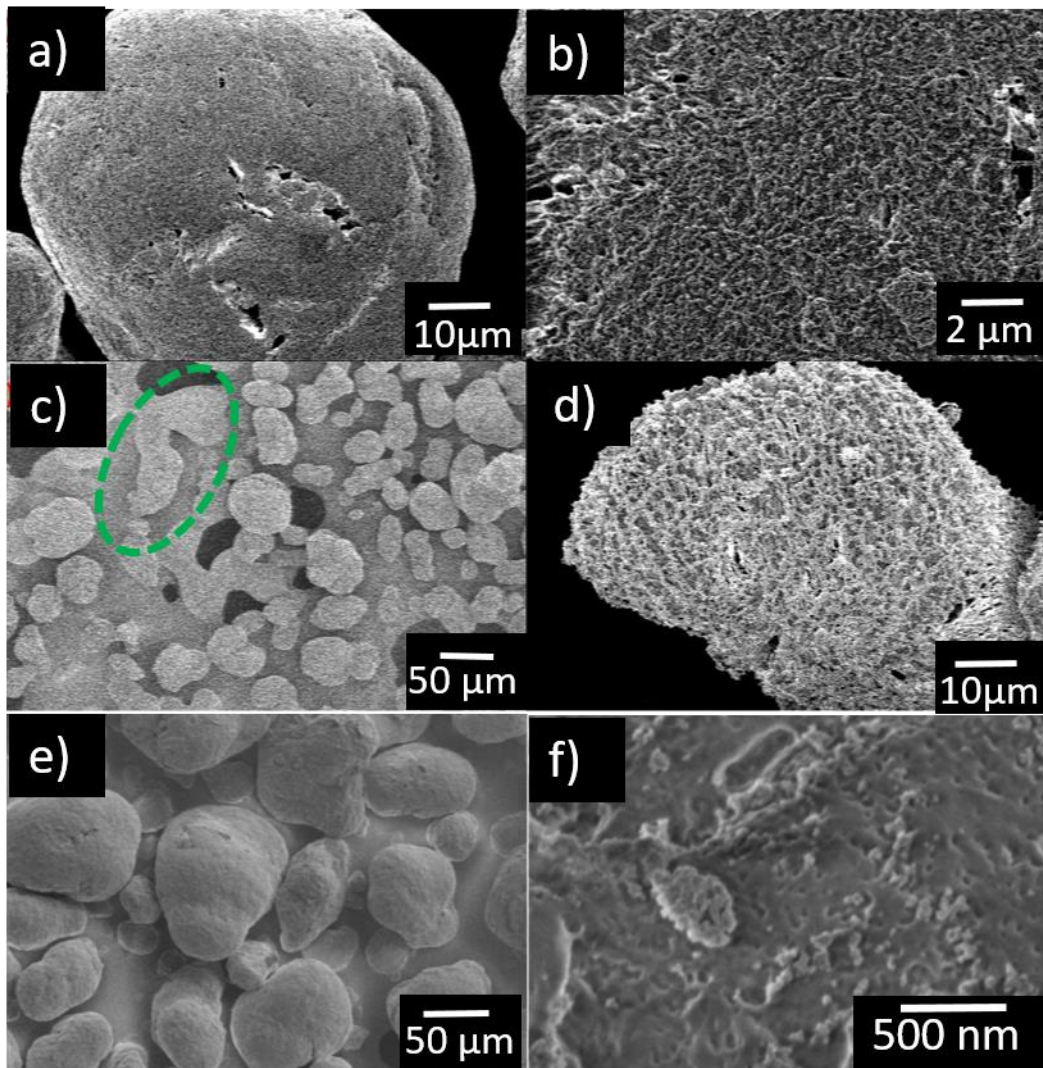


**Figure 6-8** SEM Micrographs of PA12 subjected to K-APJ at a duration of (a-b) 1minute.

And (c-d) 3 minutes.e-f) PA12 powder particles subjected to H-APJ of 6 minutes.

Hence, the atmospheric plasma jets K-APJ and H-APJ both change the surface morphology of PA12 particles whilst maintaining meltability (**Figure 6-8c**). Moreover, the plasma jet treated powder is perhaps wetttable due to increasing the porosity [59]. However, the extent

to the PA12 surface change is dependent on the PJ and further works are required on this as well as the chemical properties of the K-APJ and H-APJ treated powder.

### **Section 6.7: Conclusion**

Here we studied the effects of plasma treatment on the sintering of PA12 using different plasma techniques: low pressure air plasma treatment (LP-PT) and two atmospheric pressure plasma jets K-APJ and H-APJ.

Our results showed that the physical and chemical properties of LP-PT treated PA12 powder were altered. PA12 powder became wettable, denser and porous which results from the incorporation of oxygen groups, dissociation of carbon bonds with the accompanied removal of volatile products and amorphous components. Besides the usefulness of using LP-PT for producing wettable and porous structured powder, the melting properties of the LP-PT treated PA12 powder needs to be considered if powders are intended for the fabrication of parts by Laser Sintering. Prolonged low pressure plasma treatment resulted in poor melting behaviour in the time needed to generate target morphological changes.

K-APJ and H-APJ, on the other hand, have rapidly created porous structures for K-APJ similar to that of LP-PT for 2-3 hours. Moreover, the short K-APJ has not prevented the meltability of the PA12 powder but the rapid pore formation and melting make it difficult to control. Due to the lower power, the H-APJ was deemed the more useful treatment to observe the morphology change induced by the atmospheric Plasma jet.

Hence, we conclude that for Laser sintering applications of PA12 powder, PJ treatment technique is recommended. However, further work on characterising the chemical and physical changes of K-APJ and H-APJ treated PA12 using techniques such as FTIR and wettability analyses will be required. This testing is important to discover whether the

shorter minute exposures have made similar chemical and physical changes to the LP-PT or not.

## Section 6.8:References

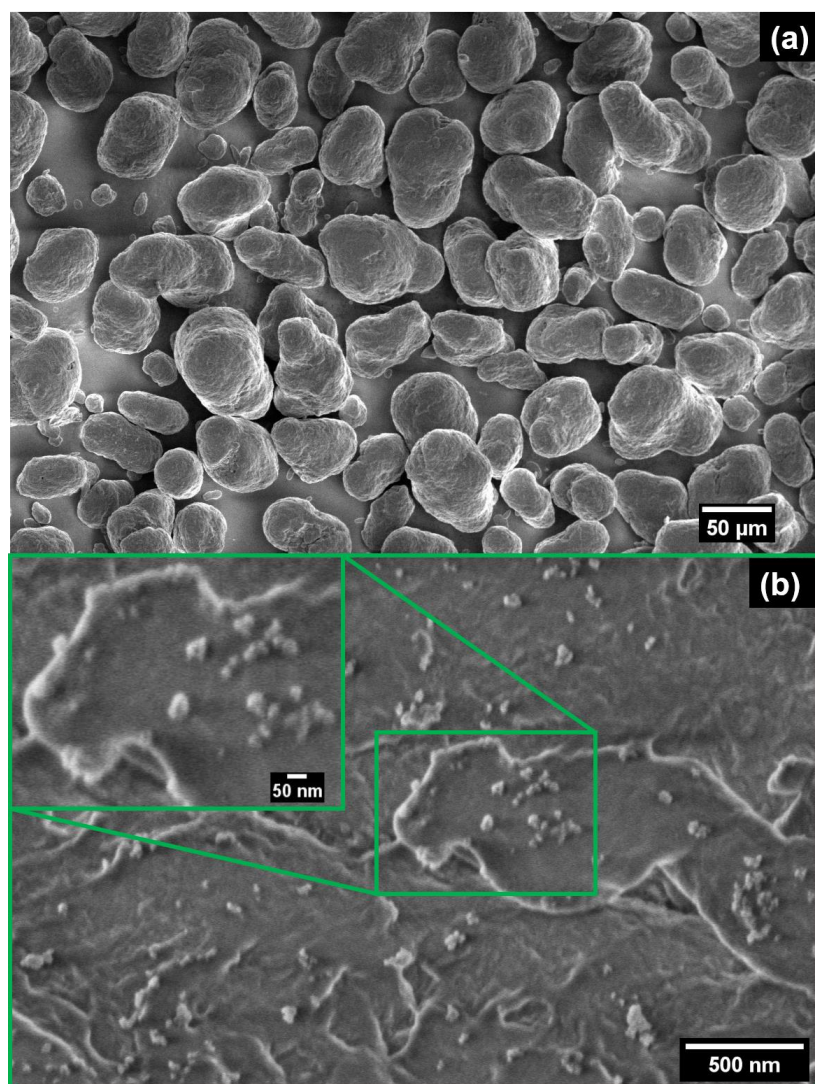
- [1] M. Pavan, T. Craeghs, R. Verhelst, O. Ducatteeuw, J. P. Kruth, and W. Dewulf, “CT-based quality control of Laser Sintering of Polymers,” *Case Stud. Nondestruct. Test. Eval.*, vol. 6, pp. 62–68, 2016.
- [2] Z. X. Low, Y. T. Chua, B. M. Ray, D. Mattia, I. S. Metcalfe, and D. A. Patterson, “Perspective on 3D printing of separation membranes and comparison to related unconventional fabrication techniques,” *J. Memb. Sci.*, vol. 523, no. May 2016, pp. 596–613, 2017.
- [3] Y. Khalil, A. Kowalski, and N. Hopkinson, “Influence of laser power on tensile properties and material characteristics of laser-sintered UHMWPE,” *Manuf. Rev.*, vol. 3, p. 15, 2016.
- [4] A. Warnakula and S. Singamneni, “Selective Laser Sintering of Nano Al<sub>2</sub>O<sub>3</sub> Infused Polyamide,” *Materials (Basel)*, vol. 10, no. 8, p. 864, 2017.
- [5] R. D. Goodridge, C. J. Tuck, and R. J. M. Hague, “Laser sintering of polyamides and other polymers,” *Prog. Mater. Sci.*, vol. 57, no. 2, pp. 229–267, 2012.
- [6] G. M. Vasquez, C. E. Majewski, B. Haworth, and N. Hopkinson, “A targeted material selection process for polymers in laser sintering,” *Addit. Manuf.*, vol. 1, pp. 127–138, 2014.
- [7] U. Ajoku, N. Hopkinson, and M. Caine, “Experimental measurement and finite element modelling of the compressive properties of laser sintered Nylon-12,” 2006.
- [8] A. Almansoori, C. Majewski, and C. Rodenburg, “Nanoclay/Polymer Composite Powders for Use in Laser Sintering Applications: Effects of Nanoclay Plasma Treatment,” *JOM*, vol. 69, no. 11, 2017.
- [9] A. Almansoori, R. Seabright, C. Majewski, and C. Rodenburg, “Feasibility of Plasma Treated Clay in Clay/Polymer Nanocomposites Powders for use Laser Sintering (LS),” in *IOP Conference Series: Materials Science and Engineering*, 2017, vol. 195, no. 1.
- [10] J. Hnilica, L. Potočňáková, M. Stupavská, and V. Kudrle, “Rapid surface treatment of polyamide 12 by microwave plasma jet,” *Appl. Surf. Sci.*, vol. 288, pp. 251–257, 2014.
- [11] R. Puffr and V. Kubanek, *Lactam Based Polyamides, Volume 1: Polymerization, structure and properties*. Boca Raton, FL: CRC Press, 1991.
- [12] L. Bao, H. Fan, Y. Chen, J. Yan, T. Yang, and Y. Guo, “Effect of surface free energy and wettability on the adhesion property of waterborne polyurethane adhesive,” *RSC Adv.*, vol. 6, no. 101, pp. 99346–99352, 2016.
- [13] P. Slepíčka, N. S. Kasálková, E. Stránská, L. Bačáková, and V. Švorčík, “Surface characterization of plasma treated polymers for applications as biocompatible carriers,” *Express Polym. Lett.*, vol. 7, no. 6, pp. 535–545, 2013.

- [14] M. Šíra, D. Trunec, P. St'ahel, V. Buršíková, and Z. Navrátil, "Surface modification of polycarbonate in homogeneous atmospheric pressure discharge," *J. Phys. D. Appl. Phys.*, vol. 41, no. 1, 2008.
- [15] Z. Gao, J. Sun, S. Peng, L. Yao, and Y. Qiu, "Surface modification of a polyamide 6 film by He/CF<sub>4</sub> plasma using atmospheric pressure plasma jet," *Appl. Surf. Sci.*, vol. 256, no. 5, pp. 1496–1501, 2009.
- [16] P. Krüger, R. Knes, and J. Friedrich, "Surface cleaning by plasma-enhanced desorption of contaminants (PEDC)," *Surf. Coatings Technol.*, vol. 112, no. 1–3, pp. 240–244, 1999.
- [17] K. Fricke *et al.*, "Atmospheric pressure plasma: A high-performance tool for the efficient removal of biofilms," *PLoS One*, vol. 7, no. 8, p. e42539, Aug. 2012.
- [18] R. Morent, N. De Geyter, J. Verschuren, K. De Clerck, P. Kiekens, and C. Leys, "Non-thermal plasma treatment of textiles," *Surf. Coatings Technol.*, vol. 202, no. 14, pp. 3427–3449, 2008.
- [19] K. Fricke, H. Steffen, T. Von Woedtke, K. Schröder, and K. D. Weltmann, "High rate etching of polymers by means of an atmospheric pressure plasma jet," *Plasma Process. Polym.*, vol. 8, no. 1, pp. 51–58, 2011.
- [20] J. Schäfer, K. Fricke, F. Mika, Z. Pokorná, L. Zajíčková, and R. Foest, "Liquid assisted plasma enhanced chemical vapour deposition with a non-thermal plasma jet at atmospheric pressure," *Thin Solid Films*, vol. 630, pp. 71–78, 2017.
- [21] U. Lommatzsch, D. Pasedag, A. Baalman, G. Ellinghorst, and H. E. Wagner, "Atmospheric pressure plasma jet treatment of polyethylene surfaces for adhesion improvement," *Plasma Process. Polym.*, vol. 4, no. SUPPL.1, pp. 1041–1045, 2007.
- [22] J. Hanusová, D. Kováčik, M. Stupavská, M. Černák, and I. Novák, "Atmospheric pressure plasma treatment of polyamide-12 foils," *Open Chem.*, vol. 13, no. 1, pp. 382–388, 2015.
- [23] A. Dupuis *et al.*, "Improving adhesion of powder coating on PEEK composite: Influence of atmospheric plasma parameters," *Appl. Surf. Sci.*, vol. 357, pp. 1196–1204, 2015.
- [24] Y. Kim, Y. Lee, S. Han, and K. J. Kim, "Improvement of hydrophobic properties of polymer surfaces by plasma source ion implantation," *Surf. Coatings Technol.*, vol. 200, no. 16–17, pp. 4763–4769, 2006.
- [25] C. K. aa. Akkan *et al.*, "Surface topography and wetting modifications of PEEK for implant applications," *Lasers Med. Sci.*, vol. 29, no. 5, pp. 1633–1639, 2014.
- [26] J. M. Grace and L. J. Gerenser, *Plasma treatment of polymers*, vol. 24, no. 3–4. 2003.
- [27] D. Breite, M. Went, A. Prager, and A. Schulze, "Tailoring membrane surface charges: A novel study on electrostatic interactions during membrane fouling," *Polymers (Basel)*, vol. 7, no. 10, pp. 2017–2030, 2015.
- [28] Y. Chang *et al.*, "Surface grafting control of PEGylated poly(vinylidene fluoride) antifouling membrane via surface-initiated radical graft copolymerization," *J. Memb. Sci.*, vol. 345, no. 1–2, pp. 160–169, 2009.
- [29] B. Van der Bruggen, "Chemical Modification of Polyethersulfone Nanofiltration

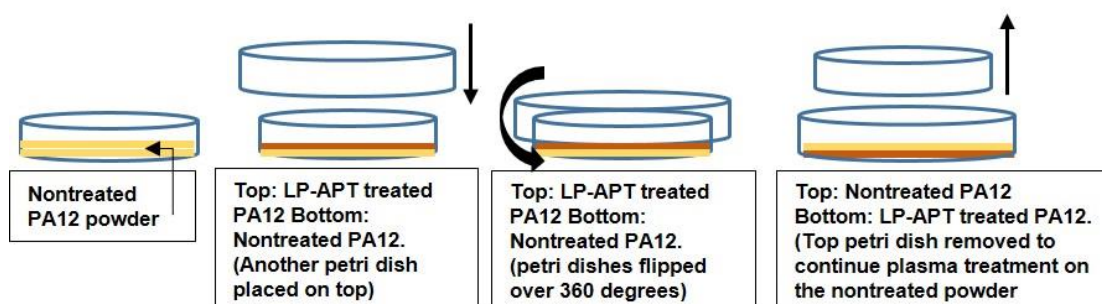
- Membranes: A Review,” *J. Appl. Polym. Surf.*, vol. 114, pp. 630–642, 2009.
- [30] K. Matsubara, M. Danno, M. Inoue, H. Nishizawa, Y. Honda, and T. Abe, “Hydrophobization of polymer particles by tetrafluoromethane (CF<sub>4</sub>) plasma irradiation using a barrel-plasma-treatment system,” *Appl. Surf. Sci.*, vol. 284, pp. 340–347, 2013.
- [31] S. W. Ha, R. Hauert, K. H. Ernst, and E. Wintermantel, “Surface analysis of chemically-etched and plasma-treated polyetheretherketone (PEEK) for biomedical applications,” *Surf. Coatings Technol.*, vol. 96, no. 2–3, pp. 293–299, 1997.
- [32] L. Zhou, Y. Qian, Y. Zhu, H. Liu, K. Gan, and J. Guo, “The effect of different surface treatments on the bond strength of PEEK composite materials (DEMA-D-13-00481),” *Dent. Mater.*, vol. 30, no. 8, pp. e209–e215, 2014.
- [33] I. Novák, M. Števiar, and I. Chodák, “Surface energy and adhesive properties of polyamide 12 modified by barrier and radio-frequency discharge plasma,” *Monatshefte fur Chemie*, vol. 137, no. 7, pp. 943–952, 2006.
- [34] P. Lennon, E. Espuche, H. Sautereau, and D. Sage, “Influence of microwave plasma treatment on the wettability and the adhesive properties of polyamides in epoxy resin,” vol. 19, pp. 273–279, 1999.
- [35] F. Dreux, S. Marais, F. Poncin-Epaillard, M. Metayer, M. Labbe, and J. M. Saiter, “Water and toluene barrier properties of a polyamide 12 modified by a surface treatment using cold plasma,” *Mater. Res. Innov.*, vol. 7, no. 3, pp. 183–190, 2003.
- [36] D. Pavlišák, J. Hnilica, A. Quade, J. Schäfer, M. Alberti, and V. Kudrle, “Functionalisation and pore size control of electrospun PA6 nanofibres using a microwave jet plasma,” *Polym. Degrad. Stab.*, vol. 108, pp. 48–55, 2014.
- [37] D. Cheneler and J. Bowen, “Degradation of polymer films,” *Soft Matter*, vol. 9, no. 2, pp. 344–358, 2013.
- [38] P. Gröning, M. Collaud Coen, and L. Schlapbach, “Polymers and cold plasmas,” *Chimia (Aarau)*, vol. 55, no. 3, pp. 171–177, 2001.
- [39] C. Canal, R. Molina, E. Bertran, and P. Erra, “Wettability, ageing and recovery process of plasma-treated polyamide 6,” *J. Adhes. Sci. Technol.*, vol. 18, no. 9, pp. 1077–1089, 2004.
- [40] K. Wudy, D. Drummer, and M. Drexler, “Characterization of polymer materials and powders for selective laser melting,” *AIP Conf. Proc.*, vol. 1593, no. May, pp. 702–707, 2014.
- [41] L. Verbelen, S. Dadbakhsh, M. Van Den Eynde, J. P. Kruth, B. Goderis, and P. Van Puyvelde, “Characterization of polyamide powders for determination of laser sintering processability,” *Eur. Polym. J.*, vol. 75, pp. 163–174, 2016.
- [42] L. Ming *et al.*, “Selective laser sintering of TiO<sub>2</sub> nanoparticle film on plastic conductive substrate for highly efficient flexible dye-sensitized solar cell application,” *J. Mater. Chem. A*, vol. 2, no. 13, pp. 4566–4573, 2014.
- [43] F. Lin, “Preparation and Characterization of Polymer TiO<sub>2</sub> Nanocomposites via In-situ Polymerization by,” University of Waterloo, 2006.
- [44] A. Dupuis, F. X. Perrin, A. Ulloa Torres, J. P. Habas, L. Belec, and J. F. Chailan,

- “Photo-oxidative degradation behavior of linseed oil based epoxy resin,” *Polym. Degrad. Stab.*, vol. 135, pp. 73–84, 2017.
- [45] R. C. Masters *et al.*, “Application of low-voltage backscattered electron imaging to the mapping of organic photovoltaic blend morphologies,” *J. Phys. Conf. Ser.*, vol. 644, no. 1, 2015.
- [46] J. M. Goddard and J. H. Hotchkiss, “Polymer surface modification for the attachment of bioactive compounds,” *Prog. Polym. Sci.*, vol. 32, no. 7, pp. 698–725, 2007.
- [47] K. Novotna *et al.*, “Adhesion and growth of vascular smooth muscle cells on nanostructured and biofunctionalized polyethylene,” *Materials (Basel)*, vol. 6, no. 5, pp. 1632–1655, 2013.
- [48] S. Rhee and J. L. White, “Crystal structure and morphology of biaxially oriented polyamide 12 films,” *J. Polym. Sci. Part B Polym. Phys.*, vol. 40, no. 12, pp. 1189–1200, 2002.
- [49] J. Han, Z. Cao, and W. Gao, “Remarkable sorption properties of polyamide 12 microspheres for a broad-spectrum antibacterial (triclosan) in water,” *J. Mater. Chem. A*, vol. 1, no. 16, pp. 4941–4944, 2013.
- [50] R. Rafiq, D. Cai, J. Jin, and M. Song, “Increasing the toughness of nylon 12 by the incorporation of functionalized graphene,” *Carbon N. Y.*, vol. 48, no. 15, pp. 4309–4314, 2010.
- [51] N. Vasanthan, “Crystallinity determination of nylon 66 by density measurement and fourier transform infrared (FTIR) spectroscopy,” *J. Chem. Educ.*, vol. 89, no. 3, pp. 387–390, 2012.
- [52] M. Porubská *et al.*, “FTIR spectroscopy study of polyamide-6 irradiated by electron and proton beams,” *Polym. Degrad. Stab.*, vol. 97, no. 4, pp. 523–531, 2012.
- [53] J. Maillo, P. Pages, E. Vallejo, T. Lacorte, and J. Gacén, “FTIR spectroscopy study of the interaction between fibre of polyamide 6 and iodine,” *Eur. Polym. J.*, vol. 41, no. 4, pp. 753–759, 2005.
- [54] A. H. Kuptsov and g. n. Zhizhin, “Handbook of Fourier Transform Raman and Infrared Spectra of Polymers,” *Bioseparation*. Elsevier, p. 536, 1998.
- [55] P. K. Chu, J. Y. Chen, L. P. Wang, and N. Huang, “Plasma surface modification of biomaterials,” *Mat. Sci. Eng. R*, vol. 36, no. 5, pp. 143–206, 2002.
- [56] Q. Guo, *Polymer morphology: Principles, characterization, and processing*. New Jersey: John Wiley and Sons, 2016.
- [57] N. Hopkinson, C. E. Majewski, and H. Zarringhalam, “Quantifying the degree of particle melt in Selective Laser Sintering®,” *CIRP Ann. - Manuf. Technol.*, vol. 58, no. 1, pp. 197–200, 2009.
- [58] K. Wudy, D. Drummer, F. Kühnlein, and M. Drexler, “Influence of degradation behavior of polyamide 12 powders in laser sintering process on produced parts,” *AIP Conf. Proc.*, vol. 1593, no. 2014, pp. 691–695, 2014.
- [59] S. Mane, S. Ponrathnam, and N. Chavan, “Effect of Chemical Crosslinking on Properties of Polymer Microbeads: A Review,” *Can. Chem. Trans.*, vol. 3, no. 4, pp. 473–485, 2016.

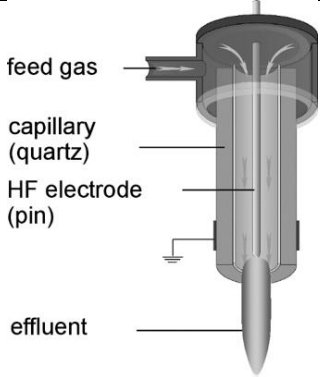
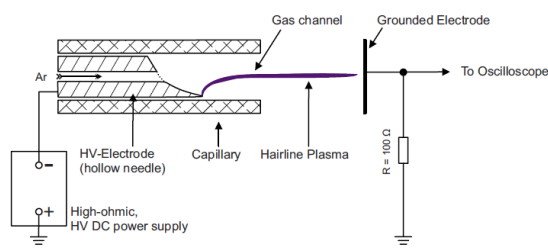
Section 6.9:Appendix (Supplementary Information)



**Figure S6-1** SEM micrograph of PA12 powder (a) and (b) high magnification SEM image of single PA12 particle covered by TiO<sub>2</sub> nanoparticles.



**Figure S6-2** A schematic diagram shows the LP-PT procedure

Source	K-APJ (Atmospheric Plasma KinPen)	H-APJ (Atmospheric Plasma Hairline Pen)
Geometry		
Characteristic diameter	1.6 mm (capillary) 1.6 mm (effluent)	1 mm (capillary) 0.1 mm (filamentary discharge)
Reactive gas	Argon	Argon
Flow rate	4.7 slm	0.5 slm
Excitation frequency	1.1 MHz	1-3 kHz self pulsed (FWHM 10 ns)
Power	1-5 W	0.1 – 0.5 W

**Figure S6-3** Table shows parameters of the two different plasma pen sources used in this work.



**Figure S6-4** A photo taken immediately after spread the untreated (white) and 1 hour treated (darker) over the top of water in petri dishes.



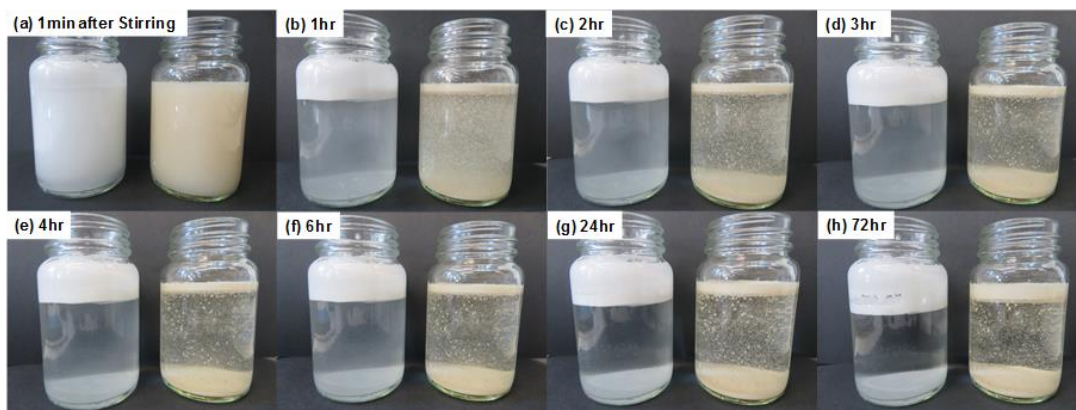


**Figure S6-5** Photos were taken to the nontreated and LP-PT treated PA12 powder after stirred in water (a) 1min, (b) 1hr, (c) 2hr, (d) 3hr, (e) 4hr, (f) 6hr, (g) 24hr, and (h) 72hr

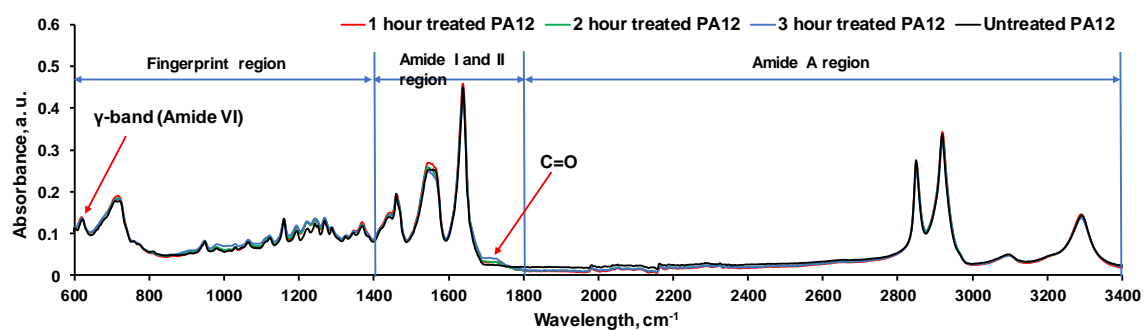


**Figure S6-6** Entire FTIR spectra of untreated PA12 and 1 hr, 2hr, and 3hr LP-PT treated PA12 powder

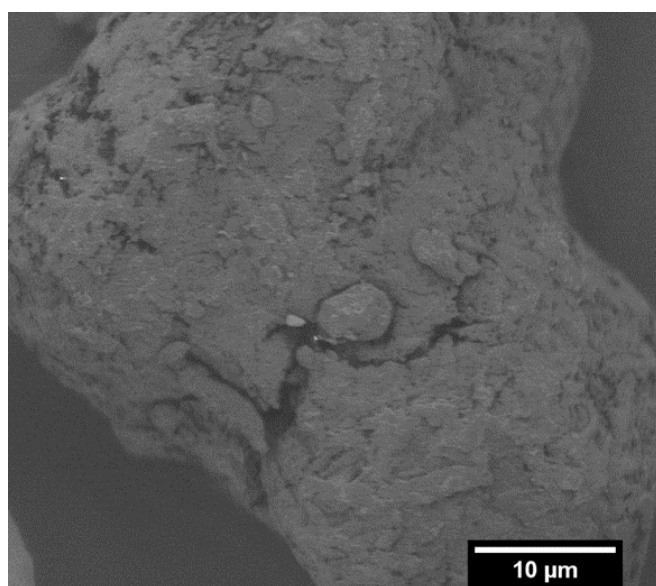


**Figure S6-7** SEM micrograph of 2 hour LP-PT treated PA12 powder

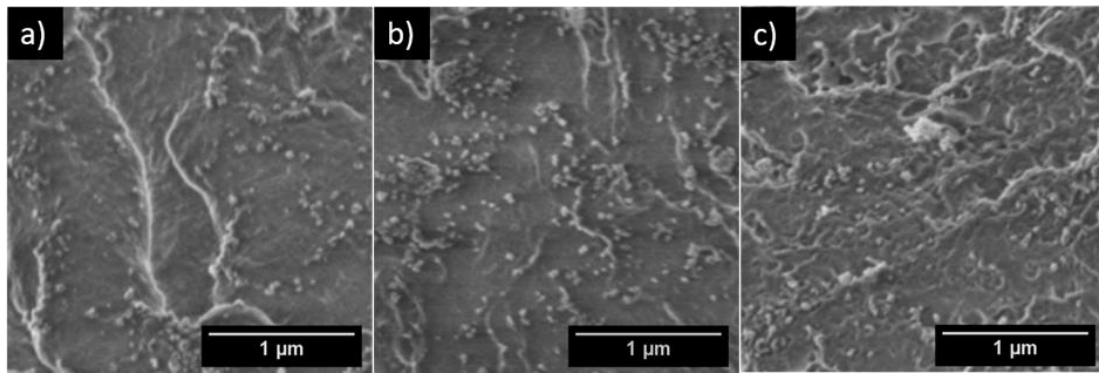


**Figure S6-8** SEM Micrographs of PA12 powder a) Untreated b) LP-PT for 6 minutes c) H-APJ for 6 minutes.

## Chapter 7: Conclusions and Future Work

### Section 7.1: Conclusions

Two polymer nanocomposites (C30B/PA12) and (I.34TCN/PA12) were prepared using a mechanical mixing method. Before mixing, Nanoclays (powders) were treated using Plasma technique. The plasma treated and untreated C30B/PA12 composite was prepared for the Downward Heat Sintering (DHS) process, while for Laser Sintering (LS), the plasma treated and untreated (I.34TCN/PA12) composites were prepared. Morphological and thermal properties were investigated. DHS and LS processes were used to make tensile test samples from both composites and PA12 matrix.

My conclusions are summarised in the following points:

(1) Plasma treatment techniques have not been linked to Laser Sintering applications and it is poorly studied. More specifically, up-to-date, the mechanical properties of the plasma treated laser sintered nanocomposites have not been studied. The research conducted here conducted that, the plasma treatment-Laser Sintering linkage is possible, and it can be a new generation of materials with improved properties.

(2) Plasma treatment was used for three objectives: surface modification of nanoclay powders for heating and laser sintering and surface modification of polymer powders for laser sintering:

- (i) Plasma treatment for nanocomposites produced by heat sintering:

The C30B/PA12 composites provided with powders, made in the dry mixing process of plasma treated C30B with PA12, through heat sintering method compare favourably to other mixing process that were previously described in the literature and are therefore encouraging for the use in Laser Sintering. We have demonstrated that large clay aggregates are avoided through the use of plasma treatment leading to smaller variations in

mechanical properties between different test specimens. The hot-stage microscopy was successfully used to determine suitable processing temperatures to produce C30B/PA12 composites. The tensile test properties (elastic modulus and tensile strength) were improved when plasma treated C30B is incorporated into PA12 powder by the dry mixing process.

(ii) Plasma treatment for nanocomposites produced by Laser Sintering:

The plasma treatment can be used to enhance the compatibility between the organic polymer PA12 and nonorganic nanoclay I.34TCN, ultimately, resulting in good processibility of complex LS parts, and most notably, improving the surface quality. It was found, the plasma treatment improves the affinity between the nanoclay and PA12 and therefore it reduced significantly the nanoclay aggregates and improved the dispersion quality. Furthermore, LP-PT can increase stiffness and promote a reduced brittleness when plasma treated nanoclays are added.

(iii) Plasma treatment for surface modification of Laser Sintering standard polymers:

Plasma treatment effects on the sintering of PA12 using air plasma treatment and plasma jets were studied. The physical and chemical properties of air plasma treated PA12 powder were altered. PA12 powder became wettable, denser and porous via the incorporation of oxygen groups, dissociation of carbon bonds with the accompanied removal of volatile products and amorphous components. Prolonged low pressure air plasma treatment resulted in poor melting behaviour in the time needed to generate target morphological changes. Plasma jets, on the other hand, have rapidly created porous structures similar to that of LP-PT for 2-3 hours without preventing the meltability of the PA12 powder.

## **Section 7.2:Future Work**

Although this work has demonstrated, for the first time, the potential for plasma-assisted polymer and polymer nanocomposites for Laser Sintering, there remain further areas for

exploration. Some suggestions and experimentations, shown below, are recommended for future work:

#### (1) Materials

This work has only focused on a specific set of nanomaterials and polymers, therefore, future work in this area requires expanding a greater range of potentially applicable materials. It is suggested applying the current methods on new fillers such as pristine MMT, or on new matrices such as new thermoplastic, or thermosetting polymers. Successful attempts on new materials would confirm the validation of the current methods for the LS of plasma assisted materials on all LS materials.

#### (2) Laser Sintered part properties

The thermal and chemical properties of the current materials were investigated via various techniques, i.e. TGA, DSC, FTIR and HSM. However, studying other properties such as fire-retardant properties to expand the material applications is also recommended, for future work. Additionally, other techniques such as Nano-indentation, flexural and bending tests could be useful in the future to examine the material performance under various loads.

#### (3) Plasma Parameters

These suggested tests and examinations might also be in parallel with further optimisation of the methods described by this thesis for example the plasma processing parameters. As such these optimisations are suggested to ensure the advantages of plasma treatment are fully exploited.

(4) Finally, a technical recommendation, if possible, would be to create a system that combines the plasma treatment and the Laser Sintering. A plasma source could be embedded into the LS chamber to treat powders before sintering. Such a novel system could save time, costs and avoid any possible reactions between the plasma treated powders and the ambient environment.